Title
Development of a Single Particle Analyzer of Mass and Mobility

Author
Elliott, Andrew Gareth

Publication Date
2018

Peer reviewed|Thesis/dissertation

Development of a Single Particle Analyzer of Mass and Mobility

by

Andrew Gareth Elliott

A dissertation submitted in partial satisfaction of the

requirements for the degree of

Doctor of Philosophy

in

Chemistry

in the

Graduate Division

of the

University of California, Berkeley

Committee in charge:

Professor Evan R. Williams, Chair
Professor Teresa Head-Gordon
Professor Hartmut Häffner

Fall 2018

Development of a Single Particle Analyzer of Mass and Mobility

by

Andrew Gareth Elliott

Abstract

Development of a Single Particle Analyzer of Mass and Mobility

by

Andrew Gareth Elliott

Doctor of Philosophy in Chemistry

University of California, Berkeley

Professor Evan R. Williams, Chair

Mass spectrometry (MS) is an important analytical tool for obtaining information about the identity, structure and function of molecules over a wide range of sizes, from small molecules up to large protein complexes. Conventional MS techniques work by measuring the mass to charge ratio (m/z) of an ensemble of ions, then using the spacing between different m/z peaks to find the ion charge states so that the masses can be determined. This approach can be difficult to use for samples with a molecular mass beyond ~1 MDa or made up of a heterogeneous mixture of molecules with similar masses, which are typically detected as a single broad, unresolved m/z peak for which the charge cannot be obtained. These samples can instead be weighed with single ion MS, in which the m/z and charge of each ion is measured individually, so other ions do not interfere with the mass measurement. The work described in this dissertation is focused on developing a new instrument for single ion MS that uses charge detection mass spectrometry (CDMS) to better analyze samples that are difficult to measure with conventional MS. New instrumentation and data analysis techniques to improve the precision of CDMS mass measurements and use CDMS for new types of measurements are demonstrated. In CDMS, ions are detected by the charge they induce as they fly through a conducting tube. A new type of CDMS detector with four detector tubes inside an ion trap is used to increase the number of measurements of each ion and reduce the uncertainty in the m/z and charge by signal averaging. A method to measure the ion energy during the trapping time from the signal pattern the ion produces was also developed. This enables the energy and mass of the ion to be determined after collisions with the background gas and after fragmentation events, as in tandem MS. The energy lost to collisions can be used to obtain information about the collision rate and size of the ions, as in ion mobility spectrometry. Monitoring the ion energy also makes it possible to normalize charge measurements for the effect of energy, improving the precision of mass measurements in CDMS.

Table of Contents

Acknowledgements

There are many people I would like to thank for the role they played in supporting me through the work leading to this dissertation. First and foremost are my parents, Simon and Julie Elliott, who are a constant source of love, advice and encouragement. I am also grateful to my brothers, Michael and Peter, for always being there to talk about anything in the world (but mostly baseball). Their support has been essential for my happiness and wellbeing.

I would also like to thank all those who helped me inside the research lab. I thank my advisor, Professor Evan Williams, for all he taught me about mass spectrometry and instrumentation, and in even more basic terms about writing, presenting and conducting scientific research. My colleagues in the Williams group were also a crucial source of assistance both as collaborators and friends. I am grateful to Dr. Sam Merenbloom and Dr. Satrajit Chakrabarty for training and guiding me early in my graduate career, and Conner Harper and Howard Lin for their hard work and insights. This research is the result of a true joint effort with each of them. I also thank Dr. Matthew DiTucci for pushing me through each stage of graduate school; Dr. Terry Chang, Dr. Catherine Going, Dr. Anna Susa and Beryl Xia for all they did to make the lab a pleasant place to work; and Dr. Daniel Mortensen, Dr. Richard Cooper and Dr. Sven Heiles for all their discussions and suggestions about my research.

Chapter 1

Introduction

1.1 Overview

Mass spectrometry can provide information about the identity, structure and physical properties of molecules. The exact mass of a molecule can be used to obtain information about its molecular formula. Fragmenting that molecule and measuring the masses of the product ions can show the structure of the parent molecule. Similarly, peptides can be sequenced by measuring the difference in mass between a series of product ions formed by fragmenting the peptide.[1] With native mass spectrometry (MS), in which biomolecular ions are generated from solutions in which they have their native or native-like structure using electrospray ionization (ESI), mass measurements also provide a way to probe protein structure and function.[2-4] Importantly, ESI kinetically traps ions so that they retain a memory of their solution-phase structure into the gas phase, such that even weakly bound noncovalent complexes are preserved.[5-11] For individual proteins, native MS combined with dissociation methods can thus be used to measure post-translational modifications.[12-14] Moreover, native MS has become an increasingly popular analytical tool for investigating biological macromolecular complexes involving proteins, nucleotides, drugs and lipids,[15-20] providing information on stoichiometry,[21-23] complex assembly,[24, 25] binding affinities,[26] and complex topology.[27, 28] Notable achievements include analyzing the enzyme 4-oxalocrotonate tautomerase,[29] characterizing the structure of the 20S proteasome,[30, 31] and measuring lipid-stabilized membrane transport protein complexes.[32-34]

Although many different biologically important macromolecules and complexes can be analyzed with native MS, it has its limitations. Current MS techniques are inadequate for weighing ions that come from complex mixtures such as large synthetic polymers.[35-38] High mass ions beyond ~1 MDa can also be challenging to measure, with the upper mass limit dependent on how homogeneous the sample is.[39-41] Highly purified 18 MDa bacteriophage HK97 virus capsids were weighed with native MS, but more heterogeneous native viruses and polymers become difficult to weigh at lower masses.[39] This deficiency occurs because conventional MS techniques are based on measuring mass to charge ratios (m/z) for ensembles of ions. Determining the ion masses therefore depends on also determining what charge state they are in which can be challenging because protein ions generated with ESI typically have multiple charges. For simple analytes, the charge state can be obtained from the m/z spacing between ions with approximately the same mass in different charge states, or with different isotopic masses in the same charge state. Heterogeneity in the ion masses, intrinsic to the sample or caused by salt or solvent adduction during the ionization process, results in many ions having very similar m/z values, filling in the spacing between charge states. Without resolved charge states, only an approximate ion mass can be obtained by assuming the ion is spherical and the average m/z corresponds to a certain charge value. Other techniques that measure the size of a molecule, such as size exclusion

chromatography[42-44] or ultracentrifugation,[45] can also provide an approximate mass measurement, but without the precision possible using MS.

An alternative way to measure ions from heterogeneous samples is with single ion MS instead of ensemble *m*/*z* measurements.[46, 47] Measuring each ion alone removes the chemical noise of other ions with similar but slightly different *m*/*z* values so that they do not interfere with making an accurate measurement of the ion. Two important factors must be considered for making single ion measurements useful. First, both charge and *m*/*z* are required to measure the mass of each ion. And second, thousands of single ions must be measured to fully characterize a complex sample with high dynamic range, so the time required to analyze each ion matters. Measuring 1,000 ions takes over 16 hours at 1 ion per minute, but only ~1.7 min at 10 ions per second. Measuring many individual ions also creates an advantage for single ion MS in making it easier to identify minor components of the sample. Two species with very different masses can have similar *m*/*z* values and be confused in a conventional mass spectrum but are separated when mass is measured directly.

A wide range of single ion MS techniques have been previously demonstrated, with variable success in measuring ions with the speed and precision necessary to produce a high-quality mass spectrum in a reasonable timeframe. The work described in this dissertation was focused on the development of a new single ion charge detection mass spectrometer. Chapter 2 provides a detailed description of the current version of the instrument. Chapter 3 presents results from a previous instrument variation, with a modified detector and simpler ion optics. New data analysis methods to measure the ion energy in situ and use that to improve charge measurements are described in Chapters 4 through 6. These measurements also enable the first single ion tandem MS and ion mobility measurements.

1.2 Single Molecule Mass Spectrometry

The problems heterogeneity causes for conventional mass spectrometry methods can be solved by measuring the mass of each ion individually. To meet this need for single molecule mass measurements, a wide array of techniques has been developed, either using specialized detection systems or adapting conventional MS methods. One type of specialized detector is the micro- or nanoelectromechanical system (NEMS), which works by measuring changes in the resonant oscillation frequency of a 0.15-200 μm vibrating cantilever or beam caused by molecules adsorbing onto the resonator.[48] NEMS devices have the advantage that neutrals can be weighed as well as ions.[49] These devices have been used to measure analytes as small as atoms by using the distribution of frequency shifts between each time step to find the size and rate of adsorption on the resonator of an ensemble of analytes.[50-52] Single molecule mass measurements of human IgM antibody (~190 kDa)[53] and many different nanoparticles ranging in size from 5 nm (~760 kDa)[53] to 1 μm (~6 TDa)[54, 55] have been made with NEMS. However, single molecule mass measurements made with current NEMS technology are sensitive to parameters such as the stiffness of the resonator[56, 57] and the exact position at which the molecule adsorbs,[48, 58, 59] leading to a mass resolution ($m/\Delta m$) of ~5.[53] Detection methods used in other fields have also been adapted for single molecule mass measurements. Nanopores can be used to weigh peptides and small polymers by measuring the amount each molecule entering the pore decreases the current flowing through it.[60-

[63] Young et al. recently demonstrated the use of interferometric scattering microscopy for mass measurements of proteins weighing 53-803 kDa, achieving an average mass accuracy of 2%.[64]

More conventional mass spectrometers can also be used for single molecule mass spectrometry. However, taking an instrument that measures only *m*/*z* and simply reducing the ion current so only a single ion is detected at a time creates little added benefit. Measuring ion masses still requires charge information which can only be obtained if the many individual *m*/*z* measurements produce a distribution in which different charge states or isotopic masses are resolved, similar to in an instrument that measures many ions at the same time. Instead, to take full advantage of measuring each ion individually, it is important to measure the charge of the ion as well as its *m*/*z*, so that the mass of each ion can be determined without information from other ions. Combining charge and *m*/*z* measurement is essential for single ion mass spectrometry.

Across the variety of single ion MS methods that have been developed, there are two general approaches to measuring the ion charge. In one approach, the ion charge is obtained by measuring the *m*/*z* of the ion several times after changing the charge of the ion. With this method, each ion produces its own charge state distribution which can be deconvolved like a simple ESI mass spectrum. In the second approach, the charge is measured directly from the signal produced by the single ion. This method is useful for techniques where ions are detected using the current induced by the ion passing by or hitting a detector. Measuring the amplitude of that current provides a second dimension of measurement for each ion, separating ions by more than their *m*/*z*. In general, more accurate charge measurements can be made with the charge stepping method, but direct charge measurements are faster. Both of these charge measurement approaches have been used to adapt conventional mass spectrometry methods for single ion MS, as discussed in the following sections.

1.2.1 Quadrupole Ion Traps

One of the most widely used single ion MS techniques is based on the quadrupole ion trap (QIT). The QIT consists of a pair of hyperbolic end cap electrodes on either side of a hyperbolic ring electrode. Ions can be trapped when an oscillating potential driven at an audio- or radio-range frequency is applied to both end caps or, more typically, to the ring electrode. The amplitude and frequency of that driving potential, along with the potentials applied to other electrodes, determine what *m*/*z* values can be stably trapped and how the ions oscillate inside the trap. Measuring *m*/*z* in a QIT thus generally involves manipulating and observing the ion oscillation pattern. One method for measuring *m*/*z* uses an additional AC potential on the end caps along with the driving potential on the ring electrode.[65] When the oscillation frequency on the end caps is tuned to the secular frequency of the ion motion along the axis between the end caps, ions are excited to oscillate further from the center of the trap. This method is commonly used for ensemble measurements in a QIT, with more intense excitation conditions so ions can be detected after they are forced to exit the trap. With the QIT oriented so the end caps are on the top and bottom of the trap, the ion *m*/*z* can also be measured by tuning a DC potential applied to the end caps to balance gravity.[66] Another method to determine the ion *m*/*z* involves tuning the amplitude and frequency of the driving potential until the ion oscillation on that axis appears as a standing star-shaped waveform.[67] However, carefully tuning several potentials and observing each ion is a slow and inexact way to

measure *m*/*z*. To improve these speed and precision problems, Gerlich and coworkers developed a QIT method in which the secular frequencies are measured directly, rather than observed to change in response to the trap conditions.[68] In their instrument, the ion is measured using the light it scatters as it passes through the trap with the driving potential set a constant frequency and amplitude. The ion path does not need to follow a special trajectory to be measured, and so the various trap potentials do not need to be retuned for each *m*/*z* measurement.

Using these optical detection methods, the only way to determine ion charge in these instruments is with charge stepping. Neither the pattern of oscillation nor the intensity of the light scattering can be directly related to a certain charge value. Charge states have been changed using UV radiation, electron bombardment, and collisions with argon ions.[67-69] The direct charge measurement method can be used instead if ions are ejected from the trap, similarly to how QITs are used for ensemble measurements. Ions exiting the trap collide with a charge collecting plate and the charge is obtained from the current induced by the ion.[70-72] This method to measure the ion charge is much faster, but also has much higher uncertainty because electronic noise affects the charge measurement and each ion can only be measured once.

Single ion QIT devices are capable of very accurate mass measurements but are ultimately of only limited general use. Gerlich and coworkers have reported resolution on the order of 10^4 for a 10 s measurement and 10^5 for an hour-long measurement.[68] Determining charge via charge stepping then requires repeating those measurements multiple times. This slow measurement process makes QIT devices ill-suited for obtaining a mass spectrum of a heterogeneous sample for which many ions must be measured to gain meaningful statistics. Instead, they are more useful for studying the properties of an individual ion in depth, such as the mass loss of an individual quantum dot.[69] Detecting ions optically also limits the range of ion sizes that can be measured in a QIT because ions smaller than ~50 nm do not scatter sufficient light to detected. However, Anderson and coworkers have demonstrated fluorescent quantum dots as small as 5 nm can be detected.[69, 73, 74]

1.2.2 FT-ICR

Another type of conventional mass spectrometer that can be used for single ion MS is the Fourier transform-ion cyclotron resonance (FT-ICR) instrument. In FT-ICR, ions are measured based on their motion inside a Penning trap, which consists of two electrostatic end cap electrodes orthogonal to a magnetic field.[75] When an ion travels off the central axis of the magnetic field, the Lorentz force from the magnet pushes the ion perpendicular to their direction of motion, causing it to rotate around the central axis of the magnetic field. The frequency of the ion rotation is related to its mass, *m*, and charge, *q*, by:

$$\omega_c = \frac{qB}{m} \qquad \text{(eq. 1.1)}$$

where ω_c is the angular rotational or cyclotron frequency and *B* is the strength of the magnetic field.[76, 77] The ion cyclotron frequency is measured using the current the ion induces on a pair of detection plates on opposite sides of the axis of the trap. The induced current increases as the ion

rotates closer towards a plate and decreases as the ion travels away, resulting in a periodic waveform that can be analyzed with a Fourier transform. To initiate this detection process, a second pair of plates is used to apply an oscillating electric field inside the tap, exciting the ion away from the center of the trap when the frequency of the applied field matches the cyclotron frequency. The *m*/*z* resolution in an FT-ICR instrument depends on the *m*/*z*, acquisition time and strength of the magnetic field.[77] The resolution reported at an *m*/*z* of 195 for an instrument with a 21 T magnet is ~5.5×10^6 in a 6 s measurement and ~2.7×10^6 in a 3 s measurement. At *m*/*z* 1022, the resolution for a 6 s measurement decreases to 1×10^6.[78]

Either approach to measuring charge for single ion MS can be used with FT-ICR instruments. The induced current by which ions are detected provides a way to use the direct approach to measure the charge of the ion. However, the amplitude of the current depends not only on the ion charge, but also on the excitation radius of the ion as it cycles inside the cell.[77] This radial dependence for the current can lead to uncertainty in the charge measurement because ions can be excited to different positions in the cell depending on the amplitude of the excitation field and the mass and phase of the ion. Measuring the ion at multiple *m*/*z* values after charge stepping reactions is more straightforward in an FT-ICR instrument. This method is effective because the ion detection is nondestructive, and ions can be effectively trapped for extended periods of time in the magnetic field in an FT-ICR cell. Similarly to in the QIT, this method is powerful for accurate charge measurements but slow.

FT-ICR instruments were first used for single ion MS by Smith and coworkers to measure individual polyethylene glycol (PEG) ions from a sample with an average molecular weight of 5 MDa.[79] These first experiments used the charge stepping method to determine charge, observing spontaneous jumps in *m*/*z* caused by background gas collisions or adding crown ethers to the ion cell to abstract adducted sodium ions.[79, 80] They also used the charge stepping approach to measure the mass of bovine serum albumin (BSA) dimer ions using reactions with ammonia to manipulate the ion charge states.[81] To measure ions with the direct charge measurement approach, they developed a method to account for the position dependence of the induced current by measuring all ions at the same radius.[82] Each ion was repeatedly measured with a higher and higher excitation amplitude, and the final measurement before the ion was pushed into the plates of the cell was assigned to a radius of 95% of the maximum radius. For heavier ions that relax to the center of the cell slowly after each measurement, a lower excitation amplitude was used on repeated measurements and the maximum amplitude signal was assigned to the 95% radius.[83] This approach reduces the uncertainty in the charge measurement caused by the ion position, but at a cost of longer measurement times. This removes the primary advantage of the direct charge measurement over the charge stepping methods, making it a less useful technique.

1.2.3 Orbitrap

The Orbitrap mass analyzer is capable of somewhat lower resolution than an FT-ICR (typically 10^5 in a 0.76 s measurement) but has the advantage that it uses an electrostatic ion trap that does not require a large superconducting magnet. The Orbitrap is based on the Kingdon trap which consists of a central electrode set to an attractive potential coaxial with an outer reference electrode.[84] Ions traveling perpendicular to the axis of the trap orbit around the central electrode

based on the balance between their inertia and their attraction to the center of the trap. In the Orbitrap, the electrodes are specially shaped to produce a harmonic potential along the axis of the trap, with a spindle shaped central and barrel shaped outer electrode.[85] Ions injected away from the minimum of the potential along the trap axis then oscillate along that axis at a frequency that depends on the ion *m*/*z* while orbiting the central electrode. Ions are detected using the current they induce on the outer electrode, which is split at the middle of the trap so that the two ends can be differentially amplified to produce a periodic signal pattern well suited for FT analysis. Because ions are detected based on the image current they induce, the Orbitrap can be used for single ion MS using the direct charge measurement method. However, like in the FT-ICR instrument, the induced current in an Orbitrap depends on the radial position of the ion inside the trap along with the ion charge. Single ions of 20+ myoglobin and GroEL have been detected with the Orbitrap, and the amplitudes of the induced currents were used to separate events where one, two or three ions were trapped.[86, 87] However, the width of the induced current distribution for the myoglobin ions was large for the single charge state investigated, and the current was not directly calibrated to a charge value.[86] Carefully controlling how the ions are injected into the trap to ensure a consistent radius can mitigate the positional effects and make the induced current a more useful way to measure the ion charge.

1.2.4 Cryodetector-TOF

Time-of-flight (TOF) mass spectrometry is a simple and useful tool for measuring the *m*/*z* of high mass ions. In a TOF instrument, the ion *m*/*z* is determined based on its velocity measured from the time the ion takes to hit a detector after an initial electrostatic acceleration. After that push, the ion kinetic energy is directly proportional to the charge of the ion and the potential used to accelerate the ion. That kinetic energy then results in a certain ion velocity depending on the mass of the ion. The ion *m*/*z* is related to its velocity, *v*, by:

$$\frac{m}{z} = \frac{2eV}{v^2} \qquad \text{(eq. 1.2)}$$

where *e* is the charge of an electron and *V* is the potential used to push the ion. Two ions with the same charge are accelerated to the same kinetic energy, but the lower mass ion ends up with a higher velocity and hits the detector first. With no traps or oscillating electric fields, the *m*/*z* range of a TOF instrument is theoretically unlimited with only a longer arrival time needed to measure high *m*/*z* ions. However, the microchannel plates used as detectors in TOF instruments effectively limit that mass range because of their decreased sensitivity to high mass ions caused by low ion velocities and detector saturation by the lower *m*/*z* ions in the ion population.[88, 89] Those conventional detectors also make TOF difficult to use as a single ion MS technique because there needs to be a way to measure the ion charge. The charge stepping approach would be challenging to implement with the destructive ion detection methods typically used for TOF instruments. However, the direct charge detection approach can be used if the microchannel plates are replaced with an energy-sensitive detector.[90] The ion charge can then be determined from the energy because the ion energy imparted by electrostatic acceleration scales linearly with charge.

Two different energy-sensitive cryodetectors have been coupled with TOF instruments. Microcalorimeters operate by using a metal absorber maintained at approximately 1 K as the target for the ions and measure the temperature rise of the metal after the ion collides with it.[91-93] The metal heats up proportionally to the energy the ion deposits in the collision. Microcalorimeters are sensitive to ions as small as protons and can be used to detect neutrals as well as ions.[94-96] However, the millisecond timeframe required for the temperature increase to dissipate in the microcalorimeter can lead to overlapping peaks and an unstable baseline temperature when many ions hit the detector in quick succession.[91] A second, faster, form of cryodetector is the superconducting tunnel junction (STJ) detector in which the energy of an ion is detected by the current produced by the ion impact on a superconducting surface.[97-99] The collision energy breaks Cooper pairs in the detector surface, freeing electrons to flow to a second superconductor separated from the first by a thin insulator and held at a potential difference. The STJ detector has been used to measure IgG antibodies, ferritin, and nanoparticles, as well as the HK97 Prohead I at 17.7 MDa with up to 30 charges.[99-104] However, the ion energy measured with the cryodetector for large ions does not increase linearly with charge and smaller ions are observed to deposit a greater percentage of their kinetic energy on the detector surface than larger ions.[91, 93, 99, 100, 105] This deficit in the energy measured leads to uncertainty in determining the ion charge from the energy. The missing measured energy has been attributed to ion fragmentation and ejection of the product ions from the detector surface and to deformation of the surface.[91, 92] The cryodetector-TOF is thus most effective for single ion MS for small ions with few charges. For larger ions, the cryodetector primarily serves as a more sensitive detector for a more conventional TOF instrument.

1.3 Charge Detection Mass Spectrometry

1.3.1 Single Tube Charge Detection Mass Spectrometry

An alternative approach to single ion mass spectrometry is to use charge detection mass spectrometry (CDMS). In CDMS, ions are measured using the charge pulse they induce as they pass through a conductive detection tube (Figure 1.1a). The duration of the charge pulse is used to obtain the ion velocity, which can be used to determine the *m*/*z* of the ion if its kinetic energy is also known, as in equation 1.2. The amplitude of the charge pulse is directly proportional to the charge of the ion. CMDS is thus similar to the FT-ICR and Orbitrap techniques in which the charge is measured non-destructively from the signal induced by the ion. However, CDMS has the advantage that for sufficiently long detector tubes (length ~4x larger than the inner diameter), the charge pulse the ion induces is essentially equal to the charge of the ion and minimally affected by the exact radial position of the ion.[106] This property makes direct charge measurements in CDMS more robust than with an FT-ICR or Orbitrap, which means an ion can be weighed effectively on a single pass through the detection tube. This single tube CDMS mass measurement takes a significantly shorter time than other single ion MS techniques, on the order of ~10-100 microseconds depending on the ion energy and *m*/*z*, as opposed to several seconds for each measurement. This analysis speed makes CDMS a much more useful tool for analyzing heterogeneous samples for which many ions must be measured to fully characterize the sample.

CDMS also has the advantage that it uses a very simple detector, consisting of just a conductive tube and amplifiers, with no need for large magnets or radio frequency (RF) power supplies.

CDMS was first developed in 1960 by Shelton, Hendricks and Wuerker to measure the mass of micron-sized iron dust particles used to investigate the effects of hypervelocity impacts.[107] The particles were ionized by contact with a tungsten filament held at 20 kV and accelerated through a 100 kV potential to reach particle velocities of 1-3 km/s. Hendricks also used CMDS to investigate the size and charge of oil droplets from electrospray.[108, 109] One difficulty in these early experiments was that only ions with at least 10^4 charges could be detected, which limited the range of samples CDMS was useful for. CDMS instruments were also hampered by the time required to process each single ion, limiting the data collection rate to well below the maximum potential rate based on the ion velocity of thousands of ions per second. Keaton et al. and Stradling et al. reported refinements to the detection system that reduced the detection limit to ~1900 charges and enabled mass measurements for 100 ions per second.[110, 111]

In 1995, Fuerstenau and Benner reported the development of a new instrument that expanded the range of samples that could be measured with CDMS.[112] Improvements to the detector electronics including adding a differentiating and integrating shaping amplifier resulted in a lower noise level and detection limit of ~425 charges. The instrument also featured an ESI source, allowing biomolecules, polymers and nanoparticles to be transferred to the gas phase with sufficiently high charge to be analyzed by CDMS. With this instrument, Benner and coworkers measured the masses of several DNA plasmid weighing 1-7 MDa as well as Lambda Phage DNA weighing 31 MDa.[112-114] They also demonstrated the use of CDMS for weighing whole viruses, such as rice yellow mottle virus and tobacco mosaic virus, which are 6.6 and 40.5 MDa, respectively.[115] Jarrold and coworkers used single tube CDMS to investigate the charging of electrospray droplets, measuring negatively charged ions with positive electrospray.[116] More recently, a similar single tube CDMS instrument developed by Doussineau et al.[117] has been used to measure a wide range of nanoparticles, from ~100 MDa amphiphilic block copolymers to ~30 GDa composite nanoparticles.[118-122] Dugourd and coworkers have also reported single tube CDMS measurements of several different amyloid fibrils, using the charge and mass distributions to characterize their heterogeneity and polymorphism.[123, 124] Although these single tube CDMS instruments have the advantage of very short analysis times, they have the disadvantage of fairly high uncertainty in the charge measurement. For example, the noise level of ±75 charges reported by Fuerstenau and Benner results in 12.5% uncertainty in the typical charge measurement of ~600 *e* for 1.2 MDa DNA ions.[112] The ~425 *e* detection limit also still restricts the range of ions that can be measured with single tube CDMS. These simple single tube CDMS instruments can also have high energy uncertainty, with no means to select or measure the ion energy. Different size ions may leave the ion source with different initial velocities due to aerodynamic acceleration, which adds to the energy provided by ion optics guiding ions towards the detector.[112, 121, 125]

1.3.2 Array Detector CDMS

One way to reduce charge measurement uncertainty is to measure each ion multiple times and signal average each individual charge measurement. This approach to improving the charge uncertainty is only possible because CDMS is a nondestructive measurement technique. Assuming

fluctuations in the charge measurement are caused by random noise, averaging reduces the uncertainty by a factor of the square root of the number of measurements. A simple and efficient way to increase the number of measurements is by using an array of detector tubes aligned in a row so that the ion passes through each tube on its way through the detector (Figure 1.1b). As an example, using an array of four detector tubes theoretically improves the noise by a factor of two. With an array detector, the measurement time increases linearly with the number of tubes used in the detector. For a four-tube array, the measurement time is only somewhat longer than for a single tube detector, still on the order of tens of microseconds per ion, so the mass measurement throughput is minimally affected.

Array detector CDMS was first implemented by Gamero-Castaño in 2007 in an instrument which featured a detector consisting of 8 tubes.[126] The first and last tubes were grounded to shield the sensing tubes, and the remaining six were used to detect ions. To separate the signal from each pass through a tube from the signal from the tube before and after it, the tubes were wired into two detection circuits, one containing the first, third and fifth detector tubes and the other the second, fourth and sixth. The separate detection channels can also be used to implement a difference amplifier by subtracting one channel from the other, lowering the detection limit by a factor of $\sqrt{2}$ by increasing the time domain S/N. Using three pairs of tubes then reduces the uncertainty in the charge measurement by a factor of $\sqrt{3}$, for a total charge noise of ~100 *e*. Gamero-Castaño used this instrument to characterize electrospray droplets with 10^4 charges, finding smaller and less highly charged ions at the edges of the spray profile.[126] Austin and coworkers have also developed an array detector CDMS instrument in which the detection electrodes were on a printed circuit board.[127-129] This design can be used to simplify the construction of a long array of detectors by because many sensors can be printed on the same board, making tube alignment straightforward. One drawback, however, is that the induced signal pattern is more dependent on the ion trajectory than when using detector tubes. Detectors containing multiple tubes can also be used to improve the energy uncertainty by changing the ion energy between measurements. Jarrold and coworkers developed an instrument in which the ion was accelerated between measurements, and another in which the ion was measured at two different floating potentials.[130, 131] The change in the ion velocity or the delay between measurements can then be used to obtain the ion energy and *m*/*z* without the influence of the ion's initial energy from aerodynamic acceleration. The instrument with floating detectors also featured the longest reported CDMS array detector, containing 22 tubes, with which they achieved a charge uncertainty of ~10 *e* and a detection limit of ~100 *e*.[131] This detection limit improvement further widens the range of ions that can be measured with CDMS, but comes at the cost of a computationally expensive autocorrelation method to observe low charge ions in the time domain.

Although array detector CDMS can be appealingly simple, it is ultimately limited in the extent to which it improves the measurement uncertainty. The number of detector tubes in the instrument is the maximum number of times each ion can be remeasured. Improving the uncertainty from a single pass by a factor of two with four tubes is fairly simple, but a ten times improvement takes 100 tubes and a 100 times improvement takes 10,000 tubes, significantly increasing the complexity. Increasing the number of tubes on a detection channel increases the capacitance, which affects the noise on that channel. The detector can be divided into smaller detection circuits to mitigate this noise, increasing the number of amplifiers and other components

required. More detector tubes also simply take up more space, necessitating a larger vacuum chamber to hold the entire detector and fine control of the ion trajectory so it passes through each tube.

1.3.3 Trapping CDMS

A second method to measure an ion multiple times is to trap the ion and force it to recirculate repeatedly through the detector (Figure 1.1c). With an ion trap, the number of times an ion can be measured is limited only by the length of time the ion can be trapped rather than length of the detector. This makes it easier to achieve more improvement in the charge uncertainty without putting together an extensive array of detectors. However, the charge uncertainty improvement comes at the cost of lower mass measurement throughput due to the longer measurement time for each ion. Additionally, trapping events in which the ion is prematurely lost from the trap can lead to extra wasted time with no ion in the detector. Selecting the trapping conditions to achieve the desired charge uncertainty while minimizing the time the trap remains empty is important to minimize the effect on the mass measurement throughput.

Ion trap CDMS was first demonstrated by Benner with an ion trap formed by a pair of electrostatic ion mirrors on either side of a single detector tube shielded to create a field-free region.[132] The ion mirrors were similar to those used by Grix et al., Zajfman and coworkers and McLuckey and coworkers for measuring ensembles of small ions.[133-137] Using an electrostatic trap rather than an RF trap minimizes the current induced on the detector by the potentials keeping the ion trapped. The trap was operated by raising the potential of the front ion mirror upon sensing an ion signal in the detector tube above a certain trigger limit set above the noise level. With this method to operate the trap, the detection limit is the same as in a single pass instrument because the trap does not close for ions that cannot be detected on their first pass through the detector. However, the charge uncertainty decreased dramatically, as low as 2.3 *e* for a pBR322 plasmid DNA ion trapped for 450 passes in 10 ms.[132] Dugourd and coworkers used a similar CDMS ion trap to investigate infrared multiphoton dissociation of individual PEG and DNA ions.[138-142] The instrument also featured a single tube detector before the ion trap to enable mass selection for the photodissociation experiments.[138] Information about ion heating and fragmentation pathways was obtained by monitoring the charge of the ion over time in the trap. However, because the ion energy changes as the ion fragments, they were unable to measure how the ion mass changed during the experiments. More recently, Continetti and coworkers developed an instrument that included a CDMS ion trap used to measure the *m*/*z* and velocity of nanoparticle ions used to study surface impact phenomena.[143] They have implemented fast data analysis methods to measure each ion in real time while the ion is still trapped. That information is then used to determine the correct sequence of potentials on a linear accelerator after the ion trap to set the desired ion velocity for the impact experiments.

Chapter 2 describes in detail the current version of the ion trap CDMS instrument discussed in this dissertation. Ions are formed by nanoelectrospray ionization and pass through four stages of differential pumping to reach the detector and ion trap. Ions enter the vacuum chamber through a commercial electrospray source, then travel through a pair of RF only ion guides to a turning quadrupole used as an energy filter to select certain ion energies to enter the detector and trap. The

detector uses a single 28.2 mm long detector tube inside a cone trap, i.e. an electrostatic ion trap where the electrodes have conical bores. The detector electronics and the schemes used to operate the trap are also discussed in Chapter 2.

A previous ion trap CDMS instrument that combines the array and ion trap methods for measuring an ion multiple times is described in Chapter 3. The detector consists of four detection tubes inside a cone trap. This design increases the number of times an ion is measured on each pass through the trap to increase the efficiency of the ion trap CDMS detection method. Because ions take longer to turn around in the trapping electrode than to travel through a single detector tube, the ion is not being actively detected for most of the time in each trapping event. Adding extra tubes to the field-free region of the trap increases the proportion of the trapping time used for measuring the ion. The instrument was used to measure 8 MDa PEG as well as nominally 50 nm and 100 nm polystyrene nanoparticles. The distribution of PEG ion masses had a maximum from 7-9 MDa with a high mass tail likely caused by PEG aggregation as well as salt and solvent adduction. The size distributions obtained for the nanoparticles by converting the measured masses to the equivalent diameter of a spherical particle were centered at ~48 nm and ~70 nm for the 50 nm and 100 nm samples, respectively. A charge uncertainty of ~2 *e* was observed for PEG ions trapped for 100 ms. This charge uncertainty is lower than the 2.3 *e* and 6.8 *e* uncertainties reported by Benner and Dugourd and coworkers, respectively.[132, 138] The uncertainty in the ion energy was also ~3x lower than in other instruments without an energy filter (which was not in this version of the instrument) because the cone trap can be operated so that only a narrow range of ion energies is trapped. However, although ions trapped for extended times were measured effectively, the longer field free detector region also led to lower trapping rates and shorter average trapping times.

To improve the trapping rates and trapping times observed in the array detector ion trap, the detector was reduced to a single tube in a heavily modified version of the instrument, as described in Chapter 2. New data analysis methods and results from the improved instrument are discussed in Chapter 4. The maximum trapping time observed for a PEG ion increased to 4 s, after which the ion was lost because the trap was opened at the end of the preset acquisition time. During that extended trapping time, the ion was observed to decrease significantly in velocity while the time to turn in the trapping electrode also decreased. The ion also fragmented 6 times, with sudden decreases in charge and jumps in velocity. To measure how the ion changed over the course of the trapping time, a method to measure the ion energy using the signal pattern induced by the ion was developed. This method to obtain the ion energy was used for the first single ion tandem MS measurements, weighing each successive fragment ion. The ion energy also provided information about the relative ion mobilities of the precursor and final fragment, which decreased in energy at different rates.

1.3.4 Fourier Transform CDMS

Ions in trapping CDMS instruments induce a regular periodic signal pattern as they pass in and out of the detector tube or tubes while oscillating inside the ion trap. For an ion trap with a single tube, the pattern of charge pulses induced on the tube and detected when no shaping amplifier is used closely resembles a simple square wave pulse train. The waveform consists of a pulse while the ion is in the tube and no pulse when the ion is turning around in the trapping

electrode. This signal pattern is well suited for analysis with a Fourier transform. Contino and Jarrold first demonstrated using FT techniques to analyze CDMS data from a detector consisting of a single tube in a conetrap.[144] The ion oscillation frequency *f*, which is obtained with the FT, is proportional to the ion *m*/*z* as

$$\frac{m}{z} = \frac{C(E,V)}{f^2} \qquad \text{(eq. 1.3)}$$

where *C* is a proportionality factor that depends on the trap geometry, ion energy *E*, and trapping potential *V*. The ion charge was determined from the amplitude of the oscillation frequency in the FT. The charge uncertainty reported for this first FT-CDMS instrument was 3.2 *e* for BSA monomer and dimer ions with 30-104 charges trapped for up to ~25 ms,[144] which is worse than the 2.3 *e* uncertainty achieved by Benner.[132] However, an advantage of this FT-CDMS technique is that it is a fast and computationally straightforward way to measure ions with less charge than the time domain noise. Lowering the charge detection limit to ~30 *e* significantly increased the range of samples that can be analyzed with CDMS. To trap ions with so few charges, the ion trap must be operated in a different way from the triggered trapping scheme used previously. Instead of closing the trap upon sensing an ion signal, the trap is instead closed at regular intervals.[144] This random trapping scheme increases the likelihood that the trap is closed with no ions, wasting the measurement time, or multiple ions, which can interfere with the single ion detection.[145, 146] Therefore, care must be taken to optimize ion optics and ion current to obtain as much useable signal as possible.

Jarrold and coworkers have made several further developments to FT-CDMS techniques to improve the charge and *m*/*z* uncertainties. Cryogenically cooling the detector electronics lowered the detection limit to 13 *e* and lowered the charge uncertainty to 2.2 *e*.[147] Reducing the pressure in the detection region of the instrument enabled longer trapping times, decreasing the detection limit to 7 *e* and the uncertainty to 0.65 *e* for a ~400 ms measurement.[145] Further extending the trapping time to 3 s and developing new data analysis methods to measure charge from the amplitude of the fundamental frequency and second harmonic pushed the charge uncertainty to 0.196 *e*.[148] With this low charge uncertainty, quantizing the charge by rounding the charge obtained for ions within 0.2 *e* of an integer charge value and culling the remaining ions decreases the likelihood an ion is assigned to the wrong charge state to 1 in 15,000. Energy selection with a dual hemispherical deflection analyzer narrowed the range of ion energies allowed into the trap, decreasing the range of oscillation frequencies for ions with a certain *m*/*z* value.[144] A new electrostatic linear ion trap was developed to minimize the effect of the ion energy on the oscillation frequency, further increasing the *m*/*z* resolution.[149] With these instrumental improvements, Jarrold and coworkers have demonstrated the use of CDMS for a wide range of new samples. Reported applications include measuring the mass and assembly kinetics of several viruses up to 50 MDa,[150-157] characterizing cargo loading into virus capsids,[158] and quantifying several classes of lipoprotein particles important for assessing the risk of cardiovascular disease.[159]

During the long trapping times often used in FT-CDMS, the ion oscillation frequency can increase significantly due to energy loss caused by collisions with the background gas. Chapter 5 demonstrates a method to use that frequency change to measure the energy lost to collisions and

obtain single-ion ion mobilities for a series of small protein ions. This method is based on equation 1.3, which shows that the energy can be obtained from the oscillation frequency if the *m*/*z* is known. Here, individual ions are assigned to a certain *m*/*z* based on their charge as obtained from their place in a resolved charge state distribution of initial oscillation frequencies. The observed increase in the oscillation frequency could indicate the ion *m*/*z* changes, but the change is too gradual to be caused by any reasonable mass loss or charge gain. The energy loss obtained from the frequency increase correlates well with collision cross sections measured with more conventional ion mobility methods. Measuring ion mobilities simultaneously with mass indicates the power of CDMS for characterizing each ion in multiple dimensions.

Although energy loss during the trapping time can be useful for making ion mobility measurements, it also affects charge measurements made using FT-CDMS. Chapter 6 discusses those energy effects and presents a way to normalize for them to improve the accuracy and uncertainty of individual ion measurements. Jarrold and coworkers have previously used the sum of the fundamental and second harmonic frequency amplitudes to measure charge.[148] However, the amplitude of each harmonic depends on the pattern of the square wave pulse train signal as well as its amplitude. Because the signal pattern is defined by the ion energy, the proportionality between charge and the amplitude of each harmonic is only constant at a single energy. The FT of a model ion signal simulated at different frequencies and energies shows how the amplitudes are affected by energy and can be used to normalize for these energy affects. Applying this normalization to a PEG ion with 2496 charges that loses ~36 eV/charge decreases the charge uncertainty from 11% to 0.04% or 1.1 *e*. This normalization is essential for high charge ions and ions that lose significant amounts of energy during their trapping time.

1.4 References

(1) Loo, J. A.; Edmonds, C. G.; Smith, R. D. Tandem mass spectrometry of very large molecules: serum albumin sequence information from multiply charged ions formed by electrospray ionization. *Anal. Chem.* **1991**, *63*, 2488-2499.

(2) Leney, A. C.; Heck, A. J. R. Native Mass Spectrometry: What is in the Name? *J. Am. Soc. Mass Spectrom.* **2016**, *28*, 5-13.

(3) Lössl, P.; van de Waterbeemd, M.; Heck, A. J. The diverse and expanding role of mass spectrometry in structural and molecular biology. *EMBO J.* **2016**, *35*, 2634-2657.

(4) Mehmood, S.; Allison, T. M.; Robinson, C. V. Mass spectrometry of protein complexes: from origins to applications. *Annu. Rev. Phys. Chem.* **2015**, *66*, 453-474.

(5) Ganem, B.; Li, Y. T.; Henion, J. D. Detection of noncovalent receptor-ligand complexes by mass spectrometry. *J. Am. Chem. Soc.* **1991**, *113*, 6294-6296.

(6) Katta, V.; Chait, B. T. Observation of the heme-globin complex in native myoglobin by electrospray-ionization mass spectrometry. *J. Am. Chem. Soc.* **1991**, *113*, 8534-8535.

(7) Clemmer, D. E.; Hudgins, R. R.; Jarrold, M. F. Naked protein conformations: cytochrome c in the gas phase. *J. Am. Chem. Soc.* **1995**, *117*, 10141-10142.

(8) Myung, S.; Badman, E. R.; Lee, Y. J.; Clemmer, D. E. Structural transitions of electrosprayed ubiquitin ions stored in an ion trap over ~10 ms to 30 s. *J. Phys. Chem. A.* **2002**, *106*, 9976-9982.

(9) van den Heuvel, R. H. H.; Heck, A. J. Native protein mass spectrometry: from intact oligomers to functional machineries. *Curr. Opin. Chem. Biol.* **2004**, *8*, 519-526.

(10) Ruotolo, B. T.; Giles, K.; Campuzano, I.; Sandercock, A. M.; Bateman, R. H.; Robinson, C. V. Evidence for Macromolecular Protein Rings in the Absence of Bulk Water. *Science.* **2005**, *310*, 1658-1661.

(11) Voronina, L.; Rizzo, T. R. Spectroscopic studies of kinetically trapped conformations in the gas phase: the case of triply protonated bradykinin. *Phys. Chem. Chem. Phys.* **2015**, *17*, 25828-25836.

(12) Synowsky, S. A.; van den Heuvel, R. H. H.; Mohammed, S.; Pijnappel, W. P.; Heck, A. J. Probing genuine strong interactions and post-translational modifications in the heterogeneous yeast exosome protein complex. *Mol. Cell. Proteomics.* **2006**, *5*, 1581-1592.

(13) Ryan, C. M.; Souda, P.; Bassilian, S.; Ujwal, R.; Zhang, J.; Abramson, J.; Ping, P.; Durazo, A.; Bowie, J. U.; Hasan, S. Post-translational modifications of integral membrane proteins resolved by top-down Fourier-transform mass spectrometry with collisionally activated dissociation. *Mol. Cell. Proteomics.* **2010**,

(14) Catherman, A. D.; Skinner, O. S.; Kelleher, N. L. Top down proteomics: facts and perspectives. *Biochem. Biophys. Res. Commun.* **2014**, *445*, 683-693.

(15) Veenstra, T. D. Electrospray ionization mass spectrometry: a promising new technique in the study of protein/DNA noncovalent complexes. *Biochem. Biophys. Res. Commun.* **1999**, *257*, 1-5.

(16) Ruotolo, B. T.; Benesch, J. L. P.; Sandercock, A. M.; Hyung, S. J.; Robinson, C. V. Ion mobility-mass spectrometry analysis of large protein complexes. *Nat. Protoc.* **2008**, *3*, 1139-1152.

(17) Sharon, M. How far can we go with structural mass spectrometry of protein complexes? *J. Am. Soc. Mass Spectrom.* **2010**, *21*, 487-500.

(18) Schmidt, C.; Kramer, K.; Urlaub, H. Investigation of protein–RNA interactions by mass spectrometry—Techniques and applications. *J. Proteom.* **2012**, *75*, 3478-3494.

(19) Laganowsky, A.; Reading, E.; Allison, T. M.; Ulmschneider, M. B.; Degiacomi, M. T.; Baldwin, A. J.; Robinson, C. V. Membrane proteins bind lipids selectively to modulate their structure and function. *Nature.* **2014**, *510*, 172-175.

(20) Pedro, L.; Quinn, R. Native mass spectrometry in fragment-based drug discovery. *Molecules.* **2016**, *21*, 984.

(21) Loo, J. A. Electrospray Ionization Mass Spectrometry: a Technology for Studying Noncovalent Macromolecular Complexes. *Int. J. Mass Spectrom.* **2000**, *200*, 175-186.

(22) Heck, A. J. R.; van den Heuvel, R. H. H. Investigation of intact protein complexes by mass spectrometry. *Mass Spectrom. Rev.* **2004**, *23*, 368-389.

(23) Hernandez, H.; Robinson, C. V. Determining the Stoichiometry and Interactions of Macromolecular Assemblies from Mass Spectrometry. *Nat. Protoc.* **2007**, *2*, 715-726.

(24) Painter, A. J.; Jaya, N.; Basha, E.; Vierling, E.; Robinson, C. V.; Benesch, J. L. P. Real-time monitoring of protein complexes reveals their quaternary organization and dynamics. *Chem. Biol.* **2008**, *15*, 246-253.

(25) Kintzer, A. F.; Sterling, H. J.; Tang, I. I.; Abdul-Gader, A.; Miles, A. J.; Wallace, B. A.; Williams, E. R.; Krantz, B. A. Role of the protective antigen octamer in the molecular mechanism of anthrax lethal toxin stabilization in plasma. *J. Mol. Biol.* **2010**, *399*, 741-758.

(26) Rostom, A. A.; Tame, J. R.; Ladbury, J. E.; Robinson, C. V. Specificity and interactions of the protein OppA: partitioning solvent binding effects using mass spectrometry. *J. Mol. Biol.* **2000**, *296*, 269-279.

(27) Heck, A. J. R. Native mass spectrometry: a bridge between interactomics and structural biology. *Nat. Methods.* **2008**, *5*, 927-933.

(28) Sharon, M.; Robinson, C. V. The role of mass spectrometry in structure elucidation of dynamic protein complexes. *Annu. Rev. Biochem.* **2007**, *76*, 167-193.

(29) Fitzgerald, M. C.; Chernushevich, I.; Standing, K. G.; Whitman, C. P.; Kent, S. B. Probing the oligomeric structure of an enzyme by electrospray ionization time-of-flight mass spectrometry. *Proc. Natl. Acad. Sci. U.S.A.* **1996**, *93*, 6851-6856.

(30) Loo, J. A.; Berhane, B.; Kaddis, C. S.; Wooding, K. M.; Xie, Y.; Kaufman, S. L.; Chernushevich, I. V. Electrospray Ionization Mass Spectrometry and Ion Mobility Analysis of the 20S Proteasome Complex. *J. Am. Soc. Mass Spectrom.* **2005**, *16*, 998-1008.

(31) Sharon, M.; Taverner, T.; Ambroggio, X. I.; Deshaies, R. J.; Robinson, C. V. Structural Organization of the 19S Proteasome Lid: Insights from MS of Intact Complexes. *PLoS Biol.* **2006**, *4*, 1314-1323.

(32) Barrera, N. P.; Di Bartolo, N.; Booth, P. J.; Robinson, C. V. Micelles protect membrane complexes from solution to vacuum. *Science.* **2008**, *321*, 243-246.

(33) Hopper, J. T. S.; Yu, Y. T.; Li, D.; Raymond, A.; Bostock, M.; Liko, I.; Mikhailov, V.; Laganowsky, A.; Benesch, J. L. P.; Caffrey, M.; Nietlispach, D.; Robinson, C. V. Detergent-free mass spectrometry of membrane protein complexes. *Nat. Methods.* **2013**, *10*, 1206-1208.

(34) Susa, A.; Lippens, J.; Xia, Z.; Loo, J.; Campuzano, I.; Williams, E. Submicrometer Emitter ESI Tips for Native Mass Spectrometry of Membrane Proteins in Ionic and Nonionic Detergents. *J. Am. Soc. Mass Spectrom.* **2018**, *29*, 203-206.

(35) Nohmi, T.; Fenn, J. B. Electrospray mass spectrometry of poly(ethylene glycols) with molecular weights up to five million. *J. Am. Chem. Soc.* **1992**, *114*, 3241-3246.

(36) O'Connor, P. B.; McLafferty, F. W. Oligomer characterization of 4-23 kDa polymers by electrospray Fourier transform mass spectrometry. *J. Am. Chem. Soc.* **1995**, *117*, 12826-12831.

(37) Lennon, J. D.; Cole, S. P.; Glish, G. L. Ion/molecule reactions to chemically deconvolute the electrospray ionization mass spectra of synthetic polymers. *Anal. Chem.* **2006**, *78*, 8472-8476.

(38) Robb, D. B.; Brown, J. M.; Morris, M.; Blades, M. W. Method of Atmospheric Pressure Charge Stripping for Electrospray Ionization Mass Spectrometry and Its Application for the Analysis of Large Poly(Ethylene Glycol)s. *Anal. Chem.* **2014**, *86*, 9644-9652.

(39) Snijder, J.; Rose, R. J.; Veesler, D.; Johnson, J. E.; Heck, A. J. Studying 18 MDa virus assemblies with native mass spectrometry. *Angew. Chem., Int. Ed.* **2013**, *52*, 4020-4023.

(40) Lössl, P.; Snijder, J.; Heck, A. J. R. Boundaries of Mass Resolution in Native Mass Spectrometry. *J. Am. Soc. Mass Spectrom.* **2014**, *25*, 906-917.

(41) Weiss, V. U.; Bereszczazk, J. Z.; Havlik, M.; Kallinger, P.; Gösler, I.; Kumar, M.; Blaas, D.; Marchetti-Deschmann, M.; Heck, A. J. R.; Szymanski, W. W.; Allmaier, G. Analysis of a Common Cold Virus and Its Subviral Particles by Gas-Phase Electrophoretic Mobility Molecular Analysis and Native Mass Spectrometry. *Anal. Chem.* **2015**, *87*, 8709-8717.

(42) Lloyd, P.; Duddaby, K.; Varney, J.; Scrivener, E.; Derrick, P.; Haddleton, D. A comparison between matrix-assisted laser desorption/ionisation time-of-flight mass spectrometry and size exclusion chromatography in the mass characterisation of

synthetic polymers with narrow molecular-mass distributions: Poly(methyl methacrylate) and poly(styrene). *Eur. J. Mass Spectrom.* **1995**, *1*, 293-300.

(43) Hong, P.; Koza, S.; Bouvier, E. S. A review size-exclusion chromatography for the analysis of protein biotherapeutics and their aggregates. *J. Liq. Chromatogr. Rel. Technol.* **2012**, *35*, 2923-2950.

(44) Mori, S. and Barth, H. G. *Size Exclusion Chromatography*, ed.; Springer: Berlin; 1999.

(45) Lebowitz, J.; Lewis, M. S.; Schuck, P. Modern analytical ultracentrifugation in protein science: a tutorial review. *Protein Sci.* **2002**, *11*, 2067-2079.

(46) Chang, H. Ultrahigh-mass mass spectrometry of single biomolecules and bioparticles. *Annu. Rev. Anal. Chem.* **2009**, *2*, 169-185.

(47) Keifer, D. Z.; Jarrold, M. F. Single-molecule mass spectrometry. *Mass Spectrom. Rev.* **2017**, *36*, 715-733.

(48) Hanay, M. S.; Kelber, S. I.; O'Connell, C. D.; Mulvaney, P.; Sader, J. E.; Roukes, M. L. Inertial imaging with nanomechanical systems. *Nat. Nanotechnol.* **2015**, *10*, 339.

(49) Sage, E.; Brenac, A.; Alava, T.; Morel, R.; Dupré, C.; Hanay, M. S.; Roukes, M. L.; Duraffourg, L.; Masselon, C.; Hentz, S. Neutral particle mass spectrometry with nanomechanical systems. *Nat. Commun.* **2015**, *6*, 6482.

(50) Jensen, K.; Kim, K.; Zettl, A. An atomic-resolution nanomechanical mass sensor. *Nat. Nanotechnol.* **2008**, *3*, 533.

(51) Chiu, H.; Hung, P.; Postma, H. W. C.; Bockrath, M. Atomic-scale mass sensing using carbon nanotube resonators. *Nano Lett.* **2008**, *8*, 4342-4346.

(52) Chaste, J.; Eichler, A.; Moser, J.; Ceballos, G.; Rurali, R.; Bachtold, A. A nanomechanical mass sensor with yoctogram resolution. *Nat. Nanotechnol.* **2012**, *7*, 301.

(53) Hanay, M. S.; Kelber, S.; Naik, A. K.; Chi, D.; Hentz, S.; Bullard, E. C.; Colinet, E.; Duraffourg, L.; Roukes, M. L. Single-protein nanomechanical mass spectrometry in real time. *Nat. Nanotechnol.* **2012**, *7*, 602.

(54) Godin, M.; Bryan, A. K.; Burg, T. P.; Babcock, K.; Manalis, S. R. Measuring the mass, density, and size of particles and cells using a suspended microchannel resonator. *Appl. Phys. Lett.* **2007**, *91*, 123121.

(55) Naik, A. K.; Hanay, M. S.; Hiebert, W. K.; Feng, X. L.; Roukes, M. L. Towards single-molecule nanomechanical mass spectrometry. *Nat. Nanotechnol.* **2009**, *4*, 445.

(56) Gil-Santos, E.; Ramos, D.; Martínez, J.; Fernández-Regúlez, M.; García, R.; San Paulo, Á; Calleja, M.; Tamayo, J. Nanomechanical mass sensing and stiffness spectrometry based on two-dimensional vibrations of resonant nanowires. *Nat. Nanotechnol.* **2010**, *5*, 641.

(57) Ruz, J. J.; Tamayo, J.; Pini, V.; Kosaka, P. M.; Calleja, M. Physics of nanomechanical spectrometry of viruses. *Sci. Rep.* **2014**, *4*, 6051.

(58) Dohn, S.; Svendsen, W.; Boisen, A.; Hansen, O. Mass and position determination of attached particles on cantilever based mass sensors. *Rev. Sci. Instrum.* **2007**, *78*, 103303.

(59) Sader, J. E.; Hanay, M. S.; Neumann, A. P.; Roukes, M. L. Mass spectrometry using nanomechanical systems: beyond the point-mass approximation. *Nano Lett.* **2018**, *18*, 1608-1614.

(60) Robertson, J. W. F.; Rodrigues, C. G.; Stanford, V. M.; Rubinson, K. A.; Krasilnikov, O. V.; Kasianowicz, J. J. Single-molecule mass spectrometry in solution using a solitary nanopore. *PNAS.* **2007**, *104*, 8207-8211.

(61) Baaken, G.; Ankri, N.; Schuler, A.; Rühe, J.; Behrends, J. C. Nanopore-Based Single-Molecule Mass Spectrometry on a Lipid Membrane Microarray. *ACS Nano.* **2011**, *5*, 8080-8088.

(62) Angevine, C. E.; Chavis, A. E.; Kothalawala, N.; Dass, A.; Reiner, J. E. Enhanced Single Molecule Mass Spectrometry via Charged Metallic Clusters. *Anal. Chem.* **2014**, *86*, 11077-11085.

(63) Robertson, J. W. F.; Reiner, J. E. The Utility of Nanopore Technology for Protein and Peptide Sensing. *Proteomics.* **2018**, *18*, 1800026.

(64) Young, G.; Hundt, N.; Cole, D.; Fineberg, A.; Andrecka, J.; Tyler, A.; Olerinyova, A.; Ansari, A.; Marklund, E. G.; Collier, M. P. Quantitative mass imaging of single biological macromolecules. *Science.* **2018**, *360*, 423-427.

(65) Wuerker, R. F.; Shelton, H.; Langmuir, R. V. Electrodynamic containment of charged particles. *J. Appl. Phys.* **1959**, *30*, 342-349.

(66) Philip, M. A.; Gelbard, F.; Arnold, S. An absolute method for aerosol particle mass and charge measurement. *J. Colloid Interface Sci.* **1983**, *91*, 507-515.

(67) Hars, G.; Tass, Z. Application of quadrupole ion trap for the accurate mass determination of submicron size charged particles. *J. Appl. Phys.* **1995**, *77*, 4245-4250.

(68) Schlemmer, S.; Illemann, J.; Wellert, S.; Gerlich, D. Nondestructive high-resolution and absolute mass determination of single charged particles in a three-dimensional quadrupole trap. *J. Appl. Phys.* **2001**, *90*, 5410-5418.

(69) Bell, D. M.; Howder, C. R.; Johnson, R. C.; Anderson, S. L. Single CdSe/ZnS nanocrystals in an ion trap: Charge and mass determination and photophysics evolution with changing mass, charge, and temperature. *ACS Nano.* **2014**, *8*, 2387-2398.

(70) Peng, W.; Lin, H.; Lin, H.; Chu, M.; Yu, A. L.; Chang, H.; Chen, C. Charge-Monitoring Laser-Induced Acoustic Desorption Mass Spectrometry for Cell and Microparticle Mass Distribution Measurement. *Angew. Chem., Int. Ed.* **2007**, *46*, 3865-3869.

(71) Nie, Z.; Cui, F.; Tzeng, Y.; Chang, H.; Chu, M.; Lin, H.; Chen, C.; Lin, H.; Yu, A. L. High-speed mass analysis of whole erythrocytes by charge-detection quadrupole ion trap mass spectrometry. *Anal. Chem.* **2007**, *79*, 7401-7407.

(72) Nie, Z.; Cui, F.; Chu, M.; Chen, C.; Chang, H.; Cai, Y. Calibration of a frequency-scan quadrupole ion trap mass spectrometer for microparticle mass analysis. *Int. J. Mass Spectrom.* **2008**, *270*, 8-15.

(73) Howder, C. R.; Bell, D. M.; Anderson, S. L. Optically detected, single nanoparticle mass spectrometer with pre-filtered electrospray nanoparticle source. *Rev. Sci. Instrum.* **2014**, *85*, 014104.

(74) Howder, C. R.; Long, B. A.; Bell, D. M.; Anderson, S. L. Thermally brightened CdSe/ZnS quantum dots as noncontact probes for surface chemistry studies of dark nanoparticles trapped in the gas phase. *J. Phys. Chem. C.* **2015**, *119*, 14561-14570.

(75) Brown, L. S.; Gabrielse, G. Geonium theory: Physics of a single electron or ion in a Penning trap. *Rev. Mod. Phys.* **1986**, *58*, 233.

(76) Comisarow, M. B.; Marshall, A. G. Fourier transform ion cyclotron resonance spectroscopy. *Chem. Phys. Lett.* **1974**, *25*, 282-283.

(77) Marshall, A. G.; Hendrickson, C. L.; Jackson, G. S. Fourier Transform Ion Cyclotron Resonance Mass Spectrometry: A Primer. *Mass Spectrom. Rev.* **1998**, *17*, 1-35.

(78) Shaw, J.; Lin, T.; Leach III, F.; Tolmachev, A.; Tolić, N.; Robinson, E.; Koppenaal, D.; Paša-Tolić, L. 21 Tesla Fourier Transform Ion Cyclotron Resonance Mass Spectrometer Greatly Expands Mass Spectrometry Toolbox. *J. Am. Soc. Mass Spectrom.* **2016**, *27*, 1929-1936.

(79) Smith, R. D.; Cheng, X.; Brace, J. E.; Hofstadler, S. A.; Anderson, G. A. Trapping, detection and reaction of very large single molecular ions by mass spectrometry. *Nature.* **1994**, *369*, 137-139.

(80) Bruce, J. E.; Cheng, X.; Bakhtiar, R.; Wu, Q.; Hofstadler, S. A.; Anderson, G. A.; Smith, R. D. Trapping, detection, and mass measurement of individual ions in a Fourier transform ion cyclotron resonance mass spectrometer. *J. Am. Chem. Soc.* **1994**, *116*, 7839-7847.

(81) Cheng, X.; Bakhtiar, R.; Van Orden, S.; Smith, R. D. Charge-state shifting of individual multiply-charged ions of bovine albumin dimer and molecular weight determination using an individual-ion approach. *Anal. Chem.* **1994**, *66*, 2084-2087.

(82) Chen, R.; Wu, Q.; Mitchell, D. W.; Hofstadler, S. A.; Rockwood, A. L.; Smith, R. D. Direct charge number and molecular weight determination of large individual ions by electrospray ionization Fourier transform ion cyclotron resonance mass spectrometry. *Anal. Chem.* **1994**, *66*, 3964-3969.

(83) Chen, R.; Cheng, X.; Mitchell, D. W.; Hofstadler, S. A.; Wu, Q.; Rockwood, A. L.; Sherman, M. G.; Smith, R. D. Trapping, detection, and mass determination of coliphage T4 DNA ions by electrospray ionization Fourier transform ion cyclotron resonance mass spectrometry. *Anal. Chem.* **1995**, *67*, 1159-1163.

(84) Kingdon, K. H. A Method for the Neutralization of Electron Space Charge by Positive Ionization at Very Low Gas Pressures. *Phys. Rev.* **1923**, *21*, 408-418.

(85) Makarov, A. Electrostatic Axially Harmonic Orbital Trapping: A High-Performance Technique of Mass Analysis. *Anal. Chem.* **2000**, *72*, 1156-1162.

(86) Makarov, A.; Denisov, E. Dynamics of ions of intact proteins in the Orbitrap mass analyzer. *J. Am. Soc. Mass Spectrom.* **2009**, *20*, 1486-1495.

(87) Rose, R. J.; Damoc, E.; Denisov, E.; Makarov, A.; Heck, A. J. High-sensitivity Orbitrap mass analysis of intact macromolecular assemblies. *Nat. Methods.* **2012**, *9*, 1084-1086.

(88) Fraser, G. W. The ion detection efficiency of microchannel plates (MCPs). *Int. J. Mass Spectrom.* **2002**, *215*, 13-30.

(89) Chen, X. Y.; Westphall, M. S.; Smith, L. M. Mass spectrometric analysis of DNA mixtures: Instrumental effects responsible for decreased sensitivity with increasing mass. *Anal. Chem.* **2003**, *75*, 5944-5952.

(90) Twerenbold, D. Biopolymer mass spectrometer with cryogenic particle detectors. *Nucl. Instrum. Methods Phys. Res.* **1996**, *370*, 253-255.

(91) Hilton, G. C.; Martinis, J. M.; Wollman, D. A.; Irwin, K. D.; Dulcie, L. L.; Gerber, D.; Gillevet, P. M.; Twerenbold, D. Impact energy measurement in time-of-flight mass spectrometry with cryogenic microcalorimeters. *Nature.* **1998**, *391*, 672.

(92) Frank, M.; Labov, S. E.; Westmacott, G.; Benner, W. H. Energy-sensitive cryogenic detectors for high-mass biomolecule mass spectrometry. *Mass Spectrom. Rev.* **1999**, *18*, 155-186.

(93) Rabin, M. W.; Hilton, G. C.; Martinis, J. M. Application of microcalorimeter energy measurement to biopolymer mass spectrometry. *IEEE Trans. Appl. Supercond.* **2001**, *11*, 242-247.

(94) Ohkubo, M.; Shigeri, Y.; Kinumi, T.; Saito, N.; Ukibe, M.; Chen, Y. E.; Kushino, A.; Kurokawa, A.; Sato, H.; Ichimura, S. Fragmentation analysis by superconducting ion detectors in matrix-assisted laser desorption/ionization (MALDI). *Nucl. Instrum. Methods Phys. Res.* **2006**, *559*, 779-781.

(95) Ohkubo, M.; Shiki, S.; Ukibe, M.; Tomita, S.; Hayakawa, S. Direct mass analysis of neutral molecules by superconductivity. *Int. J. Mass Spectrom.* **2011**, *299*, 94-101.

(96) Novotný, O.; Allgeier, S.; Enss, C.; Fleischmann, A.; Gamer, L.; Hengstler, D.; Kempf, S.; Krantz, C.; Pabinger, A.; Pies, C. Cryogenic micro-calorimeters for mass spectrometric identification of neutral molecules and molecular fragments. *J.Appl.Phys.* **2015**, *118*, 104503.

(97) Twerenbold, D.; Vuilleumier, J.; Gerber, D.; Tadsen, A.; van den Brandt, B.; Gillevet, P. M. Detection of single macromolecules using a cryogenic particle detector coupled to a biopolymer mass spectrometer. *Appl. Phys. Lett.* **1996**, *68*, 3503-3505.

(98) Frank, M.; Mears, C. A.; Labov, S. E.; Benner, W. H.; Horn, D.; Jaklevic, J. M.; Barfknecht, A. T. High-efficiency detection of 66 000 Da protein molecules using a cryogenic detector in a matrix-assisted laser desorption/ionization time-of-flight mass spectrometer. *Rapid Commun. Mass Spectrom.* **1996**, *10*, 1946-1950.

(99) Wenzel, R. J.; Matter, U.; Schultheis, L.; Zenobi, R. Analysis of megadalton ions using cryodetection MALDI time-of-flight mass spectrometry. *Anal. Chem.* **2005**, *77*, 4329-4337.

(100) Aksenov, A. A.; Bier, M. E. The analysis of polystyrene and polystyrene aggregates into the mega dalton mass range by cryodetection MALDI TOF MS. *J. Am. Soc. Mass Spectrom.* **2008**, *19*, 219-230.

(101) Ozdemir, A.; Aksenov, A. A.; Firek, B. A.; Hendrix, R. W.; Bier, M. E. In Proceeding of the 55th ASMS Conference on Mass Spectrometry and Allied Topics, Indianapolis, IN, Junes 3-7, 2007.

(102) Sipe, D. M.; Ozdemir, A.; Firek, B. A.; Hendrix, R. W.; Bier, M. E. In Proceeding of the 56th ASMS Conference on Mass Spectrometry and Allied Topics, Denver, CO, June 1-5, 2008.

(103) Plath, L. D.; Ozdemir, A.; Aksenov, A. A.; Bier, M. E. Determination of Iron Content and Dispersity of Intact Ferritin by Superconducting Tunnel Junction Cryodetection Mass Spectrometry. *Anal. Chem.* **2015**, *87*, 8985-8993.

(104) Sipe, D. M.; Plath, L. D.; Aksenov, A. A.; Feldman, J. S.; Bier, M. E. Characterization of Mega-Dalton-Sized Nanoparticles by Superconducting Tunnel Junction Cryodetection Mass Spectrometry. *ACS Nano.* **2018**, *12*, 2591-2602.

(105) Rabin, M. W.; Hilton, G. C.; Martinis, J. M. Application of ion-impact energy measurement to electrospray ionization mass spectrometry of proteins and protein mixtures. *J. Am. Soc. Mass Spectrom.* **2001**, *12*, 826-831.

(106) Weinheimer, A. J. The charge induced on a conducting cylinder by a point charge and its application to the measurement of charge on precipitation. *J. Atmos. Ocean. Technol.* **1988**, *5*, 298-304.

(107) Shelton, H.; Hendricks, C. D.; Wuerker, R. F. Electrostatic Acceleration of Microparticles to Hypervelocities. *J. Appl. Phys.* **1960**, *31*, 1243-1246.

(108) Hendricks Jr., C. D. Charged droplet experiments. *J. Colloid Sci.* **1962**, *17*, 249-259.

(109) Hendricks, C. D.; Hogan, J. Investigation of the charge-to-mass ratio of electrically sprayed liquid particles. *AIAA J.* **1965**, *3*, 296-301.

(110) Keaton, P. W.; Idzorek, G. C.; Rowton Sr., L. J.; Seagrave, J. D.; Stradling, G. L.; Bergeson, S. D.; Collopy, M. T.; Curling Jr., H. L.; McColl, D. B.; Smith, J. D. A hypervelocity - microparticle - impacts laboratory with 100-km/s projectiles. *Int. J. Impact Eng.* **1990**, *10*, 295-308.

(111) Stradling, G. L.; Idzorek, G. C.; Shafer, B. P.; Curling Jr., H. L.; Collopy, M. T.; Blossom, A. A. H.; Fuerstenau, S. Ultra-high velocity impacts: cratering studies of microscopic impacts from 3 km/s to 30 km/s. *Int. J. Impact Eng.* **1993**, *14*, 719-727.

(112) Fuerstenau, S. D.; Benner, W. H. Molecular Weight Determination of Megadalton DNA Electrospray Ions Using Charge Detection Time-of-Flight Mass Spectrometry. *Rapid Commun. Mass Spectrom.* **1995**, *9*, 1528-1538.

(113) Schultz, J. C.; Hack, C. A.; Benner, W. H. Mass Determination of Megadalton-DNA Electrospray Ions Using Charge Detection Mass Spectrometry. *J. Am. Soc. Mass Spectrom.* **1998**, *9*, 305-313.

(114) Schultz, J. C.; Hack, C. A.; Benner, W. H. Polymerase chain reaction products analyzed by charge detection mass spectrometry. *Rapid Commun. Mass Spectrom.* **1999**, *13*, 15-20.

(115) Fuerstenau, S. D.; Benner, W. H.; Thomas, J. J.; Brugidou, C.; Bothner, B.; Siuzdak, G. Mass spectrometry of an intact virus. *Angew. Chem., Int. Ed.* **2001**, *40*, 542-544.

(116) Maze, J. T.; Jones, T. C.; Jarrold, M. F. Negative Droplets from Positive Electrospray. *J. Phys. Chem. A.* **2006**, *110*, 12607-12612.

(117) Doussineau, T.; Kerleroux, M.; Dagany, X.; Clavier, C.; Barbaire, M.; Maurelli, J.; Antoine, R.; Dugourd, P. Charging megadalton poly(ethylene oxide)s by electrospray ionization. A charge detection mass spectrometry study. *Rapid Commun. Mass Spectrom.* **2011**, *25*, 617-623.

(118) Doussineau, T.; Bao, C. Y.; Antoine, R.; Dugourd, P.; Zhang, W.; D'Agosto, F.; Charleux, B. Direct Molar Mass Determination of Self-Assembled Amphiphilic Block Copolymer Nanoobjects Using Electrospray-Charge Detection Mass Spectrometry. *ACS Macro Lett.* **2012**, *1*, 414-417.

(119) Doussineau, T.; Santacreu, M.; Antoine, R.; Dugourd, P.; Zhang, W.; Chaduc, I.; Lansalot, M.; D'Agosto, F.; Charleux, B. The charging of micellar nanoparticles in electrospray ionization. *ChemPhysChem.* **2013**, *14*, 603-609.

(120) Ouadah, N.; Doussineau, T.; Hamada, T.; Dugourd, P.; Bordes, C.; Antoine, R. Correlation between the charge of polymer particles in solution and in the gas phase investigated by zeta-potential measurements and electrospray ionization mass spectrometry. *Langmuir.* **2013**, *29*, 14074-14081.

(121) Doussineau, T.; Désert, A.; Lambert, O.; Taveau, J.; Lansalot, M.; Dugourd, P.; Bourgeat-Lami, E.; Ravaine, S.; Duguet, E.; Antoine, R. Charge Detection Mass Spectrometry for the Characterization of Mass and Surface Area of Composite Nanoparticles. *J. Phys. Chem. C.* **2015**, *119*, 10844-10849.

(122) Viodé, A.; Dagany, X.; Kerleroux, M.; Dugourd, P.; Doussineau, T.; Charles, L.; Antoine, R. Coupling of size-exclusion chromatography with electrospray ionization charge-detection mass spectrometry for the characterization of synthetic polymers of ultra-high molar mass. *Rapid Commun. Mass Spectrom.* **2016**, *30*, 132-136.

(123) Doussineau, T.; Mathevon, C.; Altamura, L.; Vendrely, C.; Dugourd, P.; Forge, V.; Antoine, R. Mass determination of entire amyloid fibrils by using mass spectrometry. *Angew. Chem., Int. Ed.* **2016**, *55*, 2340-2344.

(124) Pansieri, J.; Halim, M. A.; Vendrely, C.; Dumoulin, M.; Legrand, F.; Sallanon, M. M.; Chierici, S.; Denti, S.; Dagany, X.; Dugourd, P.; Marquette, C.; Antoine, R.; Forge, V. Mass and charge distributions of amyloid fibers involved in neurodegenerative diseases: mapping heterogeneity and polymorphism. *Chem. Sci.* **2018**, *9*, 2791-2796.

(125) Elliott, A. G.; Merenbloom, S. I.; Chakrabarty, S.; Williams, E. R. Single Particle Analyzer of Mass: A Charge Detection Mass Spectrometer with a Multi-Detector Electrostatic Ion Trap. *Int. J. Mass Spectrom.* **2017**, *414*, 45-55.

(126) Gamero-Castaño, M. Induction charge detector with multiple sensing stages. *Rev. Sci. Instrum.* **2007**, *78*, 043301.

(127) Barney, B. L.; Daly, R. T.; Austin, D. E. A multi-stage image charge detector made from printed circuit boards. *Rev. Sci. Instrum.* **2013**, *84*, 114101.

(128) Barney, B. L.; Pratt, S. N.; Austin, D. E. Survivability of bare, individual Bacillus subtilis spores to high-velocity surface impact: Implications for microbial transfer through space. *Planet. Space Sci.* **2016**, *125*, 20-26.

(129) Barney, B.; Austin, D. Dynamics of rebounding Bacillus subtilis spores determined using image-charge detection. *J. Biol. Phys.* **2017**, *43*, 481-492.

(130) Mabbett, S. R.; Zilch, L. W.; Maze, J. T.; Smith, J. W.; Jarrold, M. F. Pulsed Acceleration Charge Detection Mass Spectrometry: Application to Weighing Electrosprayed Droplets. *Anal. Chem.* **2007**, *79*, 8431-8439.

(131) Smith, J. W.; Siegel, E. E.; Maze, J. T.; Jarrold, M. F. Image Charge Detection Mass Spectrometry: Pushing the Envelope with Sensitivity and Accuracy. *Anal. Chem.* **2011**, *83*, 950-956.

(132) Benner, W. H. A Gated Electrostatic Ion Trap To Repetitiously Measure the Charge and m/z of Large Electrospray Ions. *Anal. Chem.* **1997**, *69*, 4162-4168.

(133) Grix, R.; Kutscher, R.; Li, G.; Grüner, U.; Wollnik, H.; Matsuda, H. A time-of-flight mass analyzer with high resolving power. *Rapid Commun. Mass Spectrom.* **1988**, *2*, 83-85.

(134) Zajfman, D.; Heber, O.; Vejby-Christensen, L.; Ben-Itzhak, I.; Rappaport, M.; Fishman, R.; Dahan, M. Electrostatic bottle for long-time storage of fast ion beams. *Phys. Rev. A.* **1997**, *55*, R1580.

(135) Ring, S.; Pedersen, H. B.; Heber, O.; Rappaport, M. L.; Witte, P. D.; Bhushan, K. G.; Altstein, N.; Rudich, Y.; Sagi, I.; Zajfman, D. Fourier transform time-of flight mass spectrometry in an electrostatic ion beam trap. *Anal. Chem.* **2000**, *72*, 4041-4046.

(136) Zajfman, D.; Rudich, Y.; Sagi, I.; Strasser, D.; Savin, D. W.; Goldberg, S.; Rappaport, M.; Heber, O. High resolution mass spectrometry using a linear electrostatic ion beam trap. *Int. J. Mass Spectrom.* **2003**, *229*, 55-60.

(137) Hilger, R. T.; Santini, R. E.; McLuckey, S. A. Nondestructive Tandem Mass Spectrometry Using a Linear Quadrupole Ion Trap Coupled to a Linear Electrostatic Ion Trap. *Anal. Chem.* **2013**, *85*, 5226-5232.

(138) Doussineau, T.; Yu Bao, C.; Clavier, C.; Dagany, X.; Kerleroux, M.; Antoine, R.; Dugourd, P. Infrared multiphoton dissociation tandem charge detection-mass spectrometry of single megadalton electrosprayed ions. *Rev. Sci. Instrum.* **2011**, *82*, 084104.

(139) Doussineau, T.; Antoine, R.; Santacreu, M.; Dugourd, P. Pushing the Limit of Infrared Multiphoton Dissociation to Megadalton-Size DNA Ions. *J. Phys. Chem. Lett.* **2012**, *3*, 2141-2145.

(140) Antoine, R.; Doussineau, T.; Dugourd, P.; Calvo, F. Multiphoton dissociation of macromolecular ions at the single-molecule level. *Phys. Rev. A.* **2013**, *87*, 013435.

(141) Doussineau, T.; Paletto, P.; Dugourd, P.; Antoine, R. Multiphoton dissociation of electrosprayed megadalton-sized DNA ions in a charge-detection mass spectrometer. *J. Am. Soc. Mass Spectrom.* **2015**, *26*, 7-13.

(142) Halim, M. A.; Clavier, C.; Dagany, X.; Kerleroux, M.; Dugourd, P.; Dunbar, R. C.; Antoine, R. Infrared laser dissociation of single megadalton polymer ions in a gated electrostatic ion trap: the added value of statistical analysis of individual events. *Phys. Chem. Chem. Phys.* **2018**, *20*, 11959-11966.

(143) Adamson, B. D.; Miller, M. E. C.; Continetti, R. E. The aerosol impact spectrometer: a versatile platform for studying the velocity dependence of nanoparticle-surface impact phenomena. *EPJ Tech. Instrum.* **2017**, *4*, 2.

(144) Contino, N. C.; Jarrold, M. F. Charge detection mass spectrometry for single ions with a limit of detection of 30 charges. *Int. J. Mass Spectrom.* **2013**, *345-347*, 153-159.

(145) Pierson, E. E.; Contino, N. C.; Keifer, D. Z.; Jarrold, M. F. Charge Detection Mass Spectrometry for Single Ions with an Uncertainty in the Charge Measurement of 0.65 e. *J. Am. Soc. Mass Spectrom.* **2015**, *26*, 1213-1220.

(146) Keifer, D. Z.; Pierson, E. E.; Jarrold, M. F. Charge detection mass spectrometry: weighing heavier things. *Analyst.* **2017**, *142*, 1654-1671.

(147) Contino, N. C.; Pierson, E. E.; Keifer, D. Z.; Jarrold, M. F. Charge Detection Mass Spectrometry with Resolved Charge States. *J. Am. Soc. Mass Spectrom.* **2013**, *24*, 101-108.

(148) Keifer, D. Z.; Shinholt, D. L.; Jarrold, M. F. Charge Detection Mass Spectrometry with Almost Perfect Charge Accuracy. *Anal. Chem.* **2015**, *87*, 10330-10337.

(149) Hogan, J. A.; Jarrold, M. F. Optimized Electrostatic Linear Ion Trap for Charge Detection Mass Spectrometry. *J. Am. Soc. Mass Spectrom.* **2018**, *29*, 2086-2095.

(150) Keifer, D. Z.; Motwani, T.; Teschke, C. M.; Jarrold, M. F. Acquiring Structural Information on Virus Particles with Charge Detection Mass Spectrometry. *J. Am. Soc. Mass Spectrom.* **2016**, *27*, 1028-1036.

(151) Pierson, E. E.; Keifer, D. Z.; Kukreja, A. A.; Wang, J. C.; Zlotnick, A.; Jarrold, M. F. Charge Detection Mass Spectrometry Identifies Preferred Non-Icosahedral Polymorphs

in the Self-Assembly of Woodchuck Hepatitis Virus Capsids. *J. Mol. Biol.* **2016**, *428*, 292-300.

(152) Keifer, D. Z.; Pierson, E. E.; Hogan, J. A.; Bedwell, G. J.; Prevelige, P. E.; Jarrold, M. F. Charge detection mass spectrometry of bacteriophage P22 procapsid distributions above 20 MDa. *Rapid Commun. Mass Spectrom.* **2014**, *28*, 483-488.

(153) Pierson, E. E.; Keifer, D. Z.; Selzer, L.; Lee, L. S.; Contino, N. C.; Wang, J. C. -.; Zlotnick, A.; Jarrold, M. F. Detection of Late Intermediates in Virus Capsid Assembly by Charge Detection Mass Spectrometry. *J. Am. Chem. Soc.* **2014**, *136*, 3536-3541.

(154) Lutomski, C. A.; Lyktey, N. A.; Zhao, Z.; Pierson, E. E.; Zlotnick, A.; Jarrold, M. F. Hepatitis B virus capsid completion occurs through error correction. *J. Am. Chem. Soc.* **2017**, *139*, 16932-16938.

(155) Keifer, D. Z.; Motwani, T.; Teschke, C. M.; Jarrold, M. F. Measurement of the accurate mass of a 50 MDa infectious virus. *Rapid Commun. Mass Spectrom.* **2016**, *30*, 1957-1962.

(156) Lutomski, C. A.; Lyktey, N. A.; Pierson, E. E.; Zhao, Z.; Zlotnick, A.; Jarrold, M. F. Multiple Pathways in Capsid Assembly. *J. Am. Chem. Soc.* **2018**, *140*, 5784–5790.

(157) Kukreja, A. A.; Wang, J. C. -.; Pierson, E.; Keifer, D. Z.; Selzer, L.; Tan, Z.; Dragnea, B.; Jarrold, M. F.; Zlotnick, A. Structurally Similar Woodchuck and Human Hepadnavirus Core Proteins Have Distinctly Different Temperature Dependences of Assembly. *J. Virol.* **2014**, *88*, 14105-14115.

(158) Pierson, E. E.; Keifer, D. Z.; Asokan, A.; Jarrold, M. F. Resolving Adeno-Associated Viral Particle Diversity With Charge Detection Mass Spectrometry. *Anal. Chem.* **2016**, *88*, 6718-6725.

(159) Lutomski, C. A.; Gordon, S. M.; Remaley, A. T.; Jarrold, M. F. Resolution of Lipoprotein Subclasses by Charge Detection Mass Spectrometry. *Anal. Chem.* **2018**, *90*, 6353-6356.

1.5 Figure

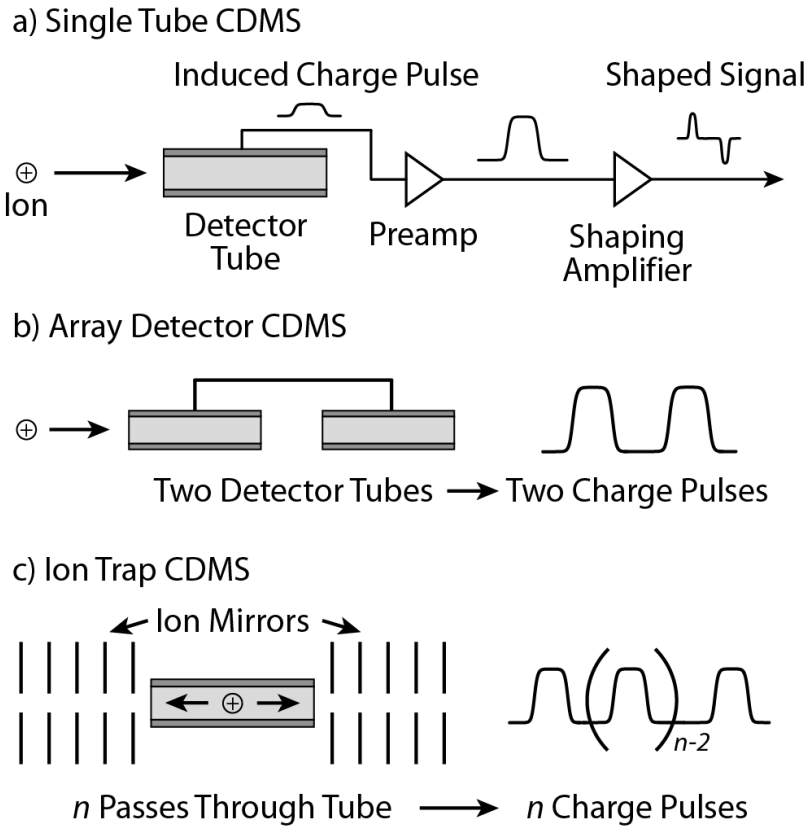

Figure 1.1: Illustration of different methods in charge detection mass spectrometry (CDMS), in which a) ions are detected based on the charge pulse they induce as they pass through a conductive detector tube. The amplitude of the pulse is proportional to the ion charge and the ion *m*/*z* is related to the velocity, obtained from the duration of the pulse. A shaping amplifier can be used to produce peaks at the beginning and end of the charge pulse to make it easier to find the velocity. Repeatedly measuring the ion with b) an array of detector tubes or c) an ion trap to reflect the ion through the tube many times improves the uncertainty in the charge and *m*/*z* measurements.

Chapter 2

Experimental

2.1 Overview

Experiments were performed on the single particle analyzer of mass and mobility, a home-built charge detection mass spectrometer that will be described in detail in this chapter. A schematic diagram of the instrument is shown in Figure 2.1. The instrument can be divided into three sections: the source region, the bender region, and the detector region. The source region consists of the electrospray emitter, a modified Z-Spray source (Waters, Milford, MA) and a pair of radio frequency (RF) only ion guides (Ardara Technologies, Ardara, PA). The second region contains the turning quadrupole (Ardara Technologies, Ardara, PA), used to select certain ion energies to enter the detector. The ion trap, charge detector, and the associated electronics are located in the third and final region of the instrument.

2.2 Source Region

Ions are formed by static nanoelectrospray ionization using borosilicate capillaries pulled to tips with an inner diameter of ~1-2 μm. Ion formation is initiated by applying a potential of +1-2 kV relative to ground to the solution with a platinum wire inserted into the tip in contact with the solution. The capillary is mounted on a movable stage and positioned so that the tip is ~2-3 mm from the instrument orifice and pointed orthogonally to the direction ions travel into the instrument.

Ions enter the instrument through a modified Z-Spray source (Waters, Milford, MA). The Z-Spray source can be divided in three parts referred to as the sample cone, source block, and extraction cone. After leaving the ESI emitter, ions make a 90° turn left from the perspective of the ions and pass through the sample cone which consists of a 7.2 mm long segment with an inner diameter of 8 mm and a segment that tapers over a length of 6 mm down to a 0.3 mm hole that is the front of the instrument. Ions then travel through a bore in the source block to make a 90° turn right through the extraction cone, 17.3 mm from the start of the source block. The bore through the source block starts at an 8 mm diameter for a depth of 3.5 mm, then tapers to a 4.5 mm diameter over a length of 2.5 mm. The extraction cone consists of a 6.7 mm long tapered skimmer with a 0.5 mm wide hole on the upstream side and 7.5 mm opening on the downstream side that opens to a 2.9 mm long, 22 mm inner diameter section used to hold the cone in place and enable differential pumping between the source block and first vacuum stage. The source block is pumped to a base pressure of ~1 Torr by a 48 CFM mechanical pump connected to the source block 23 mm beyond where ions turn into the extraction cone. The pressure can be adjusted to up to ~70 torr by throttling the pump with a diaphragm valve to improve transmission of high mass ions. The source block and sample cone are electrically connected and typically held at a potential of +250 to +350 V, with higher potentials used for polymer samples and lower potentials used for small proteins. A typical potential for the extraction cone is +220 V. The entire source block is heated with a cartridge heater, typically to 80 °C for all samples.

Ions travel from the source block to the turning quadrupole through a pair of RF-only quadrupole ion guides (Ardara Technologies, Ardara, PA). The ion guides are made up of four square stainless steel rods, with a 3.2 mm by 3.2 mm cross section, with an inscribed diameter of 5 mm. The outside edges of the rods are tapered starting 4.6 mm from the entrance to the first ion guide, so the cross section of the rods at the entrance is 3.2 mm by 0.5 mm. The first ion guide is 31.2 cm long, starting 3 mm from the downstream side of the extraction cone taper and ending 3.6 mm from the front of the second ion guide. The second ion guide is 23.2 cm long, before an exit lens electrode with a 4 mm diameter hole to allow ions into the bender chamber. The space between the two ion guides allows a gate valve to be moved into place so the source chamber can be vented to atmosphere to clean the Z-Spray source. The ion guides are powered by a self-oscillating RF power supply at a frequency of 1.89 MHz with a peak-to-peak voltage of 1480 V. The ion guides can be placed at separate DC offset potentials, typically in the range of +210 to +225 V and +180 to +195 V for the first and second ion guides, respectively. Tuning the potential difference between the extraction cone, first and second ion guides can enhance ion transmission, and the approximate ion energy can be set with the offset potential on the first ion guide. The exit lens is typically set to +100 V. The ion guides are mounted on a partial vacuum chamber holding the gate valve and MHV feedthroughs to power the ion guides. The first ion guide extends to the source through a 14.6 cm inner diameter vacuum chamber differentially pumped to a pressure of ~2 x 10^{-4} Torr by a 220 L/s turbomolecular pump (Edwards Vacuum, Burgess Hill, UK). Raising the pressure in the source block to 70 Torr increases the pressure in the ion guides to ~2 x 10^{-3} Torr. The pressure in this chamber can also be manipulated by adding nitrogen gas through a leak valve. The second ion guide extends towards the turning quadrupole inside a pair of shielding tubes to preserve the differential pumping between the source and bender chambers. When the gate valve is open, the second ion guide tubes are connected to the source chamber by a 17.3 mm diameter hole so that the exit lens forms the conductance limit.

2.3 Bender Region

After leaving the source region, the ion beam contains a certain distribution of ion energies. Ions with different energies oscillate through the trap at different frequencies, creating uncertainty in measuring the mass to charge ratio, or may not be trapped at all, depending on the ion trap settings. The electrostatic turning quadrupole is used to select certain ion energies to reach the trap. Ions with too much energy do not make the full 90° turn, and ions with too little energy turn more than 90° and hit the walls of the instrument rather than reaching the detector.

The turning quadrupole consists of four hyperbolic rods housed inside a shielding box formed by six flat plates, with one on the top and bottom of the rods and one on each side. The top and bottom of the shielding box are 5.7 cm by 5.7 cm and 1 cm thick and the side plates are 7.3 cm by 5.7 cm and 7.6 mm thick. The side plates each have a 1 cm diameter hole in the center of the plate, so ions can enter or leave through any side. The rods are 5.1 cm long and have a cross section with two 2 cm long straight edges at a 90° angle joined by a hyperbolic curve making a third edge. The rods are placed between the top and bottom plates so that the 90° corners align with the corners of the plates. The remaining four sides of the box are formed by the side plates. An additional exit lens consisting of an 8.2 mm long region with a 20.2 mm inner diameter and a 0.7 mm thick endcap with a 1 cm diameter hole through the center is also attached to one of the side plates.

The hyperbolic rods are used to create a quadrupolar field to bend ions towards the detector. Rods in opposite corners of the box are electrically connected to each other, with one pair set at a low potential and one at a high potential. This creates a saddle point at the midpoint of the bender that falls off towards the low potential rods, or inner poles, and rises towards the high potential rods, or outer poles. Ions enter between one pair of rods and follow the saddle shaped electric field to bend towards the low potential rod. In this instrument, the bender is used to deflect ions from the ion guides to make a 90° turn right from the direction of the incoming ion beam. To do this, the bender is oriented with the outer pole on the left of the ion as it enters, and the inner pole on the right, with the side holding the exit lens on the right side of the box. Additionally, the two sides the ion does not pass through, opposite the entrance and on the left of the entrance, are electrically connected. The ion energy range selected by the bender is determined by the potentials applied to the inner and outer poles as well as the top, bottom and sides of the shielding box. Typical rod potentials used are +120 V and +220 V on the inner and outer poles, respectively. Common potentials for the box are +140 V for the top, bottom and unused sides, and +170, +170 and +30 for the entrance side, exit side, and exit lens, respectively. These potentials select a distribution of ion energies with an average value of 209 eV/charge and a standard deviation of 3.2 eV/charge. These potentials can be tuned to match the maximum of the distribution of ion energies from the source. A wider range of ion energies can be passed through to the trap by lowering the potential of the inner pole to increase the difference between the poles and lowering the potentials on the top, bottom and sides of the box. For example, the distribution of ion energies transmitted has a standard deviation of ~10 eV/charge with the pole difference set to ~300 volts.

After leaving the second ion guide, ions travel 5 mm into the entrance of the turning quadrupole and are then bent towards the detector. Upon exiting the bender and exit lens, ions pass through a 22.6 mm long, 24.4 mm inner diameter insulating spacer used to help align and support the turning quadrupole in its mounting on the wall of the vacuum chamber separating the bender region and the detector region. The ions then enter the detector region through a lens shaped similarly to the bender exit lens with a smaller 1 mm through hole to form a conductance limit, typically held at a potential of -250 V to guide ions towards the detector. The bender region is differentially pumped to a typical pressure of ~5 x 10^{-7} Torr by a 540 L/s turbomolecular pump (Edwards Vacuum, Burgess Hill, UK). Raising the pressure in the source block to 70 Torr increases the pressure in the bender region to ~2 x 10^{-6} Torr.

2.4 Detector Region

Energy selected ions exiting the bender chamber through the conductance limit travel 5 mm in the final vacuum chamber before reaching the detection system, made up of a charge conducting tube inside an electrostatic ion trap. The vacuum chamber is at a pressure of ~4 x 10^{-9} Torr and is pumped by a 540 L/s turbomolecular pump (Edwards Vacuum, Burgess Hill, UK). A schematic diagram of the ion trap and detector is shown in Figure 2.2. The ion trap is based on the conetrap design of Schmidt et al.[1] in which each end of the trap consists of a single electrode with a conical bore. This design creates a focusing electric field that helps keep ions trapped for long times even if they are traveling off the trap axis, parallel or at an angle to the axis. The electrodes used here are 66 mm long with a bore that tapers from 34 mm at the wide end to 14 mm at the narrow end. The electrodes are oriented with the wide end of the bore directed at the center of the trap.

The ion trap has additional elements to shield the detector and restrict ions entering the trap. Grounded shielding plates that are 4.8 mm thick with a 6.2 mm hole through the center are placed on the interior sides of the two cone electrodes. Between those plates, the detector is housed in a 31.8 mm inner diameter shielding tube and held in place by pair of insulating spacers that mate to both the detector and shielding plates. Including the shielding plate and the detector, the total distance separating the two trapping electrodes is 37.7 mm. On the exterior of the cone electrodes, there is a 0.8 mm thick lens with a 1.5 mm hole in the center on the end ions enter the trap through, and a similar lens with a 1.0 mm hole on the back of the trap. The front lens helps restrict the number of ions entering the trap so only ions near the axis enter, and the combined pair of lenses helps with aligning the trap with the rest of the instrument.

The detector consists of a 28.2 mm long stainless steel tube with a 7.1 mm inner diameter and 9.5 mm outer diameter. The tube also has a 22.2 mm long 1.6 mm diameter post welded to the outside to connect the detector to the amplification and recording system. The tube is connected to the input of a JFET cooled to a temperature of -50 °C by a Peltier cooler on a CoolFET charge sensitive preamplifier (Amptek, Bedford, MA) that also uses an A250 preamplifier (Figure 2.2a). The preamplifier is located in a shielded box directly next to the charge conducting tube, inside the vacuum chamber. Signals are then passed to a ~10x linear amplifier located outside the vacuum chamber. The opamp in the linear amplifier has recently been changed from an Amptek A275 (used for the work in this dissertation) to a LM7171 (Texas Instruments, Dallas, TX) which can output more current, reducing signal distortion due to poor impedance matching. The signal is split after the linear amplifier, with one channel going to an analog to digital converter card (ATS9350, AlazarTech, Pointe-Claire, Canada), and the other to an additional shaping amplifier. The shaping amplifier uses a differentiator, integrator and two Amptek A275 opamps to modify the charge pulse induced by the ion to produce a leading positive peak and trailing negative peak which correspond the ion entering and exiting the detector tube. For most ion velocities observed in this instrument, this signal typically has a higher signal to noise ratio than the unshaped signal but can have distorted amplitudes depending on the ion velocity. The shaped signal is sent to a second channel on the same analog to digital converter card. Data are typically recorded at a sampling rate of 5 MHz, although the sampling rate is lowered to 2 MHz for trapping times longer than 3 s.

The trapping potential used on the cone electrodes is typically +330 V (Figure 2.2b and 2.2c). Ions traveling along the trap axis with 193 to 253 eV/charge can be trapped under these conditions. The high end of the acceptable energy range decreases by ~8 eV/charge for ions traveling up to 1° off the axis of the trap. In experiments, the back electrode of the trap is held constant at the trapping potential and the front electrode is raised and lowered to allow ions in and trap ions. Two different trapping schemes can be used to determine when to close the trap. In triggered trapping mode, the front electrode is held at ground potential until an ion is detected above the noise level inside the trap. Then, the front of the trap is raised to the same potential as the back of the trap for a preset detection time. This mode can only be used for ions that can be charged to ~300 *e* or higher, because lower charge ions cannot be detected on a single pass through the detector. The second method to operate the trap is with a random trapping scheme, in which the front potential of the trap is raised and lowered at regular intervals without knowing if an ion is present in the trap. The trapping cycle starts with the front electrode at 0 V for 1 ms, after which the electrode is raised to the trapping potential for the preset time and lowered again to 0 V to restart the trapping cycle.

2.5 Reference

(1) Schmidt, H. T.; Cederquist, H.; Jensen, J.; Fardi, A. Conetrap: A compact electrostatic ion trap. *Nucl. Instr. and Meth. in Phys. Res. B.* **2001**, *173*, 523-527.

2.6 Figures

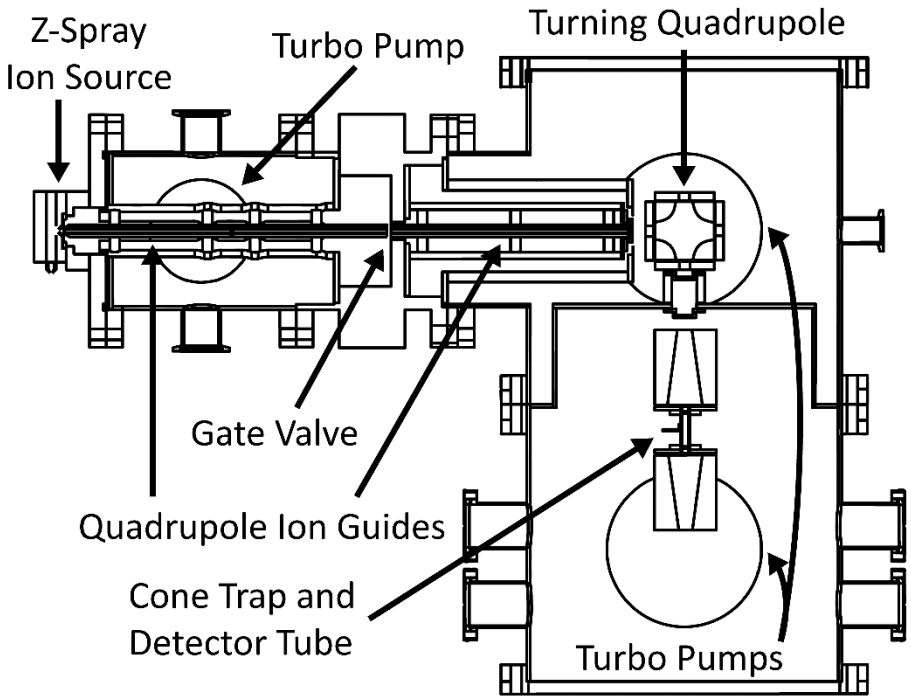

Figure 2.1: Schematic diagram of the single particle analyzer of mass and mobility (SPAMM) instrument.

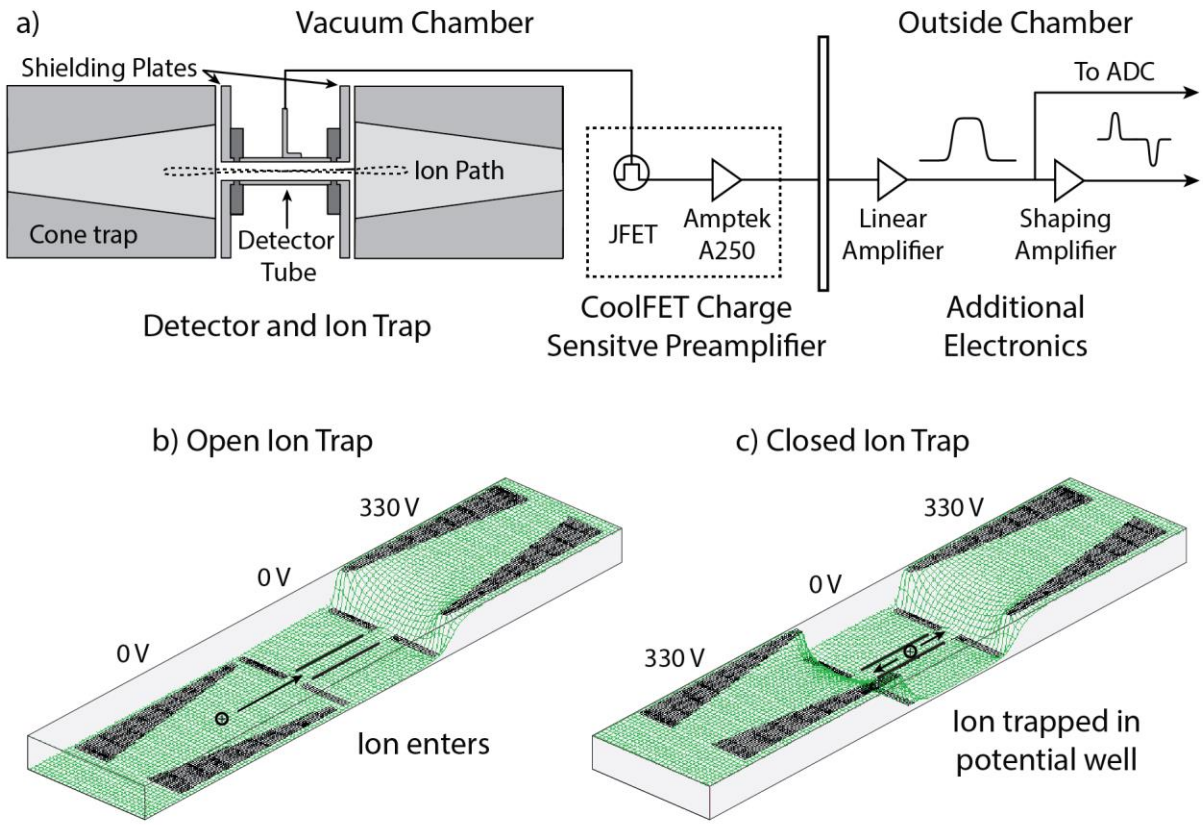

Figure 2.2: a) Schematic diagram of the ion trap and the detector tube and its associated electronics. Not shown is an additional shielding tube the detector tube is housed inside onto which the CoolFET charge sensitive preamplifier is mounted in its own shielding box inside the vacuum chamber. Also shown are potential energy surfaces produced with SIMION 8.0 for the ion trap when it is b) open and c) closed. Ions can freely enter with only one electrode at the trapping potential and are trapped by raising the potential of the second electrode to form a potential well around the detector tube.

Chapter 3

Single Particle Analyzer of Mass: A Charge Detection Mass Spectrometer with a Multi-Detector Electrostatic Ion Trap

This chapter is reproduced with permission from:

Andrew G. Elliott, Samuel I. Merenbloom, Satrajit Chakrabarty, Evan R. Williams

"Single Particle Analyzer of Mass: A Charge Detection Mass Spectrometer with a Multi-Detector Electrostatic Ion Trap" *Int. J. Mass Spectrom.* **2017**, *414*, 45-55

3.1 Abstract

A new charge detection mass spectrometer that combines array detection and electrostatic ion trapping to repeatedly measure the masses of single ions is described. This instrument has four detector tubes inside an electrostatic ion trap with conical electrodes (cone trap) to provide multiple measurements of an ion on each pass through the trap resulting in a signal gain over a conventional trap with a single detection tube. Simulations of a cone trap and a dual ion mirror trap design indicate that more passes through the trap per unit time are possible with the latter. However, the cone trap has the advantages that ions entering up to 2 mm off the central axis of the trap are still trapped, the trapping time is less sensitive to the background pressure, and only a narrow range of energies are trapped so it can be used for energy selection. The capability of this instrument to obtain information about the molecular weight distributions of heterogeneous high molecular weight samples is demonstrated with 8 MDa polyethylene glycol (PEG) and 50 and 100 nm amine modified polystyrene nanoparticle samples. The measured mass distribution of the PEG sample is centered at 8 MDa. The size distribution obtained from mass measurements of the 100 nm nanoparticle sample is similar to the size distribution obtained from transmission electron microscopy (TEM) images, but most of the smaller nanoparticles observed in TEM images of the 50 nm nanoparticles do not reach a sufficiently high charge to trigger the trap on a single pass and be detected by the mass spectrometer. With the maximum trapping time set to 100 ms, the charge uncertainty is as low as ±2 charges and the mass uncertainty is approximately 2% for PEG and polystyrene ions.

3.2 Introduction

Synthetic polymers are used in a wide variety of applications, from simple homopolymers used in common packaging materials and textiles,[1, 2] to carefully engineered copolymers and nanoparticles designed for electronics[3] and biomedical technologies.[4-6] Many properties of

polymers are related to molecular weight,[7] making accurate characterization of molecular weight distributions important to understanding and predicting polymer function. Soft ionization techniques, such as electrospray ionization (ESI) and matrix assisted laser desorption ionization (MALDI), can be used to produce gaseous ions of polymers even above 1 MDa molecular mass.[8-10] MALDI-MS can be particularly effective for mass analysis of large polymers because low charge states are typically produced, although differential ionization efficiency as a function of molecular weight can occur.[11-13] Careful matrix selection and sample preparation are important to effectively ionize MDa polymer molecules with MALDI,[14-16] and cryogenic detectors have been used to overcome low detection efficiencies associated with the large mass but low charge state ions typically formed by MALDI at high mass to charge (*m/z*) values.[15-18] ESI has the advantage that highly charged ions are produced, which lowers their *m/z* to a range where the performance of many different types of mass spectrometers excel.[19] However, the charge state distributions of each molecular ion of a heterogeneous synthetic polymer sample with a broad molecular weight distribution can overlap, limiting the size of the largest synthetic polymer than can be analyzed using ESI with conventional MS instruments.[20] A rough measure of the molecular weight of large biopolymers formed from solutions in which they have native-like spherical structures can be obtained from the *m/z* of the unresolved charge state distribution, but with significantly less accuracy than if the charge states can be determined from the mass spectral data.

An alternative way to obtain molecular weight information from a heterogeneous sample consisting of large molecules is to form and weigh individual ions so that the signal from two ions cannot overlap. There are several different methods to weigh individual ions. Quadrupole ion trap (QIT) instruments can trap single ions for extended periods of time, enabling high precision *m/z* measurements by observing the motions of the ion in the trap through light scattering or fluorescence.[21-26] The mass can be determined by making repeated *m/z* measurements after changing the charge of the ion. Single highly charged ions have also been measured with Fourier transform ion cyclotron resonance (FT-ICR)[27-31] and Orbitrap[32, 33] instruments. In FT-ICR instruments, the charge state of each ion can be obtained by measuring the ion multiple times after changing its charge, just like with the QIT.[27-29] The signal intensity induced by a single ion can also provide information about its charge state in both FT-MS techniques. However, precisely measuring the charge of a single ion from the induced current can be challenging because the amplitude of the induced current depends on the radial position of the ion in the detector as well as its charge.[34, 35] To account for this effect on single ion FT-ICR-MS, Smith and coworkers measured individual ions multiple times, exciting each ion to a larger and larger radius so that charge measurements could be made from a single known radius corresponding to a value slightly less than that of the cell.[30, 31] Because each ion must be measured several times to accurately determine its charge state, weighing an ion with these single ion detection techniques can be quite slow. The high mass precision possible with the QIT, FT-ICR or Orbitrap comes at a cost of long analysis times (many seconds to minutes) for each ion.

A faster way to measure the mass of single ions is with charge detection mass spectrometry (CDMS). Shelton and coworkers first demonstrated CDMS over 50 years ago, measuring the mass of micron sized iron particles with 10^4 charges by passing individual ions through a single conducting cylinder.[36] As each ion passes through the conductor, it induces an image charge that is proportional to the charge of the ion. The velocity of the individual ion is obtained from the tube length and from the duration of the image charge signal corresponding to the ion entering and exiting the tube. The *m/z* of the ion is determined from its energy and velocity. The mass of each ion is obtained from the independent charge and *m/z* measurements. The *m/z* and charge of each

ion are measured simultaneously in the few microseconds that it takes for the ion to pass through the detector. Thus, each ion can in principle be weighed quickly. Ions with the same *m/z* but different charge states are readily distinguished from each other because each ion is weighed individually. A true mass spectrum, versus the more conventionally measured *m/z* spectrum, is obtained for all samples as a histogram of all of the measured individual masses.

Single pass CDMS instruments similar to the design of Shelton and coworkers have been used to measure the mass of many different types of particles. Early experiments with CDMS focused on small cosmic dust particles, and instrumentation advancements resulted in improved detection limits down to 1500 charges.[37-39] Fuerstenau and coworkers expanded single pass CDMS to biomolecules and synthetic polymers and measured the mass of plasmid DNA[40] and polystyrene spheres,[40] as well as tobacco mosaic virus and rice yellow mottle virus.[41] Jarrold and coworkers observed negatively charged droplets from positive electrospray with single pass CDMS.[42] Dugourd and coworkers also used single pass CDMS to study synthetic polymers and nanoparticles over a wide size range, from low MDa polyethylene glycol (PEG) ions up to composite nanoparticles weighing tens of GDa.[43-47] In these instruments, single ions with as few as 300 charges were detected, although large uncertainties in measured *m/z* and charge values limited the overall mass precision of these measurements.

The uncertainty in CDMS measurements can be improved by signal averaging repeated measurements of the same ion. One approach is to use multiple detector tubes and measure the ion as it passes through each tube. This linear array of detector tubes improves the measurement uncertainty by a factor of $n^{½}$ where n is the number of tubes in the array. Gamero-Castaño first used this method to study micron-sized propylene carbonate droplets with a detector consisting of six cylinders.[48] The longest array detector used for CDMS thus far contained 22 detection tubes, with which Jarrold and coworkers demonstrated a charge uncertainty as low as ±9 charges.[49] Austin and coworkers developed a detector array on a printed circuit board, simplifying the design and construction of a long array detector.[50] However, a limitation of array detectors is that the detection capacitance increases with the number of detectors, which decreases the charge detection sensitivity.

Another approach to detecting an ion multiple times is to trap the ion and make it pass through the charge detection region multiple times. Dual ion mirror traps have been used to measure the *m/z* of ensembles of small ions with resolution up to ~10^5.[51-55] Benner demonstrated the use of a dual ion mirror trap for single particle CDMS with a single detector tube.[56] The ion mirror at the trap entrance is initially at ground potential until a signal pulse from an ion is detected. This signal triggers an increase in the entrance mirror potential to close the trap. A minimum of ~250 charges on an ion was necessary in order for there to be a detectable signal that would result in a trap closure. Ions were trapped for up to 450 cycles and an uncertainty in the charge measurement of single DNA ions of ±2.3 charges was reported. Dugourd and coworkers demonstrated photodissociation of individual mass selected PEG and DNA ions inside a similar ion mirror trap.[57-59]

Jarrold and coworkers used Fourier transforms to analyze CDMS data to obtain masses of single ions with as few as 7 charges.[60] Because a low charge ion produces an insufficient signal to induce a trapping event, data were obtained by raising the potential of the entrance electrode without knowing if an ion is present in the detector.[61] A Fourier transform of the resulting time domain signal from a single trapped ion results in a frequency related to the *m/z* of the ion and amplitude that is proportional to the charge of the ion. With cryogenic cooling of the detector[62] and a trapping time of 6×10^4 cycles over 3 s,[63] they demonstrated an uncertainty of ±0.196 charges

with fewer than 1 in 10^4 ions assigned to the wrong charge state. This FT-CDMS approach has extended the range of samples that can be investigated with CDMS to include small proteins, and has improved the resolution and mass measuring accuracy for large virus particles by CDMS.[60-67]

Here, we describe a new CDMS detector consisting of an array of four charge detection tubes inside an ion trap, that we refer to as the single particle analyzer of mass (SPAM). By combining both trapping and array detector approaches, ions can be trapped for hundreds of passes, and more measurements per unit time can be made because ions spend a larger fraction of time inside a detector tube. Simulations show the cone trap design developed by Schmidt et al.[68] has characteristics that are advantageous for CDMS. The performance of the instrument is tested with complex polymer and nanoparticle samples and implications for the reported size dependence of PEG ionization mechanisms are discussed.

3.3 Experimental

3.3.1 Samples

Polyethylene glycol (PEG) with a nominal molecular weight of 8 MDa and amine-modified polystyrene nanoparticles with nominal diameters of 50 nm (~41 MDa) and 100 nm (~330 MDa) were obtained from Sigma Aldrich (St Louis, MO). The PEG samples were prepared at a concentration of 0.1 mg/mL in a 50/50 water/methanol solution. The nanoparticle samples were prepared at 0.125% in a 75/25 methanol/water solution. Electron microscope images of nanoparticles were acquired on a Tecnai 12 transmission electron microscope (FEI, Hillsboro, OR). One drop of the sample solution was deposited on a copper grid for each sample. The diameters of the particles were measured from the images using Adobe Illustrator.

3.3.2 Mass Spectrometry

Experiments were performed on the single particle analyzer of mass (SPAM), a home-built charge detection mass spectrometer, a schematic of which is shown in Figure 3.1. Ions are formed by nanoelectrospray ionization using borosilicate capillaries that have tips pulled to an inner diameter of between 2 and 60 μm. A platinum wire is inserted into the capillary so as to be in contact with the sample solution. A potential of +1-2 kV with respect to instrument ground is applied to the capillary to initiate ion formation by electrospray. The resulting ions are transferred to vacuum using a Z-spray source (Waters Corporation, Milford, MA) modified to contain an extraction cone with a 0.5 mm hole to improve differential pumping between the source and first vacuum stage. Typical voltages inside the source are +335-450 V for the exterior sample cone and +205 V for the interior extraction cone and the pressure between the cones is typically 1 Torr. The source is heated to 80-90 °C to improve ion desolvation. After the extraction cone, ions enter the first vacuum stage at a pressure of 5×10^{-4} Torr then pass into a second chamber at 5×10^{-6} Torr through a grounded skimmer. A single einzel lens consisting of three stainless steel tubes guides ions to the detection chamber through a 1.0 mm conductance limit where they can be trapped at a pressure of 1×10^{-8} Torr. Transmission of large nanoparticles was improved by raising the pressure in the source block to 70 Torr by partially closing a valve to the source pump. The resulting pressures were 2×10^{-3} Torr, 2×10^{-5} Torr, and 3×10^{-8} Torr in the first, second and third chambers, respectively.

The detection system consists of four stainless steel tubes that are between two conical trapping electrodes that are based on the design of Schmidt et al.[68] The tubes have an inner diameter (ID) of 7.1 mm and are 28.2 mm long. Each tube is held in place by insulators inside a 31.8 mm ID shielding tube, and the total distance separating each trapping electrode is 127 mm. The four tubes are connected pairwise in the pattern shown in Figure 3.1b, with tubes 1 and 3 connected to one detection circuit and tubes 2 and 4 connected to a second circuit. Each pair of tubes is connected to a separate CoolFET charge sensitive preamplifier (Amptek, Bedford, MA) containing an A250 preamplifier and JFET cooled to -50 °C by a Peltier cooler. The preamps are housed in a shielded box inside the vacuum chamber, and the signal is sent to a shaping amplifier consisting of a differentiator, integrator and two voltage amplifiers (Amptek A275) and signal filter outside the vacuum chamber. Data for both channels are recorded simultaneously with a single analog to digital converter card (ATS9350, AlazarTech, Pointe-Claire, Canada) at a rate of 2 MHz. The preamplifier circuit for the A channel (tubes 1 and 3) has a 1 pF test capacitor composed of ten 10 pF 1% capacitors. To calibrate the detector, a charge pulse of known amplitude was passed through the test capacitor into the amplifier system. The charge response on the B channel (tubes 2 and 4) was later calibrated against the charge measured with signal from channel A by comparing trapped ions measured at less than 3% uncertainty in the charge and amplitude measurements from channel A and B, respectively. The response from the first and second channels is 140 μV/charge and 62 μV/charge, respectively. The noise on the second channel is correspondingly lower such that both channels have similar signal-to-noise (S/N) ratios.

An ion entering a detector tube induces an image charge of opposite sign on the tube. Inverting and shaping the square wave signal from that tube produces a pattern consisting of a leading positive peak and trailing negative peak for a positive ion. The spacing between the peaks is proportional to the velocity of the ion. If the rise time of the image charge pulse is shorter than the peaking time of the shaping amplifier, the peak widths are constant, and the amplitude of each peak is proportional to the charge of the ion. The peak widths of the PEG and nanoparticle ions are comparable to the peak width from the calibration with the test capacitor, which indicates that the peak amplitude provides a good estimate of the ion charge over the size range of the ions reported here. The standard deviation of charge measurements from an ion entering or exiting a single tube is ±105 charges, or about 10% of the average charge on an 8 MDa PEG ion. The relative standard deviation of single tube velocity measurements is 3.7%. Repeated measurements of these values for a single ion decreases the associated uncertainty by a factor of $n^{1/2}$, where n is the number of measurements.

Two different ranges of ion energies can be trapped at a single trapping potential on the cone trap, with a narrow range near the trap potential and wider range at ~60% of the trap potential.[68] In these experiments, the ion trap is only operated in the upper energy range in order to obtain energy selection. The cone electrode in the back of the trap is maintained at a single trapping potential for the entire experiment, whereas the voltage on the front is initially lower to allow ions to enter the trap. Upon sensing a charge pulse from a detector tube greater than a specified amplitude, the voltage on the front of the trap is pulsed up to the same voltage as the back of the trap through a MOSFET switch and reaches the trapping potential 20 μs after the detection of the charge pulse. For the samples studied here, trapped ions typically take at least 100 μs to return to the first cone electrode, so no ions are lost before the trap is closed. The front of the trap is held at the trapping potential for 100 ms corresponding to the time of the data acquisition. After the measurement, the front voltage is lowered for 8 ms and the acquisition program is reset

in order that the trap can trigger on the next ion detected in the trap. The upper limit of the trap cycle is 9 Hz.

Data is analyzed with a set of LABVIEW programs. Signals from trapped ions are first sorted from transients in which the detected ion was not trapped by checking for ion signal corresponding to each pass of an ion's second cycle through the trap. To account for different size ions taking different amounts of time to turn around, ion signal was identified by comparing the maximum and minimum values of the root mean square of a time interval stepped through the expected time of each pass through the detector. A different time interval was chosen for each sample, approximately equal to the time for a typical ion to pass through the detector or turn around. For each transient that contains an ion, peaks corresponding to the ion entering and leaving each detector tube are identified with a peak picking routine designed to identify signal from low charge ions based on the consistent amplitude and spacing between induced peaks. The average peak spacing and approximate peak height are determined from the group of four peaks containing the largest peak in the transient. These peaks correspond to a single pass through the detector array. Then the entire transient is scanned for groups of four peaks close to the amplitude of the initial set of peaks that are spaced at the same time interval as the initial set of peaks. With the array of peak timings and amplitudes, the *m/z*, charge and mass can be determined using the charge calibration described above. The *m/z* of the ion is proportional to the measured velocity and trapping voltage from equation 3.1:

$$\frac{m}{z} = \frac{2CeV}{v^2}, \qquad \text{(eq. 3.1)}$$

where *V* is the trapping potential, *v* is the ion velocity and *C* is a proportionality constant to convert from the trapping potential to the ion energy. A *C* value of 0.96 was determined from the range of ion energies that are trapped at a given potential using SIMION simulations. Because only ions within a narrow range of kinetic energies are trapped, there is no need for specific terms in equation 3.1 to account for aerodynamic acceleration.

3.4 Results and Discussion

3.4.1 Ion Trap Design

Two electrode designs have been used in trapping CDMS instruments: dual ion mirror traps[52, 56, 57] and cone traps.[61, 68] In order to compare the performance features of the two designs and evaluate the effects of various parameters, ion trajectory simulations were performed on the two designs in SIMION 8.0 using ions weighing 17 kDa with 21 charges for all simulations. The time for one complete cycle for a trapped ion of the same mass, kinetic energy, and charge state differs for the two traps. This effect is illustrated for an ion with a kinetic energy of 230 eV/charge in Figure 3.2a, which shows the location of the ion along the trap axis as a function of time. In the cone trap, shown in the upper trajectory, the ion travels far beyond the detector tube, penetrating deep into the electrode and takes 56 µs to return to the tube. In the ion mirror trap, shown in the lower trajectory, the ion turns around much closer to the entrance of the ion mirror, and spends only 9.3 µs outside the tube on each pass. Ions turn around faster and pass through the detector tubes more times for a given trap time with the ion mirror trap. Approximately three-fold more measurements can be made with an ion mirror trap than a cone trap for a given trap time under

these conditions. The effect of ion kinetic energy on the ion trapping time at a given trapping potential was evaluated at a trapping potential of 240 V, with a maximum trapping time set at 50 ms. These data (Figure 3.2b) show that only ions with an energy between 88% and 94% and between 96% and 98% of the trapping potential are efficiently trapped in the ion mirror trap and cone trap, respectively. The range of energies at which an ion is trapped at a given potential is much narrower for a cone trap, with a 2% range in the ion energy compared to 6% for the ion mirror trap. Thus, a cone trap can be used as an energy filter for the trapped ion. This narrow range of energies for successful ion trapping reduces the uncertainty in the *m/z* measurement for each ion in the absence of other energy filters prior to the trap.

The ion trapping time also depends on the initial radial position and the angle at which an ion enters the trap.[56, 57] The effect of the starting position on the trapping time of an ion in each trap was investigated with ions starting in a direction parallel to the trap axis, but up to 3 mm off center. The fraction of the 50 ms maximum trapping time the ion remains in the trap is shown as a function of the distance from the center of the trap axis in Figure 3.2c. The acceptance diameter for the cone trap is 3.5 mm, which is about two times greater than that of the ion mirror trap. To determine the effects of pressure and angular dispersion on trapping time, ion trajectories starting on center but with initial trajectories up to 1.4° off the trap axis were simulated at 10^{-5} to 10^{-7} Torr using a hard sphere collision model in SIMION (Figure 3.2d). Ions entering up to 0.2° off center were trapped for similar lengths of time in each trap, but beyond that angle, ions in the ion mirror trap were quickly lost from the trap at each pressure tested. Trapping times in the cone trap are greater than 1 ms at pressures up to 10^{-6} Torr at entrance angles up to 1.0°. In addition to better energy selection features, the cone trap also has greater tolerance for ions entering the trap on trajectories off its central axis.

3.4.2 Mass Measurement of a Single Ion

To illustrate the mass measurement of a single ion with sufficient charge to induce an observable signal upon a single pass through each detection tube, a transient signal from each of the two detector channels for a single ion obtained from a sample of 100 nm polystyrene beads is shown in Figure 3.3. Each time an ion passes through the detector tubes, it induces eight voltage pulses corresponding to each time the ion enters or exits a single tube, with four pulses on each detection channel. Peaks A and B on the upper trace (channel A) are the result of the ion entering and exiting the first detector tube, respectively. As the ion enters the second tube, it then induces peak C on the lower trace (channel B), and peak D as it leaves the second tube. Peaks E and F correspond to the ion in the third detector tube, and peaks G and H the ion in the fourth tube. After the ion turns around, it induces the same pulse pattern on its way back through the detector tubes, with points A' and B' from tube four, C' and D' from tube three, E' and F' from tube two, and G' and H' from tube one, in a repeating pattern until the ion is lost from the trap. This ion was trapped for 63 ms, during which time it traveled 56 cycles (112 passes) through the trap at a velocity of 562 m/s in the field free region of the trap and had 624 ± 4 charges. The trap potential was 340 V, corresponding to a kinetic energy of 327 eV/charge. Thus, the *m/z* of this ion is 199,000 ± 4,000 and its mass is 124 ± 3 MDa.

The mass measurements made with each set of tubes are similar for each ion despite the greater gain in channel A for tubes one and three. For the ion shown in Figure 3.3, the charges and masses obtained from the two separately measured channels are 622 ± 5 charges and 124 ± 3 MDa for tubes one and three and 625 ± 6 charges and 125 ± 3 MDa for tubes two and four. These charge

uncertainties correspond to the standard deviation of the mean of the charge measurements. With four charge measurements per pass and 112 passes, the charge of this ion was measured 448 times on each channel, which decreases the uncertainty by a factor of 21, from ±105 charges for a single measurement to ±5 charges for the entire measurement. For 701 ions that were trapped for more than 2 cycles through the trap, a correlation plot of the mass obtained from each channel produces a best fit line with a slope of 0.9974 and an R^2 of 0.9705.

3.4.3 Trap Performance

It is essential to trap ions for an extended period of time in order to make precise mass and charge measurements. Only ions within a narrow range of energies are trapped which provides energy selection. Only ions that complete at least two cycles are used for determining the masses of individual molecules in each sample, which is approximately 1% of all ions entering the detector array in the present configuration. The uncertainty in the charge and velocity measurement decreases with an increasing number of passes through a detector tube. The distribution of trap residence times and corresponding charge uncertainties from a single detection channel for the 376 trapped ions from an 8 MDa PEG sample (Figure 3.4) illustrates the advantages of a longer trapping time to improve the precision of the charge measurement. The uncertainty in the measured charge is 1% for ions that are trapped for more than 10 ms or 30 cycles, which represents approximately 20% of the trapped ions. Approximately 10% of the ions are trapped for at least 30 ms (100 cycles), at which point, the charge uncertainty is ±3 charges. Jarrold and coworkers have reported CDMS measurements with lower charge uncertainties of ±2 charges for protein ions trapped for 30 ms,[60] and as low as ±0.196 charges for a trapping time of 3 seconds.[63] However, smaller ions travel faster and can complete more cycles in a given time, resulting in more measurements and lower uncertainty in the charge measurement. For ions trapped for 400 tube transits (equivalent to the signal induced on one channel in 100 cycles in our detector), the charge uncertainty reported by Jarrold and coworkers is approximately ±3 charges,[64] which is similar to the results reported here for 8 MDa PEG.

The trapping time for different mass ions was investigated using 50 and 100 nm polystyrene beads, and 8 MDa PEG. Approximately 10% of the trapped nanoparticles remained trapped for the entire 100 ms duration of each trapping event, but just one PEG ion out of 376 was trapped for that length of time. However, the 100 nm polystyrene spheres are much larger and travel slower than the PEG ions, resulting in a time per cycle that is on average three times longer. Because of this longer cycle time, no ions from the sample of 100 nm polystyrene spheres were trapped for more than 120 cycles in the 100 ms, which is similar to the number of cycles PEG ions made in 30 ms. About 10% of ions from all three samples were trapped for approximately 100 cycles indicating that the trapping efficiency for a given number of cycles does not depend significantly on the molecular weight within this range. The charge uncertainties for the nanoparticles are around ±2 charges for ions trapped for the longest times, which is similar to that obtained for the smaller PEG ions in the same number of cycles.

3.4.4 Polyethylene Glycol

In order to obtain useful information about the distribution of molecular weights of the many compounds that may be present at different concentrations in a complex mixture, it is necessary to weigh many ions individually. For a more uniform sample, fewer ions are necessary

to provide useful information. Mass information about an 8 MDa PEG sample was obtained by weighing 376 individual ions, and a mass spectrum that is made up from a histogram of the individual masses is shown in Figure 3.5. The distribution has a maximum around 7-9 MDa with a full-width-half-maximum (FWHM) of 6 MDa, and a high mass tail that extends up to 39 MDa. There are also peaks apparent at 14 and 25 MDa. The maximum in this mass distribution is about the same as the reported average molecular weight, and the peaks at 14 and 25 MDa likely correspond to dimers and trimers. The dispersity index calculated from the measured masses is 1.4, consistent with reported dispersity indexes for MDa PEGs which range from 1.4 to 2.8.[69, 70] Approximately half of the ions have between 600 and 1000 charges, with a maximum of about 1100 charges for an ion at 8 MDa and up to 2900 charges for the largest ions trapped (~40 MDa). As a result, the *m/z* spectrum is centered at ~10,000 with only three ions below *m/z* = 6,000.

These mass measurements are similar to those reported by Dugourd and coworkers who used CDMS to measure the molecular weight of a 7 MDa polyethylene glycol sample.[43] They found that the molecular weight was near the expected value and had a similarly broad distribution of 7 MDa FWHM. This broad peak was attributed to the inherent dispersity in the sample, which is the likely cause of the broad range of masses in both measurements. They also reported that the 7 MDa PEG ions charged to a similar level as what is reported here.

3.4.5 Ionization Mechanism of Polyethylene Glycol

Fenn and coworkers reported ESI mass spectra of PEGs between 400 Da and 5 MDa and used the *m/z* of the ions together with a modeled charge capacity to deduce mechanistic information about how PEG ions are formed by ESI.[71, 72] In their model, PEG ions theoretically reach a maximum charge state in a linear zigzag conformation, with charges evenly spaced along the entire length of the ion. The maximum charge state decreased with increasing ion mass up to 20-30 kDa relative to the maximum charge for a theoretical linear ion. For PEG samples weighing more than 17.5 kDa, they observed a broad peak between *m/z* 600 and 1200 which they assigned to intact PEG molecular ions. The maximum reported charge state for these larger ions was 4200 charges for 5 MDa PEG, and the reported maximum charge for each ion increased relative to the modeled maximum charge with increasing mass. Based on these data, they concluded PEG molecules smaller than 20-30 kDa are ionized by an ion evaporation mechanism, whereas larger PEG ions are instead formed by a charge residue mechanism necessary in order to reach high charge states.

The maximum charge states for MDa PEG ions reported by Fenn and coworkers[71, 72] are significantly higher than those measured with CDMS reported here and by Dugourd and coworkers.[43, 57] None of the mass spectra for PEGs beyond 3.3 kDa measured previously by Fenn and coworkers had peaks with a resolvable charge state distribution with which the mass or charge of those ions could be determined. The quadrupole mass spectrometer used in the earlier experiments had a *m/z* limit of 1500, well below where PEG molecular ions are observed in our experiments. Although there may be some difference in the extent of charging in these experiments owing to differences in solution or instrument conditions, our data, which show much lower charging for large, intact PEG molecules, indicate that the ions reported by Fenn and workers to be intact large PEG molecules are more likely to be smaller fragments. Thus, our data bring into question the mechanistic conclusions about the size dependence of the ion formation mechanisms deduced from this prior data. It is important to note that the Rayleigh limit charge for a spherical 8 MDa water droplet is 223 charges, a value much lower than the charge states observed here and

by Dugourd and coworkers. This indicates that the ions in our experiments are unfolded to a large extent in the ESI droplets prior to ion formation.

3.4.6 Amine-modified Polystyrene Nanoparticles

To evaluate the accuracy with which information about the molecular weights of larger, more complex samples can be obtained, samples of 50 and 100 nm amine modified polystyrene nanoparticles were measured. The mass spectrum of the 50 nm sample obtained by CDMS (Figure 3.6a) has a maximum at 35 MDa, with a FWHM of 6 MDa. The approximate sizes of the ions measured in SPAM can be obtained from these mass measurements by assuming these particles are spherical with a density of 1.05 g/mL (value reported by the manufacturer). Figure 3.6b shows the mass spectrum converted into a size distribution, with a maximum at 48 nm, near the manufacturer stated size of the sample. To obtain independent information about the size distribution, the nanoparticle sample was imaged using transmission electron microscopy (TEM) (Figure 3.6d). The size distribution measured from those images (Figure 3.6c) shows a broad range of particle sizes peaking at 40 nm. In contrast, no ions smaller than 43 nm were detected by CDMS.

The larger particle distribution obtained by MS is an artifact of how the CDMS measurement was made. To ensure the trap only closed when an ion was present, the trap was set to operate in a triggering mode, in which ions are only trapped when they induced a signal corresponding to at least ~575 charges on their first pass through the detector. Ions with fewer than 575 charges are still trapped when constructive interference between ion signal and noise is above the trigger limit, but few ions with less than 400 charges were trapped. The measured charge of the trapped ions and the Rayleigh limit charge for a water droplet as a function of size are shown in Figure 3.7. Most of the ions have charge that is close to, but slightly less than the Rayleigh limit, with an average value of 92% of the Rayleigh limit charge. The Rayleigh limit charge for a 45 nm nanoparticle is 425, which is close to the minimum necessary to occasionally trigger a trapping event. This threshold for trapping results in the majority of ions smaller than 46 nm not being detected. Improvements in the detector electronics or cooling to liquid nitrogen temperatures would improve the detection limit. The random trapping method used by Jarrold and coworkers can also be used to detect ions with as few as 7 charges,[60] but this method of data acquisition is less efficient because some trapping events occur when there are no ions or multiple ions present.

In order to more fully evaluate the mass accuracy of the instrument, measurements were made on a sample of 100 nm amine-modified polystyrene beads that should be sufficiently large to consistently charge above the trigger threshold. The CDMS mass spectrum and resulting size distribution of this sample are shown in Figure 3.8a and 3.8b, respectively. The sample contains a broad range of particle sizes, with a maximum between 66 and 76 nm, and an average size of 78 nm. The particle sizes measured by CDMS are much smaller than that indicated by the manufacturer. The distribution measured from TEM images (Figure 3.8c and d) is also broad, with a wide peak stretching from 60 to 80 nm and an average size of 70 nm. The CDMS and TEM data show a similar distribution of sizes, but the average size from CDMS measurements is slightly higher. Salt or solvent adduction may increase the particle masses measured by CDMS, shifting the size distribution larger than that of the bare particles in the TEM images. The size distribution measured from TEM images may also be slightly lower than the true distribution due to uncertainties in determining the edges of the nanoparticles in the images. Uncertainty in the density used to obtain the nanoparticle diameter from the CDMS mass measurements may also contribute to the differences between the two measured size distributions.

3.4.7 Effects of Aerodynamic Acceleration on Ion Energy

Another potential source of uncertainty in measuring the mass of a single ion is aerodynamic acceleration from the gas expansion that takes place in the ESI source. In molecular beams of small molecules, dilute gases accelerate to approach the speed of the background gas, with some velocity slip.[73] Large ions can also travel near the velocity of the neutral gas in an expansion, which increases the ion kinetic energy above that provided by electrostatic acceleration alone. Fuerstenau and Benner reported this effect for 314 nm polystyrene nanoparticles for which the initial velocity in the expansion was as much as 90% of the velocity measured in the detector tube of a single pass CDMS instrument.[40] In contrast, the expansion velocity was just 10% of the measured velocity for smaller DNA and PEG ions. If this initial velocity is not considered, the mass measurements would be lower than the actual mass of the particle. To account for aerodynamic acceleration, Dugourd and coworkers measured the mass of several standard sized nanoparticles to create a calibration curve between measured and actual particle masses.[45, 46]

In the experiments reported here, a narrow range of ion kinetic energies is selected using the trap potential. In order to investigate the effect of aerodynamic acceleration on the mass measurement made at a single trap potential, mass spectra of the 100 nm polystyrene bead sample were obtained at different trap potentials. The size distribution measured at each trapping potential is shown in Figure 3.9. The masses of the ions that are trapped increase with increasing trap potentials. At the lowest potential (300 V), no ions larger than 61 nm were trapped. In contrast, no ions smaller than 78 nm were trapped at the highest potential (390 V). At each trapping potential, only a 6-8 eV/charge range of ion energies is trapped. However, the range of ion energies is nearly 100 eV/charge. Thus, just a fraction of the entire ion distribution is measured at a single trap potential, and the mass and particle kinetic energy are related.

At a given velocity, ion kinetic energy is directly proportional to mass. However, for large globular ions like these nanoparticles, charging and thus the kinetic energy per charge both increase proportionally to the square root of the mass of the ion.[74] A 90 nm ion has approximately six times the mass of a 50 nm ion and therefore has approximately six times the kinetic energy if both ions have the same velocity, but just 2.4 times the charge. An average particle size of 51 nm and 92 nm is trapped at 300 V (Figure 3.9a) and 380 V (Figure 3.9i), respectively. With an electrostatic acceleration of 200 eV/charge, the ions trapped at 300 V have 86 eV/charge initial kinetic energy, and the ions trapped at 380 V have 163 eV/charge initial kinetic energy, 1.9 times more than the smaller particles. This ratio is close to, but less than, the energy per charge difference if the two ions were accelerated to the same initial velocity. This is consistent with the velocity slip increasing with particle size during aerodynamic acceleration.

Due to these energy effects of aerodynamic acceleration, the range of masses that can be measured is heavily influenced by the trap potential. For complex samples containing a broad range of particle sizes or masses, using many trapping voltages is important to effectively measuring the sample distribution. In the future, trapping and collisionally cooling ions before they are introduced into the trap, or increasing collisional cooling of the ions after the ESI source could be used to decouple the effects of aerodynamic acceleration from the ion energy in these trapping experiments.

3.5 Conclusions

A new charge detection mass spectrometer combines a four-tube detector array within a cone trap. Using multiple detector tubes compensates for the slower turning time for the cone trap, so that a similar number of measurements are made in a cone trap and an ion mirror trap with a single detector tube in the same length of time for ions with the same *m/z*. Simulations show that the cone trap has greater tolerance for ions entering the trap off the central axis, can operate at higher pressures, and is more effective for energy selection than the ion mirror trap. The charge measurement uncertainty with this instrument is ±3 charges and ±2 charges for 8 MDa PEG ions trapped for 30 ms and 100 ms, respectively. These charge uncertainties are similar to those reported by Jarrold and coworkers for a similar number of measurements,[64] but somewhat higher than those reported for a similar measurement time[60] due to the higher *m/z* and lower velocity of the high mass PEG ions.

The mass distribution of 8 MDa PEG is centered near the nominal mass of the sample and has a dispersity consistent with measurements made with other analytical techniques.[69, 70] The directly measured charges of intact 8 MDa PEG ions are much lower than previously reported for large PEG ions where charge state resolution was not achieved,[72] bringing into question mechanistic information about ion formation deduced from the earlier data. The size distribution obtained from mass measurements of 100 nm polystyrene nanoparticles indicates the nanoparticles are smaller than reported by the manufacturer, which is consistent with data from TEM images. The mass uncertainty of the 8 MDa PEG and polystyrene nanoparticle ions is approximately 2% and does not depend on mass within this size range. These results indicate single ion CDMS is a useful method for measuring molecular weight distributions of large, heterogeneous, polymer samples. These results also show that aerodynamic acceleration can adversely affect mass measurements when there is a wide range of masses. This can be overcome by trapping or collisionally cooling ions prior to their injection into the trap. Addition of an ion energy filter will decrease the uncertainty in ion energy and will lead to more precise mass measurements.

3.6 Acknowledgements

The authors thank Waters Corporation for their generous donation of equipment, including the Z-spray source used in this work, the Robert D. Ogg Electron Microscope Lab at the University of California, Berkeley for use of the Tecnai 12 transmission electron microscope, and the National Institutes of Health (R01GM096097 and Grant 5F32GM093593-02 for fellowship support for S.I.M) and the Swiss National Science Foundation (Grant P2BSP2_148624 for fellowship support for S.C.) for funding.

3.7 References

(1) Siracusa, V.; Rocculi, P.; Romani, S.; Rosa, M. D. Biodegradable polymers for food packaging: a review. *Trends Food Sci. Technol.* **2008**, *19*, 634-643.

(2) Chen, G. Q.; Patel, M. K. Plastics derived from biological sources: present and future: a technical and environmental review. *Chem. Rev.* **2012**, *112*, 2082-2099.

(3) Kim, J. K.; Yang, S. Y.; Lee, Y.; Kim, Y. Functional nanomaterials based on block copolymer self-assembly. *Prog. Polym. Sci.* **2010**, *35*, 1325-1349.

(4) Rösler, A.; Vandermeulen, G. W. M.; Klok, H. Advanced drug delivery devices via self-assembly of amphiphilic block copolymers. *Adv. Drug Deliv. Rev.* **2012**, *64*, 270-279.

(5) Tyrrell, Z. L.; Shen, Y.; Radosz, M. Fabrication of micellar nanoparticles for drug delivery through the self-assembly of block copolymers. *Prog. Polym. Sci.* **2010**, *35*, 1128-1143.

(6) Alexandridis, P. Amphiphilic copolymers and their applications. *Curr. Opin. Colloid Interface Sci.* **1996**, *1*, 490-501.

(7) Albanese, A.; Tang, P. S.; Chan, W. C. The effect of nanoparticle size, shape, and surface chemistry on biological systems. *Annu. Rev. Biomed. Eng.* **2012**, *14*, 1-16.

(8) Hanton, S. D. Mass Spectrometry of Polymers and Polymer Surfaces. *Chem. Rev.* **2001**, *101*, 527-570.

(9) Gruendling, T.; Weidner, S.; Falkenhagen, J.; Barner-Kowollik, C. Mass spectrometry in polymer chemistry: a state-of-the-art up-date. *Polym. Chem.* **2010**, *1*, 599-617.

(10) Charles, L. MALDI of synthetic polymers with labile end-groups. *Mass Spectrom. Rev.* **2014**, *33*, 523-543.

(11) Lloyd, P.; Duddaby, K.; Varney, J.; Scrivener, E.; Derrick, P.; Haddleton, D. A comparison between matrix-assisted laser desorption/ionisation time-of-flight mass spectrometry and size exclusion chromatography in the mass characterisation of synthetic polymers with narrow molecular-mass distributions: Poly(methyl methacrylate) and poly(styrene). *Eur. J. Mass Spectrom.* **1995**, *1*, 293-300.

(12) Martin, K.; Spickermann, J.; Rader, H. J.; Mullen, K. Why Does Matrix-assisted Laser Desorption/Ionization Time-of-flight Mass Spectrometry Give Incorrect Results for Broad Polymer Distributions? *Rapid Commun. Mass Spectrom.* **1996**, *10*, 1471-1474.

(13) Sakurada, N.; Fukuo, T.; Arakawa, R.; Ute, K.; Hatada, K. Characterization of poly(methyl methacrylate) by matrix-assisted laser desorption/ionization mass spectrometry. A comparison with supercritical fluid chromatography and gel permeation chromatography. *Rapid Commun. Mass Spectrom.* **1998**, *12*, 1895-1898.

(14) Schriemer, D. C.; Li, L. Detection of High Molecular Weight Narrow Polydisperse Polymers up to 1.5 Million Daltons by MALDI Mass Spectrometry. *Anal. Chem.* **1996**, *68*, 2721-2725.

(15) Wenzel, R. J.; Matter, U.; Schultheis, L.; Zenobi, R. Analysis of megadalton ions using cryodetection MALDI time-of-flight mass spectrometry. *Anal. Chem.* **2005**, *77*, 4329-4337.

(16) Aksenov, A. A.; Bier, M. E. The analysis of polystyrene and polystyrene aggregates into the mega dalton mass range by cryodetection MALDI TOF MS. *J. Am. Soc. Mass Spectrom.* **2008**, *19*, 219-230.

(17) Chen, X. Y.; Westphall, M. S.; Smith, L. M. Mass spectrometric analysis of DNA mixtures: Instrumental effects responsible for decreased sensitivity with increasing mass. *Anal. Chem.* **2003**, *75*, 5944-5952.

(18) Plath, L. D.; Ozdemir, A.; Aksenov, A. A.; Bier, M. E. Determination of Iron Content and Dispersity of Intact Ferritin by Superconducting Tunnel Junction Cryodetection Mass Spectrometry. *Anal. Chem.* **2015**, *87*, 8985-8993.

(19) Snijder, J.; Rose, R. J.; Veesler, D.; Johnson, J. E.; Heck, A. J. Studying 18 MDa virus assemblies with native mass spectrometry. *Angew. Chem., Int. Ed.* **2013**, *52*, 4020-4023.

(20) O'Connor, P. B.; McLafferty, F. W. Oligomer characterization of 4-23 kDa polymers by electrospray Fourier transform mass spectrometry. *J. Am. Chem. Soc.* **1995**, *117*, 12826-12831.

(21) Wuerker, R. F.; Shelton, H.; Langmuir, R. V. Electrodynamic containment of charged particles. *J. Appl. Phys.* **1959**, *30*, 342-349.

(22) Philip, M. A.; Gelbard, F.; Arnold, S. An absolute method for aerosol particle mass and charge measurement. *J. Colloid Interface Sci.* **1983**, *91*, 507-515.

(23) Hars, G.; Tass, Z. Application of quadrupole ion trap for the accurate mass determination of submicron size charged particles. *J. Appl. Phys.* **1995**, *77*, 4245-4250.

(24) Schlemmer, S.; Illemann, J.; Wellert, S.; Gerlich, D. Nondestructive high-resolution and absolute mass determination of single charged particles in a three-dimensional quadrupole trap. *J. Appl. Phys.* **2001**, *90*, 5410-5418.

(25) Nie, Z.; Tzeng, Y.; Chang, H.; Chiu, C.; Chang, C.; Chang, C.; Tao, M. Microscopy-based Mass Measurement of a Single Whole Virus in a Cylindrical Ion Trap. *Angew. Chem., Int. Ed.* **2006**, *45*, 8131-8134.

(26) Cai, Y.; Peng, W. P.; Kuo, S. J.; Lee, Y. T.; Chang, H. C. Single-particle mass spectrometry of polystyrene microspheres and diamond nanocrystals. *Anal. Chem.* **2002**, *74*, 232-238.

(27) Smith, R. D.; Cheng, X.; Brace, J. E.; Hofstadler, S. A.; Anderson, G. A. Trapping, detection and reaction of very large single molecular ions by mass spectrometry. *Nature* **1994**, *369*, 137-139.

(28) Cheng, X.; Bakhtiar, R.; Van Orden, S.; Smith, R. D. Charge-state shifting of individual multiply-charged ions of bovine albumin dimer and molecular weight determination using an individual-ion approach. *Anal. Chem.* **1994**, *66*, 2084-2087.

(29) Bruce, J. E.; Cheng, X.; Bakhtiar, R.; Wu, Q.; Hofstadler, S. A.; Anderson, G. A.; Smith, R. D. Trapping, detection, and mass measurement of individual ions in a Fourier transform ion cyclotron resonance mass spectrometer. *J. Am. Chem. Soc.* **1994**, *116*, 7839-7847.

(30) Chen, R.; Wu, Q.; Mitchell, D. W.; Hofstadler, S. A.; Rockwood, A. L.; Smith, R. D. Direct charge number and molecular weight determination of large individual ions by electrospray ionization Fourier transform ion cyclotron resonance mass spectrometry. *Anal. Chem.* **1994**, *66*, 3964-3969.

(31) Chen, R.; Cheng, X.; Mitchell, D. W.; Hofstadler, S. A.; Wu, Q.; Rockwood, A. L.; Sherman, M. G.; Smith, R. D. Trapping, detection, and mass determination of coliphage T4 DNA ions by electrospray ionization Fourier transform ion cyclotron resonance mass spectrometry. *Anal. Chem.* **1995**, *67*, 1159-1163.

(32) Makarov, A.; Denisov, E. Dynamics of ions of intact proteins in the Orbitrap mass analyzer. *J. Am. Soc. Mass Spectrom.* **2009**, *20*, 1486-1495.

(33) Rose, R. J.; Damoc, E.; Denisov, E.; Makarov, A.; Heck, A. J. High-sensitivity Orbitrap mass analysis of intact macromolecular assemblies. *Nat. Methods.* **2012**, *9*, 1084-1086.

(34) Marshall, A. G.; Hendrickson, C. L.; Jackson, G. S. Fourier Transform Ion Cyclotron Resonance Mass Spectrometry: A Primer. *Mass Spectrom. Rev.* **1998**, *17*, 1-35.

(35) Makarov, A. Electrostatic Axially Harmonic Orbital Trapping: A High-Performance Technique of Mass Analysis. *Anal. Chem.* **2000**, *72*, 1156-1162.

(36) Shelton, H.; Hendricks, C. D.; Wuerker, R. F. Electrostatic Acceleration of Microparticles to Hypervelocities. *J. Appl. Phys.* **1960**, *31*, 1243-1246.

(37) Hendricks Jr., C. D. Charged droplet experiments. *J. Colloid Sci.* **1962**, *17*, 249-259.

(38) Keaton, P. W.; Idzorek, G. C.; Rowton Sr., L. J.; Seagrave, J. D.; Stradling, G. L.; Bergeson, S. D.; Collopy, M. T.; Curling Jr., H. L.; McColl, D. B.; Smith, J. D. A hypervelocity - microparticle - impacts laboratory with 100-km/s projectiles. *Int. J. Impact Eng.* **1990**, *10*, 295-308.

(39) Stradling, G. L.; Idzorek, G. C.; Shafer, B. P.; Curling Jr., H. L.; Collopy, M. T.; Blossom, A. A. H.; Fuerstenau, S. Ultra-high velocity impacts: cratering studies of microscopic impacts from 3 km/s to 30 km/s. *Int. J. Impact Eng.* **1993**, *14*, 719-727.

(40) Fuerstenau, S. D.; Benner, W. H. Molecular Weight Determination of Megadalton DNA Electrospray Ions Using Charge Detection Time-of-Flight Mass Spectrometry. *Rapid Commun. Mass Spectrom.* **1995**, *9*, 1528-1538.

(41) Fuerstenau, S. D.; Benner, W. H.; Thomas, J. J.; Brugidou, C.; Bothner, B.; Siuzdak, G. Mass spectrometry of an intact virus. *Angew. Chem., Int. Ed.* **2001**, *40*, 542-544.

(42) Maze, J. T.; Jones, T. C.; Jarrold, M. F. Negative Droplets from Positive Electrospray. *J. Phys. Chem. A.* **2006**, *110*, 12607-12612.

(43) Doussineau, T.; Kerleroux, M.; Dagany, X.; Clavier, C.; Barbaire, M.; Maurelli, J.; Antoine, R.; Dugourd, P. Charging megadalton poly(ethylene oxide)s by electrospray ionization. A charge detection mass spectrometry study. *Rapid Commun. Mass Spectrom.* **2011**, *25*, 617-623.

(44) Doussineau, T.; Bao, C. Y.; Antoine, R.; Dugourd, P.; Zhang, W.; D'Agosto, F.; Charleux, B. Direct Molar Mass Determination of Self-Assembled Amphiphilic Block Copolymer Nanoobjects Using Electrospray-Charge Detection Mass Spectrometry. *ACS Macro Lett.* **2012**, *1*, 414-417.

(45) Ouadah, N.; Doussineau, T.; Hamada, T.; Dugourd, P.; Bordes, C.; Antoine, R. Correlation between the charge of polymer particles in solution and in the gas phase investigated by zeta-potential measurements and electrospray ionization mass spectrometry. *Langmuir.* **2013**, *29*, 14074-14081.

(46) Doussineau, T.; Désert, A.; Lambert, O.; Taveau, J.; Lansalot, M.; Dugourd, P.; Bourgeat-Lami, E.; Ravaine, S.; Duguet, E.; Antoine, R. Charge Detection Mass Spectrometry for the Characterization of Mass and Surface Area of Composite Nanoparticles. *J. Phys. Chem. C.* **2015**, *119*, 10844-10849.

(47) Viodé, A.; Dagany, X.; Kerleroux, M.; Dugourd, P.; Doussineau, T.; Charles, L.; Antoine, R. Coupling of size-exclusion chromatography with electrospray ionization charge-detection mass spectrometry for the characterization of synthetic polymers of ultra-high molar mass. *Rapid Commun. Mass Spectrom.* **2016**, *30*, 132-136.

(48) Gamero-Castaño, M. Induction charge detector with multiple sensing stages. *Rev. Sci. Instrum.* **2007**, *78*, 043301.

(49) Smith, J. W.; Siegel, E. E.; Maze, J. T.; Jarrold, M. F. Image Charge Detection Mass Spectrometry: Pushing the Envelope with Sensitivity and Accuracy. *Anal. Chem.* **2011**, *83*, 950-956.

(50) Barney, B. L.; Daly, R. T.; Austin, D. E. A multi-stage image charge detector made from printed circuit boards. *Rev. Sci. Instrum.* **2013**, *84*, 114101.

(51) Grix, R.; Kutscher, R.; Li, G.; Grüner, U.; Wollnik, H.; Matsuda, H. A time-of-flight mass analyzer with high resolving power. *Rapid Commun. Mass Spectrom.* **1988**, *2*, 83-85.

(52) Zajfman, D.; Heber, O.; Vejby-Christensen, L.; Ben-Itzhak, I.; Rappaport, M.; Fishman, R.; Dahan, M. Electrostatic bottle for long-time storage of fast ion beams. *Phys. Rev. A.* **1997**, *55*, R1580.

(53) Ring, S.; Pedersen, H. B.; Heber, O.; Rappaport, M. L.; Witte, P. D.; Bhushan, K. G.; Altstein, N.; Rudich, Y.; Sagi, I.; Zajfman, D. Fourier transform time-of flight mass spectrometry in an electrostatic ion beam trap. *Anal. Chem.* **2000**, *72*, 4041-4046.

(54) Zajfman, D.; Rudich, Y.; Sagi, I.; Strasser, D.; Savin, D. W.; Goldberg, S.; Rappaport, M.; Heber, O. High resolution mass spectrometry using a linear electrostatic ion beam trap. *Int. J. Mass Spectrom.* **2003**, *229*, 55-60.

(55) Hilger, R. T.; Santini, R. E.; McLuckey, S. A. Nondestructive Tandem Mass Spectrometry Using a Linear Quadrupole Ion Trap Coupled to a Linear Electrostatic Ion Trap. *Anal. Chem.* **2013**, *85*, 5226-5232.

(56) Benner, W. H. A Gated Electrostatic Ion Trap to Repetitiously Measure the Charge and m/z of Large Electrospray Ions. *Anal. Chem.* **1997**, *69*, 4162-4168.

(57) Doussineau, T.; Yu Bao, C.; Clavier, C.; Dagany, X.; Kerleroux, M.; Antoine, R.; Dugourd, P. Infrared multiphoton dissociation tandem charge detection-mass spectrometry of single megadalton electrosprayed ions. *Rev. Sci. Instrum.* **2011**, *82*, 084104.

(58) Doussineau, T.; Antoine, R.; Santacreu, M.; Dugourd, P. Pushing the Limit of Infrared Multiphoton Dissociation to Megadalton-Size DNA Ions. *J. Phys. Chem. Lett.* **2012**, *3*, 2141-2145.

(59) Antoine, R.; Doussineau, T.; Dugourd, P.; Calvo, F. Multiphoton dissociation of macromolecular ions at the single-molecule level. *Phys. Rev. A.* **2013**, *87*, 013435.

(60) Pierson, E. E.; Contino, N. C.; Keifer, D. Z.; Jarrold, M. F. Charge Detection Mass Spectrometry for Single Ions with an Uncertainty in the Charge Measurement of 0.65 e. *J. Am. Soc. Mass Spectrom.* **2015**, *26*, 1213-1220.

(61) Contino, N. C.; Jarrold, M. F. Charge detection mass spectrometry for single ions with a limit of detection of 30 charges. *Int. J. Mass Spectrom.* **2013**, *345-347*, 153-159.

(62) Contino, N. C.; Pierson, E. E.; Keifer, D. Z.; Jarrold, M. F. Charge Detection Mass Spectrometry with Resolved Charge States. *J. Am. Soc. Mass Spectrom.* **2013**, *24*, 101-108.

(63) Keifer, D. Z.; Shinholt, D. L.; Jarrold, M. F. Charge Detection Mass Spectrometry with Almost Perfect Charge Accuracy. *Anal. Chem.* **2015**, *87*, 10330-10337.

(64) Pierson, E. E.; Keifer, D. Z.; Contino, N. C.; Jarrold, M. F. Probing higher order multimers of pyruvate kinase with charge detection mass spectrometry *Int. J. Mass Spectrom.* **2013**, *337*, 50-56.

(65) Keifer, D. Z.; Pierson, E. E.; Hogan, J. A.; Bedwell, G. J.; Prevelige, P. E.; Jarrold, M. F. Charge detection mass spectrometry of bacteriophage P22 procapsid distributions above 20 MDa. *Rapid Commun. Mass Spectrom.* **2014**, *28*, 483-488.

(66) Pierson, E. E.; Keifer, D. Z.; Selzer, L.; Lee, L. S.; Contino, N. C.; Wang, J. C. -.; Zlotnick, A.; Jarrold, M. F. Detection of Late Intermediates in Virus Capsid Assembly by Charge Detection Mass Spectrometry. *J. Am. Chem. Soc.* **2014**, *136*, 3536-3541.

(67) Pierson, E. E.; Keifer, D. Z.; Asokan, A.; Jarrold, M. F. Resolving Adeno-Associated Viral Particle Diversity with Charge Detection Mass Spectrometry. *Anal. Chem.* **2016**, *88*, 6718-6725.

(68) Schmidt, H. T.; Cederquist, H.; Jensen, J.; Fardi, A. Conetrap: A compact electrostatic ion trap. *Nucl. Instr. and Meth. in Phys. Res. B.* **2001**, *173*, 523-527.

(69) Chen, X. L.; Jenekhe, S. A. Solubilization and encapsulation of fullerenes by amphiphilic block copolymers. *Langmuir.* **1999**, *15*, 8007-8017.

(70) Kremer, M.; Pothmann, E.; Roessler, T.; Baker, J.; Yee, A.; Blanch, H.; Prausnitz, J. M. Pore-size distributions of cationic polyacrylamide hydrogels varying in initial monomer concentration and cross-linker/monomer ratio. *Macromolecules.* **1994**, *27*, 2965-2973.

(71) Wong, S. F.; Meng, C. K.; Fenn, J. B. Multiple charging in electrospray ionization of poly(ethylene glycols). *J. Phys. Chem.* **1988**, *92*, 546-550.

(72) Nohmi, T.; Fenn, J. B. Electrospray mass spectrometry of poly(ethylene glycols) with molecular weights up to five million. *J. Am. Chem. Soc.* **1992**, *114*, 3241-3246.

(73) Becker, E. W.; Bier, K.; Henkes, W. Strahlen aus kondensierten Atomen und Molekeln im Hochvakuum. *Z. Physik.* **1956**, *146*, 333-338.

(74) Fernandez de la Mora, J. Electrospray ionization of large multiply charged species proceeds via Dole's charged residue mechanism. *Anal. Chim. Acta.* **2000**, *406*, 93-104.

3.8 Figures

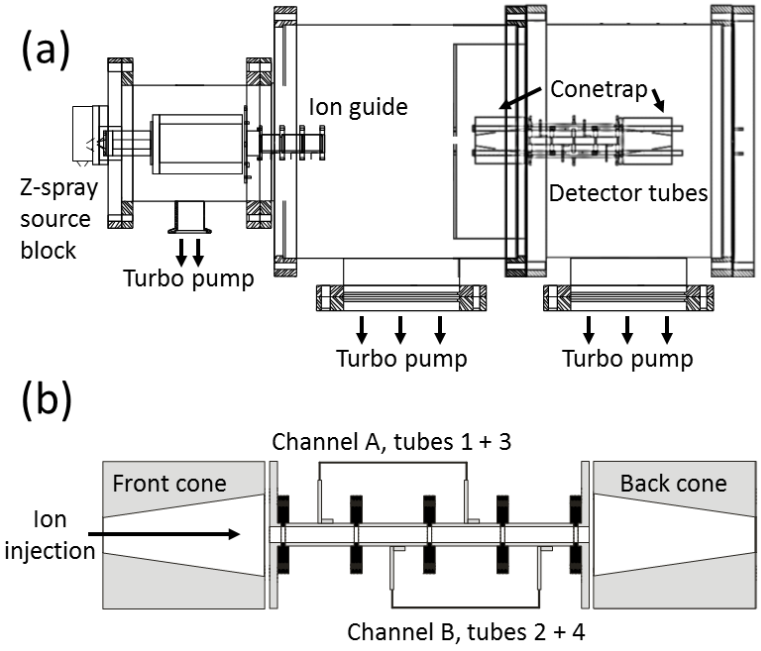

Figure 3.1: Schematic diagrams of a) the single particle analyzer of mass (SPAM) instrument and b) the combined ion trap and detector array.

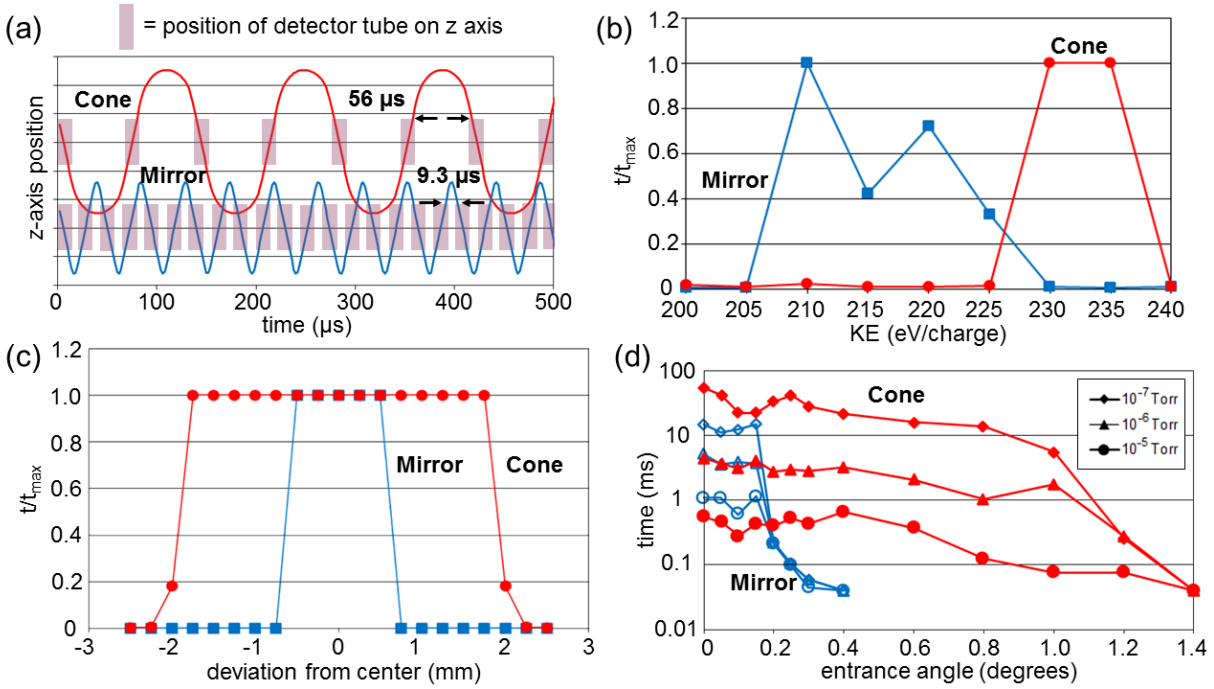

Figure 3.2: Comparison of trapping performance of cone trap and electrostatic ion trap (EIT), showing a) position of the ion inside the two traps as a function of time, b) the length of time an ion is trapped relative to the maximum trapping time of 50 ms at different trapping voltages, and c) entrance radii, and d) the length of time an ion is trapped for at different entrance angles at pressures of 10^{-5}, 10^{-6}, and 10^{-7} Torr.

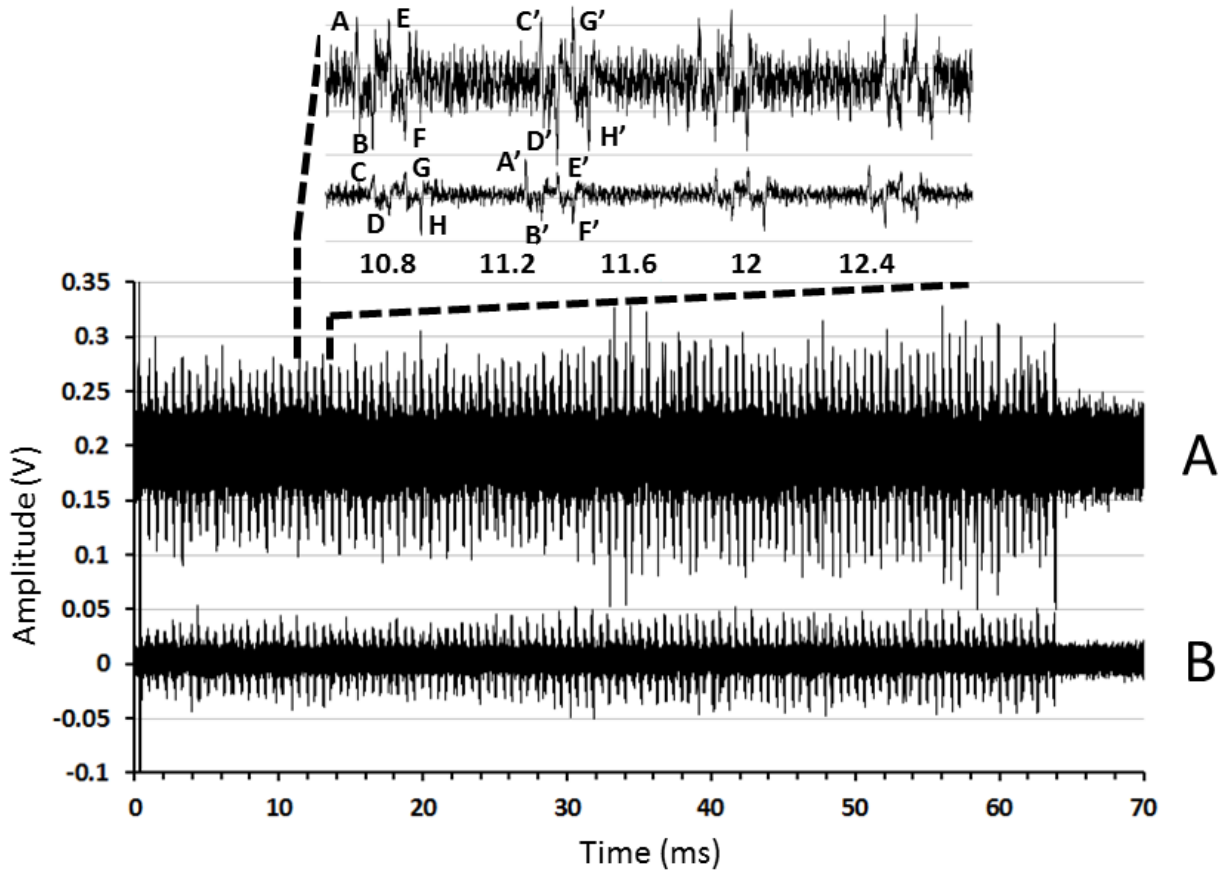

Figure 3.3: Transient recorded for a single polystyrene nanoparticle ion that was trapped for 63 ms. The upper transient shows the data from channel A, and the lower transient the data from channel B. The inset is an expansion of both channels between 10.6 ms and 12.75 ms.

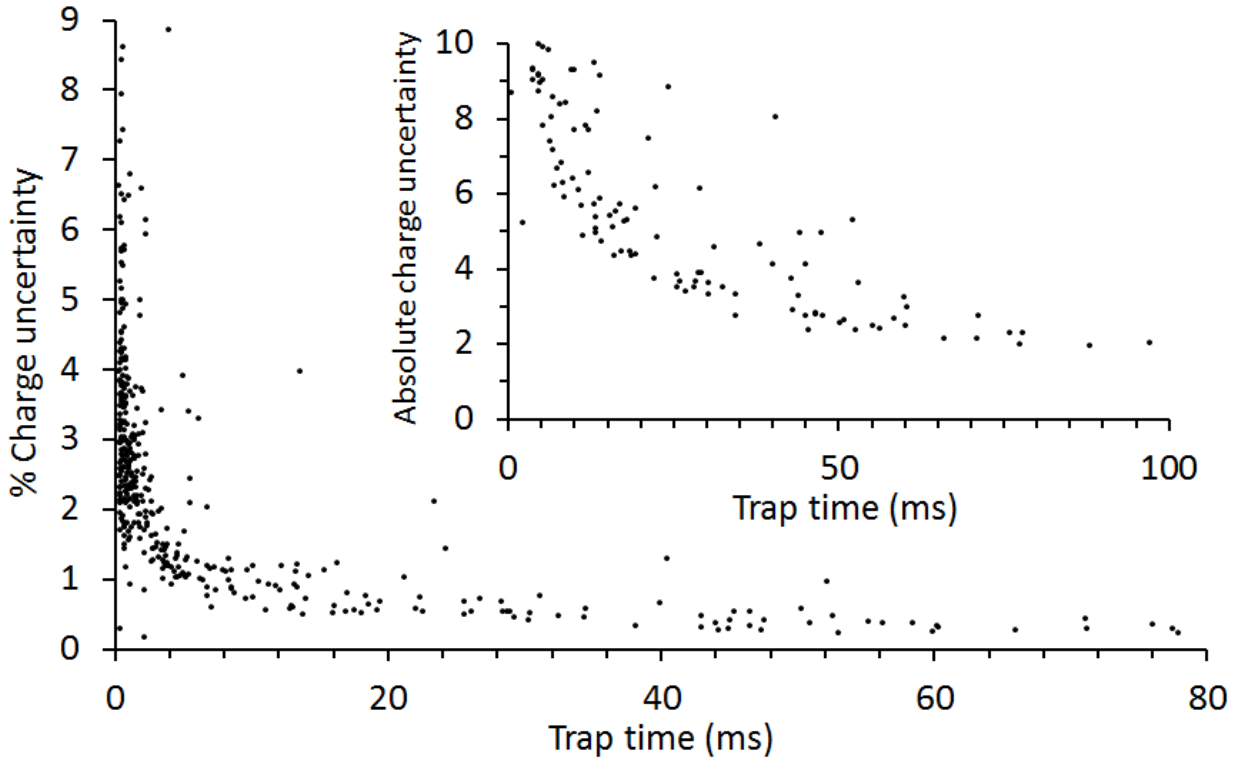

Figure 3.4: Data showing percent uncertainty in measured charge versus the length of ion trapping time for 376 PEG ions with a nominal 8 MDa mass. The inset shows the trapping time of all ions with an absolute charge uncertainty less than 10 charges, as low as 2 charges for ions trapped for approximately 100 ms.

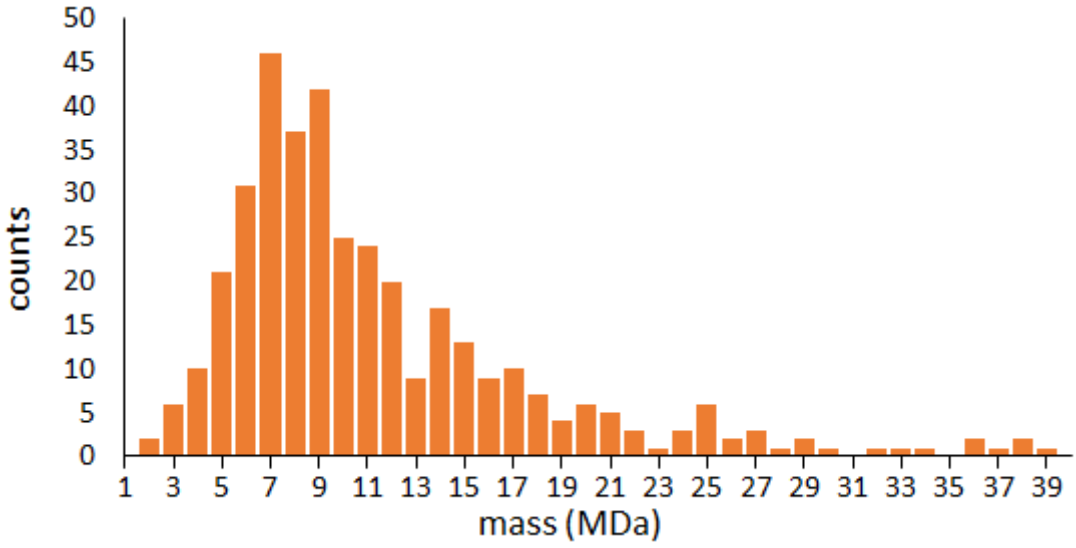

Figure 3.5: Histogram of 376 PEG ion masses making up a mass spectrum of a sample of nominal molecular weight 8 MDa.

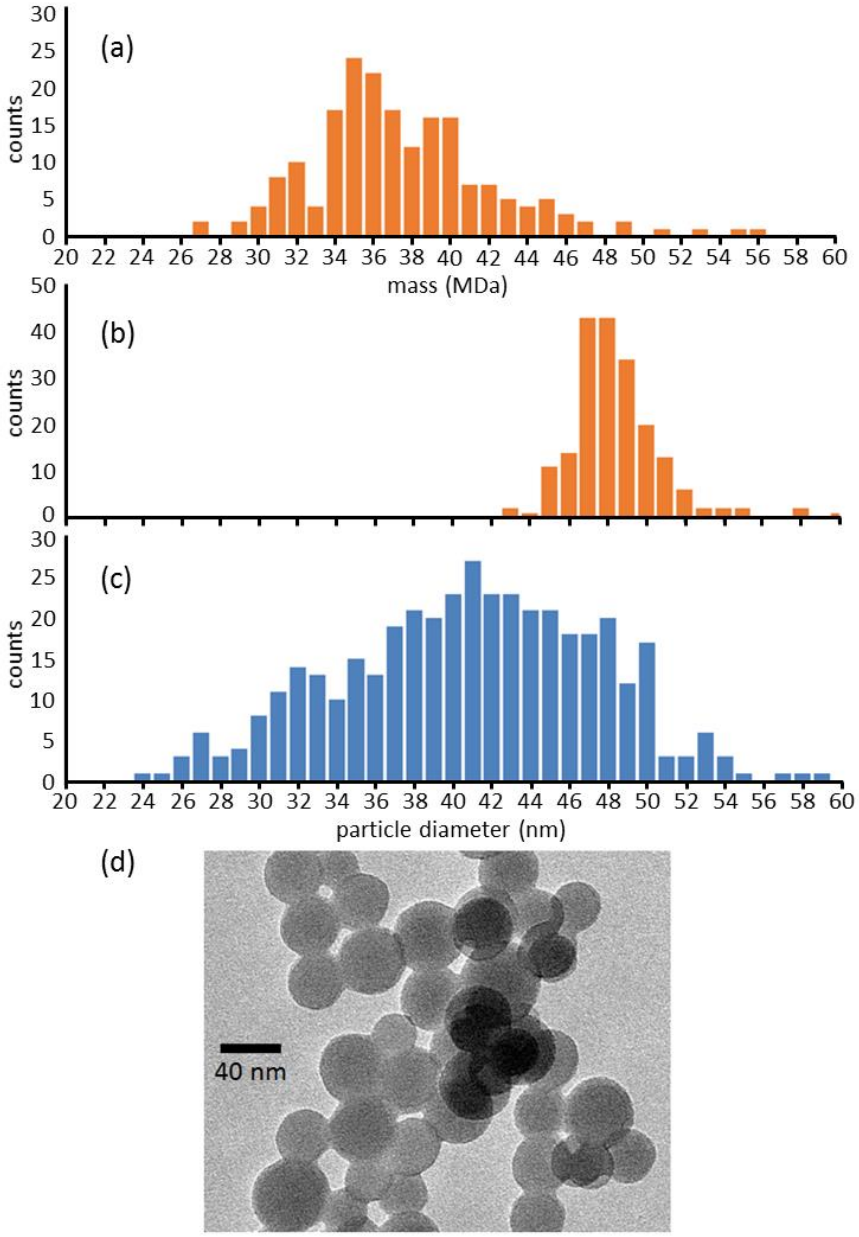

Figure 3.6: Data from a nominal 50 nm amine-modified polystyrene nanoparticle sample: a) mass spectrum measured with SPAM, b) size distribution determined from mass spectrum, c) size distribution determined from TEM images, and d) TEM image of the nanoparticle sample.

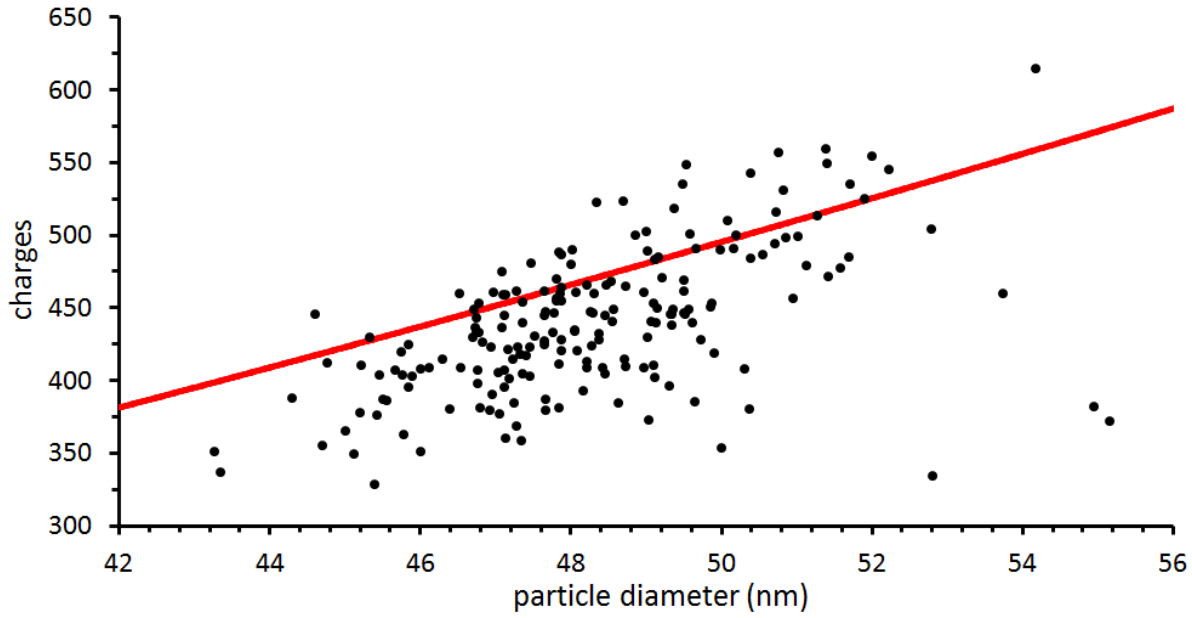

Figure 3.7: Measured charge of ions from the 50 nm nanoparticle sample versus their diameter determined from the mass data obtained with SPAM. The line shows the Rayleigh limit charge for a water droplet of a given size. Relatively few ions are detected below ~400 charges, indicating the threshold for detecting an ion from a single induced signal.

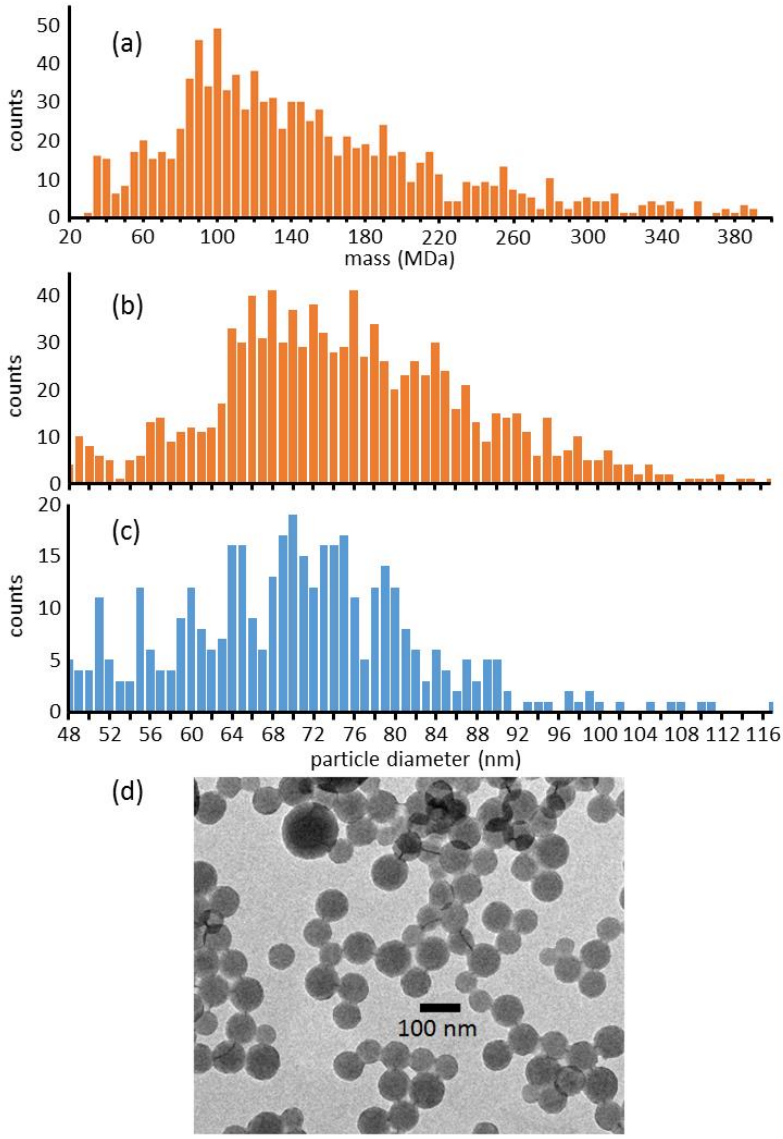

Figure 3.8: Data from a nominal 100 nm amine-modified polystyrene nanoparticle sample: a) mass spectrum measured by SPAM, b) size distribution determined from the mass spectrum, c) size distribution determined from TEM images, d) relative trapping rate at each particle size, e) TEM image of the nanoparticle sample.

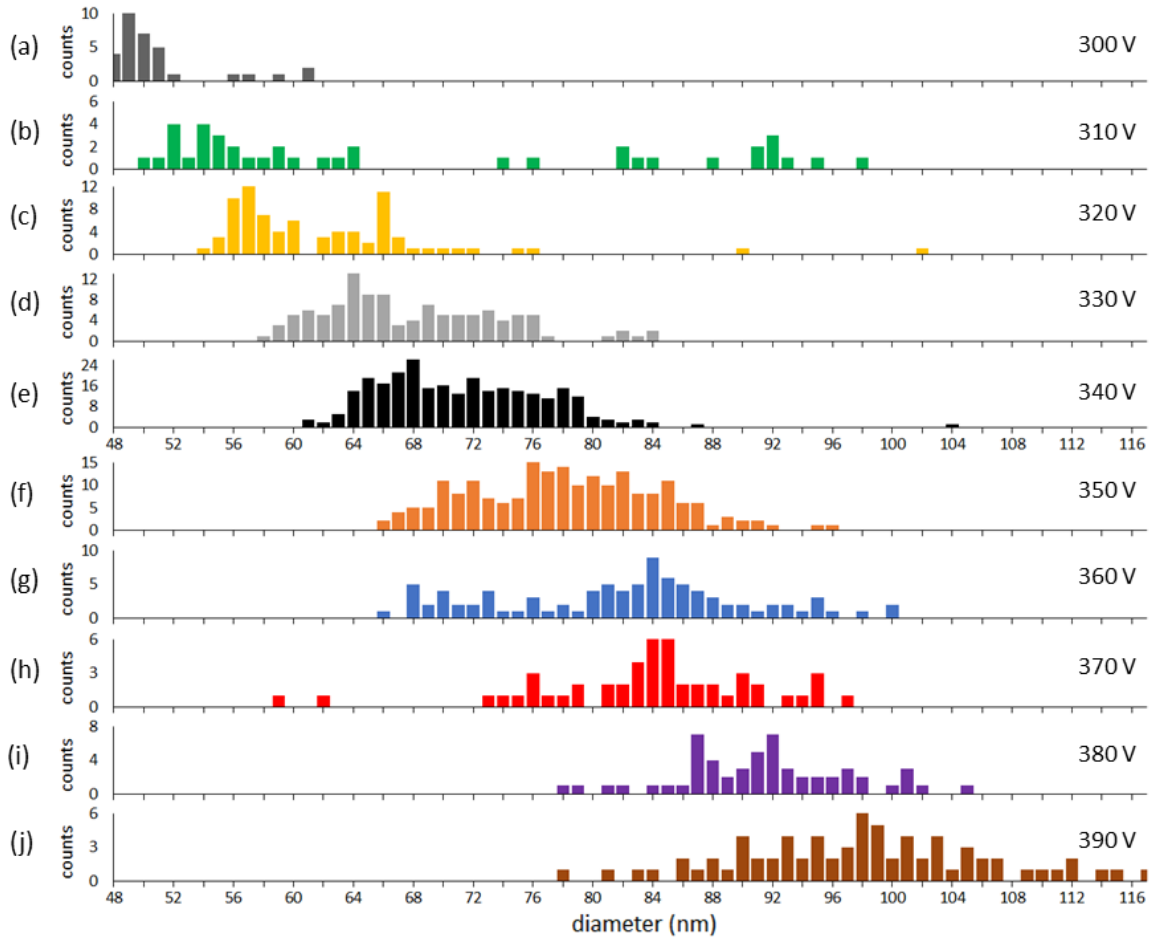

Figure 3.9: Size distribution of ions from a nominal 100 nm amine-modified polystyrene nanoparticle sample measured at different trapping voltages, a) 300 V, b) 310 V, c) 320 V, d) 330 V, e) 340 V, f) 350 V, g) 360 V, h) 370 V, i) 380 V, and j) 390 V.

Chapter 4

Mass, Mobility and MS^n Measurements of Single Ions Using Charge Detection Mass Spectrometry

This chapter is reproduced with permission from:

Andrew G. Elliott, Conner C. Harper, Haw-Wei Lin, Evan R. Williams

"Mass, Mobility and MS^n Measurements of Single Ions Using Charge Detection Mass Spectrometry" *Analyst* **2017**, *142* (15), 2760-2769

4.1 Abstract

Charge detection mass spectrometry is used to measure the mass, charge, MS^n and mobility of an individual ion produced by electrospray ionization of an 8 MDa polyethylene glycol sample. The charge detection mass spectrometer is an electrostatic ion trap that uses cone electrodes and a single tube detector and can detect ions for up to the full trapping time of 4.0 s. The time-domain signal induced on the detector tube by a single multiply charged ion can be complex owing to sequential fragmentation of the original precursor ion as well as increasing oscillation frequencies of the single ion owing to collisions with background gas that reduce the kinetic energy of the ion inside the trap. Simulations show that the ratio of the time for the ion to turn around inside the cone region of the trap to the time for the ion to travel through the detector tube is constant with *m*/*z* and increases with the ion energy per charge. By measuring this ratio, the kinetic energy of an ion can be obtained with good precision (~1%) and this method to measure ion kinetic energies eliminates the necessity of ion energy selection prior to trapping for high precision mass measurement of large molecules in complex mixtures. This method also makes it possible to measure the masses of each sequential fragment ion formed from the original precursor ion. MS^7 of a single multiply charged PEG molecule is demonstrated, and from these ion energy measurements and effects of collisions on the ion motion inside the trap, information about the ion mobility of the precursor ion and its fragments is obtained.

4.2 Introduction

Mass spectrometry (MS) is widely used to obtain the masses of large molecules, macromolecular complexes,[1, 2] as well as to probe binding affinities[3] and the kinetics or thermodynamics of protein complex assembly.[4, 5] Tandem MS can provide information about protein identity and structural information about molecular subunits in a complex.[6-8] In combination with ion mobility spectrometry (IMS), information about the shapes of molecules and their arrangements in a complex can be obtained.[9-11] Samples consisting of a heterogeneous mixture of components, particularly those with molecular masses beyond ~1 MDa, can be

challenging to analyze with MS. With electrospray ionization (ESI), the charge states of large ions are typically determined from the *m*/*z* spacing between adjacent peaks in the charge-state distribution of a molecule. Heterogeneity in the sample or in the ion population due to salt or other non-specific molecular interactions can lead to overlapping charge states that can be difficult or impossible to resolve. Charge-state resolution has been attained for highly purified samples of virus capsids as large as 18 MDa,[12] but the masses of more heterogeneous native viruses are more difficult to effectively measure with MS owing to spectral overlap.[13] High molecular weight synthetic polymers, such as polyethylene glycol, can be especially challenging to analyze owing to the large number of molecular masses in a single sample.[14-19] Without charge-state resolution, molecular weight can be roughly estimated from the *m*/*z* range of the charge-state distribution for a highly purified sample assuming that the molecules have nearly spherical structures.[20]

One solution to this problem of sample heterogeneity for high mass ions is to measure the charge as well as the *m*/*z* of an isolated single ion so that the mass of the ion can be determined without interference from other ions. Information about the masses of molecules in the sample can be obtained from many repeated measurements of individual or single ions. Several techniques for weighing single multiply charged ions have been developed that rely on either changing the charge of the ion between *m*/*z* measurements thereby producing a charge-state distribution that originates from a single precursor ion or by measuring the charge directly from current induced by the ion as it passes near a detection electrode. The charge shifting method has been implemented with quadrupole ion trap (QIT) instruments that detect ions using light scattering or fluorescence[21-26] and Fourier-transform ion cyclotron resonance (FT-ICR) instruments.[27, 28] These techniques are capable of very high precision mass measurements of single ions, but the process for weighing individual ions can be slow. The charge of single ions has also been measured directly from the amplitude of the induced current with FT-ICR MS, which depends on the position of the ion in the cell so that careful calibration of ion excitation radius is required for each ion.[29]

Another way to directly measure the charge and mass of a single multiply charged ion is to use charge detection mass spectrometry (CDMS). In CDMS, an ion passes through a conductive tube inducing a signal from which the velocity and charge of the ion is determined from the duration and amplitude of the charge pulse, respectively.[30] The *m*/*z* of the ion is determined from its velocity and energy per charge, and the mass is determined from the *m*/*z* and charge. CDMS was first used in the 1960s to measure the masses of micron sized cosmic dust particles[30-33] and has since been used to measure the masses of viruses,[34] DNA,[35, 36] and a wide variety of synthetic polymers and nanoparticles.[18, 35, 37-40] This basic single tube CDMS is much faster than the FT-ICR and QIT techniques for single ions because each ion is measured in the few microseconds it takes to pass once through the detector tube, but the measurement of mass is much less precise.[34]

Recent developments in CDMS have improved the uncertainty in the mass and charge measurements by repeatedly measuring a single ion. Benner first demonstrated this technique by using an electrostatic dual ion mirror trap to reflect ions through the charge detector many times.[41] Ions were trapped for up to 10 ms, during which time they made up to 450 passes through the detection electrode, which reduced the charge uncertainty to ±2.3 charges. Jarrold and coworkers have reported further improvements to the charge measurement accuracy, down to ±0.196 charges, with cryogenic cooling of the detector[42] and extending the trapping time to 6×10^4 cycles in 3 s.[43] They also demonstrated a limit of detection of seven charges, which was achieved by analyzing CDMS data with a Fourier transform (FT).[43-45] With these improvements, they have used CDMS to obtain mass spectra of large protein complexes and viruses with much greater

resolution and accuracy than was previously possible.[43, 45-51] Dugourd and coworkers have also demonstrated an ion trapping CDMS instrument, which they used to investigate the photodissociation of mass selected PEG and DNA ions.[52-55] However, only the rate of dissociation of the ions was obtained because fragment ions were quickly lost from the trap. Anderson and coworkers have also measured rates of mass loss from individual quantum dots in a QIT.[56] The CDMS ion trap design has also been combined with an array detector and used to measure the mass of synthetic polymers and nanoparticles.[19]

Recently, Jarrold and co-workers showed that signals induced by a single hepatitis B virus capsid trapped in CDMS can gradually shift in frequency with time as a result of collisions with background gas and a change in mass which they attribute to solvent loss.[57] In addition, they found that the oscillation frequency of some of the trapped ions can change suddenly as a result of fragmentation. By comparing frequency shifts measured for a large number of ions with results from ion simulations, they deduced that these ions lost a single charge and about 1000 Da in mass. They attributed this fragmentation to loss of a singly charged solvent cluster and suggested that this fragmentation process was induced by the electric fields inside the trap.

Here, we demonstrate a CDMS instrument for MS^n and ion mobility measurements on a single multiply charged ion that we call a single particle analyzer of mass and mobility (SPAMM). This instrument uses electrospray ionization, two quadrupole ion guides, a turning quadrupole that makes possible ion energy selection, and an electrostatic ion trap consisting of a single detector tube and two cone electrodes. Simulations show that both the time it takes an ion to turn around in the cone region of the trap and the time it takes an ion to pass through the detection tube depend on ion energy. The ratio between the turnaround time and the time to travel through the tube is independent of mass and m/z but does depend on the ion energy per charge. By measuring this ratio, the energy and mass of a single ion can be determined even for ions that lose energy with time or for ions that fragment inside the trap. This makes it possible to determine the masses of sequential fragment ions formed from the initial precursor ion thereby enabling MS^n measurements of single multiply charged ions. From the energy lost via collisions with background gas in the trap, information about the ion mobility is obtained.

4.3 Experimental

Polyethylene glycol (PEG) with a nominal molecular weight of 8 MDa was obtained from Sigma Aldrich (St Louis, MO, USA) and prepared at a concentration of 60 nM in a 1:1 water-methanol solution. Experiments were performed using the single particle analyzer of mass and mobility (SPAMM), a home-built charge detection mass spectrometer (Figure 4.1). Ions are formed by nanoelectrospray ionization and transferred to vacuum using a modified Z-spray source (Waters, Milford, MA). Ions are guided through the next vacuum stages by a pair of RF-only quadrupole ion guides and an energy selective electrostatic turning quadrupole (both Ardara Technologies, Ardara, PA). The offset potential of +204 V in the first ion guide defines the nominal energy of the ions. Ions are then accelerated though a 1.0 mm conductance limit into a final vacuum chamber with a pressure of 5×10^{-9} Torr where they are trapped and detected. The detection system is a modified version of a design described elsewhere,[19] with one detector tube inside a cone trap instead of four. The trapping potential is set to +330 V and a triggered trapping scheme is used. An ion entering a detector tube induces an image charge of opposite sign on the tube which is inverted and shaped to produce a leading positive peak and trailing negative peak for a positive ion. The amplitude of each peak is proportional to the charge of the ion, and the

spacing between the peaks is proportional to the velocity of the ion.[19] Data is analyzed with a program designed to find peaks of a consistent size and spacing that is described in detail elsewhere.[19] Additional experimental detail is provided in Supporting Information.

4.4 Results and Discussion

4.4.1 Transient Signal of Polyethylene Glycol at Long Trap Times

Trapping an individual ion and measuring its induced signal for a long time can increase the accuracy with which the charge and mass of the ion can be measured. For example, Jarrold and coworkers reported a charge uncertainty for pyruvate kinase of ±0.65 and ±0.196 for measurement times of 400 ms[45] and 3 s,[43] respectively. However, both the frequency and the intensity of the signal for an individual ion in an electrostatic CDMS instrument can change with time,[52, 57] making analysis of the resulting time-domain data more complex. This effect is illustrated in Figure 4.2, which shows the induced signal from an ion formed from an 8 MDa PEG sample that was trapped for the entire set trapping time of 4.0 s. Although signal persists for the entire 4.0 s transient, the signal amplitude decreases significantly at 2.27 s and 2.48 s. This occurs due to ion fragmentation, which lowers both the charge and the mass of the remaining trapped fragment ion. The fragment formed at 2.48 s was trapped for the remainder of the recording time, indicating that fragment ions can remain on a stable trajectory in the trap even after multiple fragmentation events occur. Although only a single product ion is trapped after each fragmentation event, two product ions resulting from a single cleavage of a multiply charged ion have been trapped for other ions. Fragmentation and subsequent product ion trapping occurs in the first 100 ms for approximately 5% of the PEG ions that are trapped for at least two cycles. Fragmentation at early times may be due to metastable dissociation as a result of collisions prior to trapping, but at longer times, fragmentation is likely induced by collisions with background gases inside the trap that can effectively compete with ion cooling by radiative emission.[58]

The oscillation frequency of the ions inside the trap changes with time (Figure 4.2, top). For example, the precursor ion completes 7 passes in a 250 μs window 5 ms into the transient but makes 8 passes through the trap in the same time period two seconds later (Figure 4.2, top expansion) before a significant discrete change in mass as a result of fragmentation occurs. The ion velocity in the field free region inside the detector tube decreases from 2650 ± 5 m/s to 2561 ± 5 m/s between the first 10 ms and 2.10-2.11 s. In the same period, the turnaround time or the time between each pass through the tube decreases from 23.4 μs to 19.7 μs. This occurs because the kinetic energy of the ion decreases while its charge remains constant, which results in less penetration of the ion into the cone electrodes and corresponding faster turnaround times. The total time required for each cycle decreases over the trapping time, changing from 34.7 μs in the first 10 ms to 31.4 μs between 2.10-2.11 s. Because the effect on the turnaround time in the region where there is an electric field is larger than the effect on the tube transit time in the field free region, the overall ion oscillation frequency increases as the ion loses energy. The final fragment shows a similar trend. Between the time that it first appears at 2.48 s and the end of the recording, the tube transit time increases from 14.0 μs to 14.2 μs, but the turnaround time decreases from 32.3 μs to 30.7 μs.

A Fourier-transform of the entire 4.0 s transient (Figure 4.2) results in a relatively complex frequency domain spectrum shown in Figure 4.3a. There are multiple fundamental ion oscillation frequencies from the precursor ion and its consecutive fragmentation products. The presence of

more than three peaks indicates that there are more fragmentation events than the three different amplitudes discernable in Figure 4.2 suggest. These features are relatively broad and have low intensity due to ion energy loss and frequency shifts that occur while the ion is trapped. Additional peaks occur at higher frequency (region not shown) and correspond to harmonics, primarily the second and fourth harmonics of these fundamental frequencies.

The wide peaks around 22 kHz and from ~29-32 kHz correspond to the signal from 2.48-4.0 s and from 0-2.27 s, respectively, and the peaks at 24.0 kHz, 25.4 kHz, and 28.1 kHz are from signal between those times. Significantly, the peak heights are not proportional to the charge of each ion in this full-length transform. The two broad FT peaks have similar intensity despite originating from signals that differ in amplitude by a factor of two. This effect is due to the frequency shift that occurs with time. In contrast, the ion charge visible in the transient is fairly consistent between 2.27 s and 2.48 s, and yet the peaks at 24.0 kHz, 25.4 kHz and 28.1 kHz vary widely in intensity because of the different lifetimes of the fragment ions that produce each of these frequencies.

4.4.2 Short-time Fourier Transform

The effect of increasing oscillation frequency, ion energy loss, and ion fragmentation in the ion trap, all of which can occur during long trap times, can be more readily observed by Fourier transforming smaller segments of the time-domain data (Figure 4.3b-h). Transformation of 50 ms segments of time-domain data for initial times ranging from 0 to 2.00 s results in a single peak that slowly increases in frequency from 28.7 kHz to 31.9 kHz (Figure 4.3b) over this time period. A peak at lower frequency appears after 2.11 s when the frequency jumps from 31.9 kHz to 31.2 kHz (Figure 4.3c). These results show that the original ion survives for 2.11 s before a significant discrete change in mass and charge occurs as a result of fragmentation and that a product ion is trapped thereafter. Similar fragmentation events occur at 2.24 s, 2.27 s, 2.43 s, 2.46 s and 2.48 s to produce sequential fragment ions with oscillation frequencies of 30.5 kHz, 28.1 kHz, 25.4 kHz, 24.0 kHz, and 21.6 kHz, respectively (Figure 4.3c-h; regions where these frequencies appear on the full FT, Figure 4.3a, are color coded to correspond to the regions of the segmented FTs, Figure 4.3b-3h). The charge of each consecutive fragment ion decreases. The number of charges on each ion, determined from the first 10 ms of the transient and the first 10 ms after each fragmentation event occurs is 1274 ± 5, 1225 ± 5, 1141 ± 5, 979 ± 5, 819 ± 5, 773 ± 5, and 623 ± 5. The low precision in the measured charge is a result of using only 10 ms of data to obtain this value.

The mass of an ion is determined from the measured charge and m/z of each ion. The latter can be obtained from the frequency of the ion if the energy of the ion is known. Previous CDMS techniques have relied on estimating the ion energy based on the ion optics potentials[18, 19, 35] or using an energy filter to select a narrow range of ion energies to enter the detector.[44] Here, the initial energy per charge of the precursor ion is selected using a turning quadrupole as an energy filter. However, the energy of an ion changes with time owing both to fragmentation and to collisions with background gases. The energy cannot be determined from solely the frequency of the oscillation unless the m/z is known. Jarrold and coworkers obtained the energy lost to collisions with background gas by using a model to partition ion oscillation frequency shifts due to solvent evaporation and collisional damping using an assumed cross section and pressure of nitrogen gas.[57] In cases where a discrete frequency jump was observed, they obtained an average charge and mass loss by modeling data measured for an ensemble of individual ions. However, the latter method cannot be applied to just one ion. In order to determine both the energy loss and

mass of each of the fragment ions throughout their lifetime in the trapping cell, a method to obtain the energy of each individual ion from the signal pattern it induces was developed.

4.4.3 Determining Energy per Charge of a Single Ion

The energy per charge of each ion must be known to determine the mass of an ion in CDMS. A new method to determine the ion kinetic energy per charge is described which is based on the ratio of the time required for an ion to turn around in the cone electrode and the travel time through the detection electrode. An ion with more energy per charge spends less time in the detector but takes a longer time to return to it after traveling further into the cone electrode. The ratio of these time values depends on the energy per charge. This method to measure ion energy makes it possible to weigh single ions with good precision without using an energy filter.

In order to evaluate the relationships between the ion energy, the travel time through the detection tube and the turnaround time in the trap used in this instrument, ion trajectory simulations were performed in SIMION 8.0. The trapping potential was set to 330 V in all simulations, the same value used experimentally. The effects of mass and m/z on the turning times of an ion with an initial kinetic energy of 204 eV/charge were investigated with 80 kDa and 8 MDa ions ranging in charge from 5 to 44 and 100 to 1450, respectively. The turning time, tube transit time and the ratio between the two are shown as a function of m/z in Figure 4.4a. The turning time and tube transit time increase with m/z but do not depend on the mass of the ion. However, the ratio of the turning time divided by the tube transit time, or turning time ratio, stays constant over the entire m/z range, with each ion taking 1.74 times longer to turn around than to travel through the detector tube. To determine the relationship between the turning time ratio and kinetic energy per charge, trajectories for ions weighing 8 MDa with 1000 charges and initial energy per charge from 193 eV to 253 eV were simulated (Figure 4.4b). This energy range was selected because ions outside this range do not have stable trajectories and are not trapped under the conditions of these experiments.[19, 59] The turning time ratio increases nonlinearly with energy, from 1.62 at 193 eV/charge to 2.45 at 253 eV/charge.

Ions enter the trap through a 1.5 mm diameter hole that is concentric with the central axis of the trap. Thus, some ions may have initial trajectories that are offset by as much as 0.75 mm. The dependence of the turning time ratio on the initial position of the ion was evaluated by starting the same set of ions parallel to the trap at 0.5 and 1 mm off center. The turning time ratio to energy relationship for these ions is shown in the inset of Figure 4.4b. Ions turn around faster when they are off the central axis, leading to an uncertainty in the ion energy of approximately 0.5% at a given turning time ratio.

Ions entering the trap chamber with a trajectory up to 1.5° off parallel can also make an entire pass through the detector, although ions traveling that far off axis are not stably trapped. For ions entering at 1° off parallel, the turning time ratio is lower than that of an ion with the same energy that travels parallel to the trap and 1 mm off center, resulting in an overall uncertainty in the ion energy of ~1% (see Supporting Information). Jarrold and co-workers reported an uncertainty in ion energy of 0.45% using a dual hemispherical deflection analyzer to select ion energies before they enter the detector.[44] By using the turning time ratio to measure energy, a wider range of initial energies can be admitted into the trap so that signal can be improved with little effect on mass accuracy. Moreover, this method makes it possible to measure the energy per charge of each ion, including sequential fragment ions or individual ions that lose energy through collisions.

4.4.4 MS^n of a Single Ion

Using the relationship between the turning time ratio and energy per charge (Figure 4.4), the mass and energy of each ion, including fragment ions formed during a single trapping event, as well as ions that lose energy through collisions, can be determined with high precision. This is illustrated in Figure 4.5, which shows how the mass of the ion formed from the 8 MDa PEG sample evolved during the 4.0 s trapping event. The initial mass of the ion, determined from the field-free velocity, charge and energy per charge measured during the first 10 ms is 8.11 ± 0.09 MDa. The charge and energy per charge of this ion are 1274 ± 5 and 231.6 ± 2.3 eV, respectively. The mass of this ion during the time between 2.10 and 2.11 s is 7.59 ± 0.09 MDa. The charge and energy per charge of this ion are 1289 ± 5, 200.1 ± 2.0 eV, respectively. These measurements indicate that the charge of the initial ion may have increased marginally during this time, which could occur by pickup of small ions, such as Na^+ or even the loss of an anion of clustered salt, such as Cl^-. This phenomenon has been observed previously for single ion measurements in FT-ICR MS of PEG.[28] However, it is clear that the mass of the ion decreased significantly over this same time period, from 8.11 ± 0.09 MDa initially to 7.59 ± 0.09 MDa at 2.1 s. This is likely due to evaporation of solvent or other species that adduct onto the ion and evaporate as neutral species. This slow mass loss is substantially greater than that observed by Jarrold and coworkers[57] and may be due to the larger size and charge of this ion. These data also show that the ion lost ~13.6% of its initial kinetic energy within this 2.1 s period.

The masses of each sequential fragment ion, shown as individual frequencies as a function of time in Figure 4.3, are determined from the measured charge and from the energy determined from the Figure 4.4 calibration data. These masses for the first through sixth fragment ion are 7.52 ± 0.09 MDa, 7.25 ± 0.08 MDa, 7.09 ± 0.09 MDa, 6.69 ± 0.09 MDa, 6.67 ± 0.09 MDa, and 6.42 ± 0.10 MDa, respectively (Table 4.1). The evolution of the mass of the trapped ion as a function of time is shown in Figure 4.5. In addition to the decrease in mass, the ion also increases in m/z after each discrete fragmentation event. As a result, the energy per charge of each trapped fragment ion increases (or stays approximately the same, as in the case of the first fragment). This trend may be due to the fact that only ions within a certain energy per charge range are trapped. If the precursor ion is near the low end of the trapping range, product ions with lower m/z may have too little energy per charge to be trapped. Similarly, fragment ions with higher m/z than the precursor may not be trapped if the precursor is near the high end of the trapping range.

As is the case for the original precursor ion, the frequency of the last fragment ion formed by MS^7 changes with time, but at a much lower rate. The charge of this last fragment ion is 621 ± 5 at 2.48-2.49 s and 613 ± 5 at 3.99-4.00 s and thus does not change significantly with time. The mass also does not change significantly over this same time frame (6.42 ± 0.10 MDa and 6.32 ± 0.09 MDa, respectively). Thus, the shift in frequency is entirely attributable to collisional damping of the ion motion in the trap. Ion energy loss from the induced charge in the detection circuit is negligible.[57]

This is the first determination of the masses of individual fragment ions formed from a single precursor ion with CDMS. Because only one ion is trapped initially, the precursor of each fragment is known, indicating that CDMS is potentially useful for obtaining MS^n of single ions (MS^7 is demonstrated here).

4.4.5 Ion Mobility

Ion mobility, broadly defined, is the ability of a charged particle to move through a resistive medium. Under certain conditions, such as a homogeneous low electric field typically used in drift ion mobility, the drift time is directly proportional to the collision cross section.[60] In other techniques to measure ion mobilities, such as traveling wave ion mobility and high-field asymmetric waveform ion mobility, the relationship between drift time and cross section is more complex.[61-63] Information about collisional cross sections has also been obtained at low pressure from the decay rate of signals in FT-ICR MS due to packet dephasing that correlates with drift ion mobility measurements.[64, 65]

Another way to obtain information about the mobility or collisional cross section of an individual ion with the instrument reported here is from the decay in the ion velocity over time due to collisions with the background gas. These ion mobility measurements are inherently different from those made with more conventional methods, because there is no driving electric field, the pressure is far lower, and collisions occur over a wide range of ion velocities, from zero when the ion turns around to thousands of meters per second in the field free region of the detector. However, the rate at which an ion loses velocity to collisions is related to the collision rate and the reduced mass of the ion and collision gas. The collision rate of the ion inside the trap in turn depends on its collisional cross section and velocity as well as the residual gas pressure.

For ions that do not change in mass while they are inside the trap, such as the final fragment ion, the velocity decay due to collisions is straightforward to measure. The final fragment slows from 2143 ± 8 m/s to 2107 ± 8 m/s between 2.48 s and 4.00 s for a loss of 1.7%. Determining the decrease in velocity caused by collisions for ions that change in mass, such as the initial precursor, is more complex. Jarrold and coworkers obtained the frequency shift due to collisions by fitting their data to a model that incorporates both mass loss and collision energy loss for ions with a known cross section.[57] Because we can measure how the energy of each ion evolves with time directly, the effects of collisional dampening and effects of mass loss on the ion frequency can be deconvolved without knowing an ion collisional cross section. In the absence of collisions, the velocity of an ion that gradually loses mass will increase because some of the mass will be lost in the cone electrode. This process was simulated using SIMION for an ion that loses a constant mass per unit time. Without collisions, the velocity of the precursor ion increases from 2650 m/s to 2686 m/s (see Supporting Information). The final velocity of the PEG ion at ~2.1 s is 2561 ± 5 m/s, which is 4.7% lower than the computed velocity of the dissociating precursor in the absence of collisions. After normalizing for the different lifetimes and average oscillation frequencies of the precursor ion and the sixth fragment ion formed by MS^7, the rate at which the precursor ion loses velocity due to collisions per cycle is 43% greater than that for the product ion. However, if the precursor and product ions were both spherical and had the same density, the cross section of the precursor would be only ~17% larger. This indicates that the shape of the precursor and the fragment ion are significantly different. Obtaining a meaningful collisional cross section from these ion mobility data is not straightforward owing to the range of velocities of the ions inside the trap. However, this observation constitutes the first single-ion ion mobility measurement and is a unique way to probe the gas-phase structure of individual ions.

The velocity lost by the ions to collisions also has important implications on the precision with which the *m*/*z* of an ion can be measured with CDMS. Velocity or frequency measurements after longer trapping times will lead to a systematic error if the change in the ion kinetic energy due to collisions is not taken into account. Thus, although long trapping times can improve charge measurement uncertainties, effects of collisions should be taken into account in order to make

precise *m*/*z* measurements. This effect can be minimized by reducing the pressure inside the trap and by measuring the frequency as a function of time and extrapolating these values to zero time, which would correspond to the initial frequency of the ion in the absence of collisions.

4.4.6 Fragmentation Mechanism of Polyethylene Glycol

The progression of fragmentation and charge loss provides information about the gas-phase structure of this large PEG ion. The initial charge of the precursor ion, 1274 ± 5, is significantly higher than the 223 charges calculated for the Rayleigh limit for a spherical 8 MDa water droplet, indicating that these ions are initially in a more extended geometry. The gradual loss of neutral mass in the first 2 s likely corresponds to slow desolvation or loss of neutral salt clusters from the ion. This is consistent with a narrowing of the precursor peak with time (Figure 4.3b). Upon the formation of the sixth product ion, the original precursor lost ~50% of its initial charge, but only ~20% of its initial mass. The *m*/*z* of this fragment is ~60% greater than that of the precursor. If the charge were evenly distributed along a fully elongated ion, then fragmentation would remove a similar fraction of the charge and mass and the *m*/*z* of the ion would remain roughly the same over the entire trapping time. In contrast, these results indicate that the ion has regions that are more highly charged, and that these segments are lost during fragmentation. These results also indicate that there is a less highly charged region of the ion and this is the part of the original precursor ion that remains trapped for the duration of the experiment.

A simplified illustration for a conformation of the PEG ion, which combines both high and low charge regions and is consistent with all of these data, is shown in Figure 4.6. The proposed conformation consists of three domains, with one central domain in the middle of the polymer chain where the charge per polymer unit density is low, and two more highly charged and more fully extended regions at each end of the polymer. More extended regions should accommodate a higher charge to subunit ratio owing to a larger separation between charges. Fernandez de la Mora and coworkers have proposed similar structures for PEG ions weighing 6-20 kDa with 3-15 charges based on observations that within each charge state, the ion cross section decreases upon crossing certain mass thresholds.[66, 67] The fragmentation events of the original precursor ion correspond to the ion losing part or all of each more highly charged extension thereby removing a higher ratio of charge to mass from the ion. The third fragment ion lost half of the charges that are eventually lost to produce the sixth fragment ion, consistent with the loss of just one end of the ion. The final fragment ion loses velocity significantly more slowly than the precursor and has a significantly lower rate of collisional damping than expected based just on mass, which is consistent with the loss of the extended regions of the original ion.

4.5 Conclusions

The combination of mass, charge, energy, MS^7 and ion mobility measurements on a single multiply charged ion formed from an 8 MDa PEG sample and trapped in an electrostatic ion trap for 4.0 s is demonstrated. The initially trapped precursor ion loses energy both by loss of neutral molecules, most likely evaporation of residual solvent or salt clusters, and through collisions with residual background gas in the trap. Six fragmentation events occur over the 4.0 s trapping time and can be readily observed by segmenting the time-domain data into smaller periods for analysis by Fourier transform. Because the ion energies change with time, either as a result of fragmentation or by collisions with residual background gas, it is not possible to obtain the masses

of the fragments or measure the energy change with time from just the initial precursor energy. A novel method to obtain the energy per charge is described that uses the ratio of the turnaround time of an ion to the transit time of an ion through the detection tube. This ratio does not depend on mass or *m*/*z* but does depend strongly on ion energy. By measuring the energy of the trapped ion as a function of time, information about how the mass and mobility of the ion evolves with time as a result of sequential fragmentation is obtained. This technique for measuring ion energy makes selecting the initial precursor ion energy with an energy filter unnecessary and eliminates imprecision in mass measurements as a result of changes in energy after energy selection occurs. MS^7 is demonstrated here, but it should be possible to extend this to higher stages of MS by using longer trapping times or by inducing fragmentation with energy deposition methods, such as laser photodissociation.

The oscillation frequency of PEG ions that do not fragment increases due to kinetic energy loss due to collisions with background gas. As the ion loses energy, the turning time decreases more quickly than the time to travel through the detector tube increases. The rate at which the ion loses energy and increases in frequency depends on the rate of collisions with gases. Compared to the original precursor, the sixth fragment ion loses energy and velocity to collisions even more slowly than expected based on mass, which is consistent with the survival of a more compact region of the original precursor. Obtaining collisional cross sections from this mobility data is complicated owing to the range of ion velocities in the trap, but recent results with measurements of cross sections in FT-ICR MS suggest that it may be possible to obtain information about collisional cross sections from these single ion data. Although these results and analysis are shown for only one ion, similar features in the time-domain data of other individual ions are observed. To obtain useful information from a complex sample, many such measurements on individual ions are required in order to get a statistically meaningful result. Although more data analysis is required, these results clearly show a route to obtaining information about structure through both MS^n and mobility measurements on individual ions weighed using CDMS. These methods extend the widely used techniques of tandem MS and ion mobility spectrometry to complex mixtures of large molecules that cannot be analyzed using conventional MS instrumentation.

4.6 Acknowledgements

The authors thank Waters Corporation for their generous donation of equipment, including the Z-spray source used in this work, and the National Institutes of Health (R01GM096097) for funding.

4.7 References

(1) Heck, A. J. R. Native mass spectrometry: a bridge between interactomics and structural biology. *Nat. Methods.* **2008**, *5*, 927-933.

(2) Loo, J. A. Electrospray Ionization Mass Spectrometry: A Technology for Studying Noncovalent Macromolecular Complexes. *Int. J. Mass Spectrom.* **2000**, *200*, 175-186.

(3) Rostom, A. A.; Tame, J. R.; Ladbury, J. E.; Robinson, C. V. Specificity and interactions of the protein OppA: partitioning solvent binding effects using mass spectrometry. *J. Mol. Biol.* **2000**, *296*, 269-279.

(4) Kintzer, A. F.; Thoren, K. L.; Sterling, H. J.; Dong, K. C.; Feld, G. K.; Tang, I. I.; Zhang, T. T.; Williams, E. R.; Berger, J. M.; Krantz, B. A. The protective antigen component of anthrax toxin forms functional octameric complexes. *J. Mol. Biol.* **2009**, *392*, 614-629.

(5) Painter, A. J.; Jaya, N.; Basha, E.; Vierling, E.; Robinson, C. V.; Benesch, J. L. P. Real-time monitoring of protein complexes reveals their quaternary organization and dynamics. *Chem. Biol.* **2008**, *15*, 246-253.

(6) Hernandez, H.; Robinson, C. V. Determining the Stoichiometry and Interactions of Macromolecular Assemblies from Mass Spectrometry. *Nat. Protoc.* **2007**, *2*, 715-726.

(7) Snijder, J.; Heck, A. J. R. Analytical Approaches for Size and Mass Analysis of Large Protein Assemblies. *Annu. Rev. Anal. Chem.* **2014**, *7*, 43-64.

(8) Zhou, M.; Wysocki, V. H. Surface induced dissociation: dissecting noncovalent protein complexes in the gas phase. *Acc. Chem. Res.* **2014**, *47*, 1010-1018.

(9) Loo, J. A.; Berhane, B.; Kaddis, C. S.; Wooding, K. M.; Xie, Y.; Kaufman, S. L.; Chernushevich, I. V. Electrospray Ionization Mass Spectrometry and Ion Mobility Analysis of the 20S Proteasome Complex. *J. Am. Soc. Mass Spectrom.* **2005**, *16*, 998-1008.

(10) Ruotolo, B. T.; Benesch, J. L. P.; Sandercock, A. M.; Hyung, S. J.; Robinson, C. V. Ion mobility-mass spectrometry analysis of large protein complexes. *Nat. Protoc.* **2008**, *3*, 1139-1152.

(11) Sterling, H. J.; Kintzer, A. F.; Feld, G. K.; Cassou, C. A.; Krantz, B. A.; Williams, E. R. Supercharging Protein Complexes from Aqueous Solution Disrupts their Native Conformations. *J. Am. Soc. Mass Spectrom.* **2012**, *23*, 191-200.

(12) Snijder, J.; Rose, R. J.; Veesler, D.; Johnson, J. E.; Heck, A. J. Studying 18 MDa virus assemblies with native mass spectrometry. *Angew. Chem., Int. Ed.* **2013**, *52*, 4020-4023.

(13) Weiss, V. U.; Bereszczak, J. Z.; Havlik, M.; Kallinger, P.; Gösler, I.; Kumar, M.; Blaas, D.; Marchetti-Deschmann, M.; Heck, A. J. R.; Szymanski, W. W.; Allmaier, G. Analysis of a Common Cold Virus and Its Subviral Particles by Gas-Phase Electrophoretic Mobility Molecular Analysis and Native Mass Spectrometry. *Anal. Chem.* **2015**, *87*, 8709 8717.

(14) Nohmi, T.; Fenn, J. B. Electrospray mass spectrometry of poly(ethylene glycols) with molecular weights up to five million. *J. Am. Chem. Soc.* **1992**, *114*, 3241-3246.

(15) O'Connor, P. B.; McLafferty, F. W. Oligomer characterization of 4-23 kDa polymers by electrospray Fourier transform mass spectrometry. *J. Am. Chem. Soc.* **1995**, *117*, 12826-12831.

(16) Lennon, J. D.; Cole, S. P.; Glish, G. L. Ion/molecule reactions to chemically deconvolute the electrospray ionization mass spectra of synthetic polymers. *Anal.Chem.* **2006**, *78*, 8472-8476.

(17) Robb, D. B.; Brown, J. M.; Morris, M.; Blades, M. W. Method of Atmospheric Pressure Charge Stripping for Electrospray Ionization Mass Spectrometry and Its Application for the Analysis of Large Poly(Ethylene Glycol)s. *Anal. Chem.* **2014**, *86*, 9644-9652.

(18) Doussineau, T.; Kerleroux, M.; Dagany, X.; Clavier, C.; Barbaire, M.; Maurelli, J.; Antoine, R.; Dugourd, P. Charging megadalton poly(ethylene oxide)s by electrospray ionization. A charge detection mass spectrometry study. *Rapid Commun. Mass Spectrom.* **2011**, *25*, 617-623.

(19) Elliott, A. G.; Merenbloom, S. I.; Chakrabarty, S.; Williams, E. R. Single Particle Analyzer of Mass: A Charge Detection Mass Spectrometer with a Multi-Detector Electrostatic Ion Trap. *Int. J. Mass Spectrom.* **2017**, *414*, 45-55.

(20) Fernandez de la Mora, J. Electrospray ionization of large multiply charged species proceeds via Dole's charged residue mechanism. *Anal. Chim. Acta.* **2000**, *406*, 93-104.

(21) Wuerker, R. F.; Shelton, H.; Langmuir, R. V. Electrodynamic containment of charged particles. *J. Appl. Phys.* **1959**, *30*, 342-349.

(22) Philip, M. A.; Gelbard, F.; Arnold, S. An absolute method for aerosol particle mass and charge measurement. *J. Colloid Interface Sci.* **1983**, *91*, 507-515.

(23) Hars, G.; Tass, Z. Application of quadrupole ion trap for the accurate mass determination of submicron size charged particles. *J. Appl. Phys.* **1995**, *77*, 4245-4250.

(24) Schlemmer, S.; Illemann, J.; Wellert, S.; Gerlich, D. Nondestructive high-resolution and absolute mass determination of single charged particles in a three-dimensional quadrupole trap. *J. Appl. Phys.* **2001**, *90*, 5410-5418.

(25) Nie, Z.; Tzeng, Y.; Chang, H.; Chiu, C.; Chang, C.; Chang, C.; Tao, M. Microscopy-based Mass Measurement of a Single Whole Virus in a Cylindrical Ion Trap. *Angew. Chem., Int. Ed.* **2006**, *45*, 8131-8134.

(26) Cai, Y.; Peng, W. P.; Kuo, S. J.; Lee, Y. T.; Chang, H. C. Single-particle mass spectrometry of polystyrene microspheres and diamond nanocrystals. *Anal. Chem.* **2002**, *74*, 232-238.

(27) Smith, R. D.; Cheng, X.; Brace, J. E.; Hofstadler, S. A.; Anderson, G. A. Trapping, detection and reaction of very large single molecular ions by mass spectrometry. *Nature.* **1994**, *369*, 137-139.

(28) Bruce, J. E.; Cheng, X.; Bakhtiar, R.; Wu, Q.; Hofstadler, S. A.; Anderson, G. A.; Smith, R. D. Trapping, detection, and mass measurement of individual ions in a Fourier transform ion cyclotron resonance mass spectrometer. *J. Am. Chem. Soc.* **1994**, *116*, 7839-7847.

(29) Chen, R.; Wu, Q.; Mitchell, D. W.; Hofstadler, S. A.; Rockwood, A. L.; Smith, R. D. Direct charge number and molecular weight determination of large individual ions by electrospray ionization Fourier transform ion cyclotron resonance mass spectrometry. *Anal. Chem.* **1994**, *66*, 3964-3969.

(30) Shelton, H.; Hendricks, C. D.; Wuerker, R. F. Electrostatic Acceleration of Microparticles to Hypervelocities. *J. Appl. Phys.* **1960**, *31*, 1243-1246.

(31) Hendricks Jr., C. D. Charged droplet experiments. *J. Colloid Sci.* **1962**, *17*, 249-259.

(32) Keaton, P. W.; Idzorek, G. C.; Rowton Sr., L. J.; Seagrave, J. D.; Stradling, G. L.; Bergeson, S. D.; Collopy, M. T.; Curling Jr., H. L.; McColl, D. B.; Smith, J. D. A hypervelocity - microparticle - impacts laboratory with 100-km/s projectiles. *Int. J. Impact Eng.* **1990**, *10*, 295-308.

(33) Stradling, G. L.; Idzorek, G. C.; Shafer, B. P.; Curling Jr., H. L.; Collopy, M. T.; Blossom, A. A. H.; Fuerstenau, S. Ultra-high velocity impacts: cratering studies of microscopic impacts from 3 km/s to 30 km/s. *Int. J. Impact Eng.* **1993**, *14*, 719-727.

(34) Fuerstenau, S. D.; Benner, W. H.; Thomas, J. J.; Brugidou, C.; Bothner, B.; Siuzdak, G. Mass spectrometry of an intact virus. *Angew. Chem., Int. Ed.* **2001**, *40*, 542-544.

(35) Fuerstenau, S. D.; Benner, W. H. Molecular Weight Determination of Megadalton DNA Electrospray Ions Using Charge Detection Time-of-Flight Mass Spectrometry. *Rapid Commun. Mass Spectrom.* **1995**, *9*, 1528-1538.

(36) Schultz, J. C.; Hack, C. A.; Benner, W. H. Mass Determination of Megadalton-DNA Electrospray Ions Using Charge Detection Mass Spectrometry. *J. Am. Soc. Mass Spectrom.* **1998**, *9*, 305-313.

(37) Doussineau, T.; Bao, C. Y.; Antoine, R.; Dugourd, P.; Zhang, W.; D'Agosto, F.; Charleux, B. Direct Molar Mass Determination of Self-Assembled Amphiphilic Block Copolymer Nanoobjects Using Electrospray-Charge Detection Mass Spectrometry. *ACS Macro Lett.* **2012**, *1*, 414-417.

(38) Ouadah, N.; Doussineau, T.; Hamada, T.; Dugourd, P.; Bordes, C.; Antoine, R. Correlation between the charge of polymer particles in solution and in the gas phase investigated by zeta-potential measurements and electrospray ionization mass spectrometry. *Langmuir.* **2013**, *29*, 14074-14081.

(39) Doussineau, T.; Désert, A.; Lambert, O.; Taveau, J.; Lansalot, M.; Dugourd, P.; Bourgeat-Lami, E.; Ravaine, S.; Duguet, E.; Antoine, R. Charge Detection Mass Spectrometry for

the Characterization of Mass and Surface Area of Composite Nanoparticles. *J. Phys. Chem. C.* **2015**, *119*, 10844-10849.

(40) Viodé, A.; Dagany, X.; Kerleroux, M.; Dugourd, P.; Doussineau, T.; Charles, L.; Antoine, R. Coupling of size-exclusion chromatography with electrospray ionization charge-detection mass spectrometry for the characterization of synthetic polymers of ultra-high molar mass. *Rapid Commun. Mass Spectrom.* **2016**, *30*, 132-136.

(41) Benner, W. H. A Gated Electrostatic Ion Trap To Repetitiously Measure the Charge and m/z of Large Electrospray Ions. *Anal. Chem.* **1997**, *69*, 4162-4168.

(42) Contino, N. C.; Pierson, E. E.; Keifer, D. Z.; Jarrold, M. F. Charge Detection Mass Spectrometry with Resolved Charge States. *J. Am. Soc. Mass Spectrom.* **2013**, *24*, 101-108.

(43) Keifer, D. Z.; Shinholt, D. L.; Jarrold, M. F. Charge Detection Mass Spectrometry with Almost Perfect Charge Accuracy. *Anal. Chem.* **2015**, *87*, 10330-10337.

(44) Contino, N. C.; Jarrold, M. F. Charge detection mass spectrometry for single ions with a limit of detection of 30 charges. *Int. J. Mass Spectrom.* **2013**, *345-347*, 153-159.

(45) Pierson, E. E.; Contino, N. C.; Keifer, D. Z.; Jarrold, M. F. Charge Detection Mass Spectrometry for Single Ions with an Uncertainty in the Charge Measurement of 0.65 e. *J. Am. Soc. Mass Spectrom.* **2015**, *26*, 1213-1220.

(46) Pierson, E. E.; Keifer, D. Z.; Contino, N. C.; Jarrold, M. F. Probing higher order multimers of pyruvate kinase with charge detection mass spectrometry *Int. J. Mass Spectrom.* **2013**, *337*, 50-56.

(47) Pierson, E. E.; Keifer, D. Z.; Selzer, L.; Lee, L. S.; Contino, N. C.; Wang, J. C. -.; Zlotnick, A.; Jarrold, M. F. Detection of Late Intermediates in Virus Capsid Assembly by Charge Detection Mass Spectrometry. *J. Am. Chem. Soc.* **2014**, *136*, 3536-3541.

(48) Keifer, D. Z.; Pierson, E. E.; Hogan, J. A.; Bedwell, G. J.; Prevelige, P. E.; Jarrold, M. F. Charge detection mass spectrometry of bacteriophage P22 procapsid distributions above 20 MDa. *Rapid Commun. Mass Spectrom.* **2014**, *28*, 483-488.

(49) Pierson, E. E.; Keifer, D. Z.; Asokan, A.; Jarrold, M. F. Resolving Adeno-Associated Viral Particle Diversity With Charge Detection Mass Spectrometry. *Anal. Chem.* **2016**, *88*, 6718-6725.

(50) Keifer, D. Z.; Motwani, T.; Teschke, C. M.; Jarrold, M. F. Acquiring Structural Information on Virus Particles with Charge Detection Mass Spectrometry. *J. Am. Soc. Mass Spectrom.* **2016**, *27*, 1028 1036.

(51) Keifer, D. Z.; Motwani, T.; Teschke, C. M.; Jarrold, M. F. Measurement of the accurate mass of a 50 MDa infectious virus. *Rapid Commun. Mass Spectrom.* **2016**, *30*, 1957-1962.

(52) Doussineau, T.; Yu Bao, C.; Clavier, C.; Dagany, X.; Kerleroux, M.; Antoine, R.; Dugourd, P. Infrared multiphoton dissociation tandem charge detection-mass spectrometry of single megadalton electrosprayed ions. *Rev. Sci. Instrum.* **2011**, *82*, 084104.

(53) Doussineau, T.; Antoine, R.; Santacreu, M.; Dugourd, P. Pushing the Limit of Infrared Multiphoton Dissociation to Megadalton-Size DNA Ions. *J. Phys. Chem. Lett.* **2012**, *3*, 2141-2145.

(54) Antoine, R.; Doussineau, T.; Dugourd, P.; Calvo, F. Multiphoton dissociation of macromolecular ions at the single-molecule level. *Phys. Rev. A.* **2013**, *87*, 013435.

(55) Doussineau, T.; Paletto, P.; Dugourd, P.; Antoine, R. Multiphoton dissociation of electrosprayed megadalton-sized DNA ions in a charge-detection mass spectrometer. *J. Am. Soc. Mass Spectrom.* **2015**, *26*, 7-13.

(56) Bell, D. M.; Howder, C. R.; Johnson, R. C.; Anderson, S. L. Single CdSe/ZnS nanocrystals in an ion trap: Charge and mass determination and photophysics evolution with changing mass, charge, and temperature. *ACS Nano.* **2014**, *8*, 2387-2398.

(57) Keifer, D. Z.; Alexander, A. W.; Jarrold, M. F. Spontaneous Mass and Charge Losses from Single Multi-Megadalton Ions Studied by Charge Detection Mass Spectrometry. *J. Am. Soc. Mass Spectrom.* **2017**, *28*, 498-506.

(58) Price, W. D.; Williams, E. R. Activation of Peptide Ions by Blackbody Radiation: Factors That Lead to Dissociation Kinetics in the Rapid Energy Exchange Limit. *J. Phys. Chem. A.* **1997**, *101*, 8844-8852.

(59) Schmidt, H. T.; Cederquist, H.; Jensen, J.; Fardi, A. Conetrap: A compact electrostatic ion trap. *Nucl. Instr. and Meth. in Phys. Res. B.* **2001**, *173*, 523-527.

(60) Clemmer, D. E.; Jarrold, M. F. Ion Mobility Measurements and their Applications to Clusters and Biomolecules. *J. Mass. Spectrom.* **1997**, *32*, 577-592.

(61) Kanu, A. B.; Dwivedi, P.; Tam, M.; Matz, L.; Hill, H. H. Ion mobility–mass spectrometry. *J. Mass Spectrom.* **2008**, *43*, 1-22.

(62) Shvartsburg, A. A.; Smith, R. D. Fundamentals of traveling wave ion mobility spectrometry. *Anal. Chem.* **2008**, *80*, 9689-9699.

(63) Kolakowski, B. M.; Mester, Z. Review of applications of high-field asymmetric waveform ion mobility spectrometry (FAIMS) and differential mobility spectrometry (DMS). *Analyst.* **2007**, *132*, 842-864.

(64) Yang, F.; Voelkel, J. E.; Dearden, D. V. Collision Cross Sectional Areas from Analysis of Fourier Transform Ion Cyclotron Resonance Line Width: A New Method for Characterizing Molecular Structure. *Anal. Chem.* **2012**, *84*, 4851-4857.

(65) Anupriya; Jones, C. A.; Dearden, D. V. Collision Cross Sections for 20 Protonated Amino Acids: Fourier Transform Ion Cyclotron Resonance and Ion Mobility Results. *J. Am. Soc. Mass Spectrom.* **2016**, *27*, 1366-1375.

(66) Larriba, C.; Fernandez de la Mora, J. The Gas Phase Structure of Coulombically Stretched Polyethylene Glycol Ions. *J Phys Chem B.* **2012**, *116*, 593-598.

(67) Larriba, C.; Fernandez de la Mora, J.; Clemmer, D. E. Electrospray Ionization Mechanisms for Large Polyethylene Glycol Chains Studied Through Tandem Ion Mobility Spectrometry. *J. Am. Soc. Mass Spectrom.* **2014**, *25*, 1332-1345.

4.8 Table and Figures

Table 4.1: Mass, charge, *m*/*z* and energy of the precursor and each fragment ion.

	Time (ms)	*m*/*z*	Charge	Mass (MDa)	Energy per charge (eV)
Precursor (initial)	0.5–10.5	6360 ± 70	1274 ± 5	8.11 ± 0.09	231.6 ± 2.3
Precursor (final)	2100–2110	5890 ± 60	1289 ± 5	7.59 ± 0.09	200.1 ± 2.0
Fragment 1	2114–2124	6140 ± 70	1225 ± 5	7.52 ± 0.09	198.3 ± 2.0
Fragment 2	2243–2253	6360 ± 70	1141 ± 5	7.25 ± 0.08	204.2 ± 2.0
Fragment 3	2268–2278	7240 ± 80	979 ± 5	7.09 ± 0.09	213.4 ± 2.1
Fragment 4	2425.5–2435.5	8170 ± 90	819 ± 5	6.69 ± 0.09	231.6 ± 2.3
Fragment 5	2462–2472	8620 ± 100	773 ± 5	6.67 ± 0.09	242.3 ± 2.4
Fragment 6 (initial)	2482–2492	10 340 ± 130	621 ± 5	6.42 ± 0.10	246.1 ± 2.5
Fragment 6 (final)	3990–4000	10 320 ± 130	613 ± 5	6.32 ± 0.09	237.3 ± 2.4

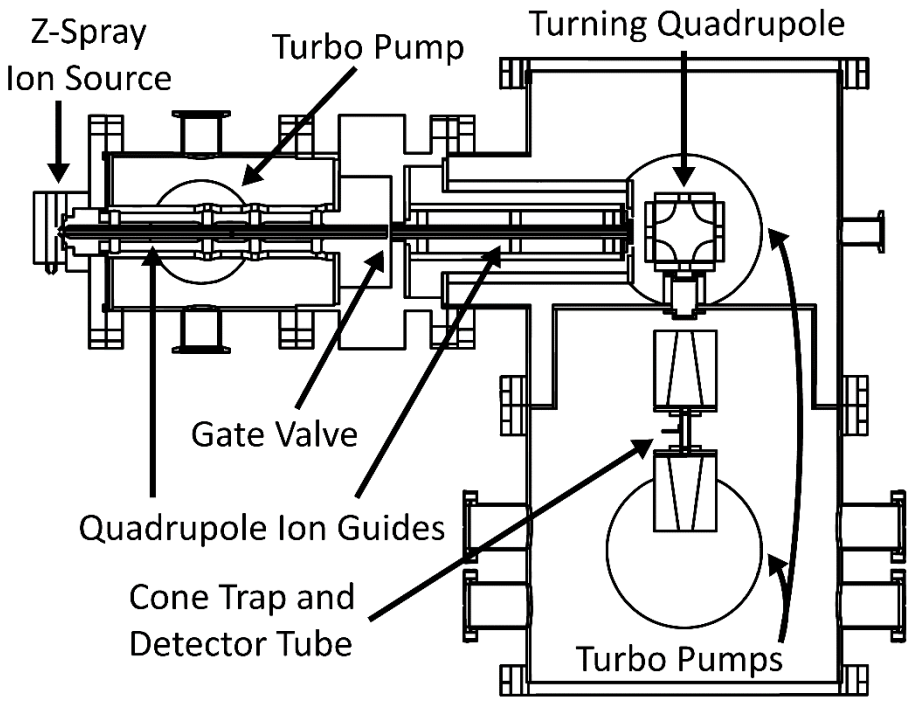

Figure 4.1: Schematic diagram of the single particle analyzer of mass and mobility (SPAMM) instrument.

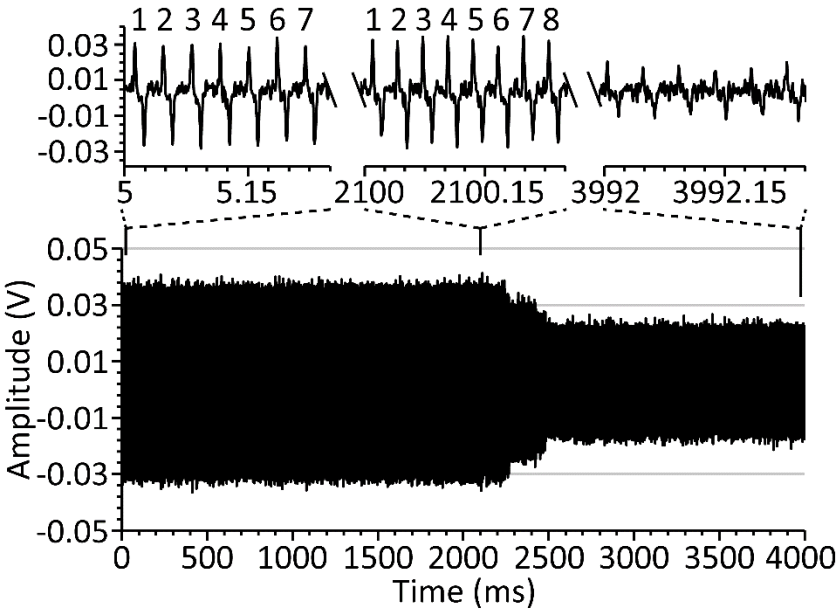

Figure 4.2: Time-domain signal of an individual 8 MDa PEG ion trapped for 4 s. The insets show expansions of 250 μs long segments of the transient signal, demonstrating the changes in the signal due to collisions with the background gas, which decrease the ion kinetic energy and induce ion fragmentation.

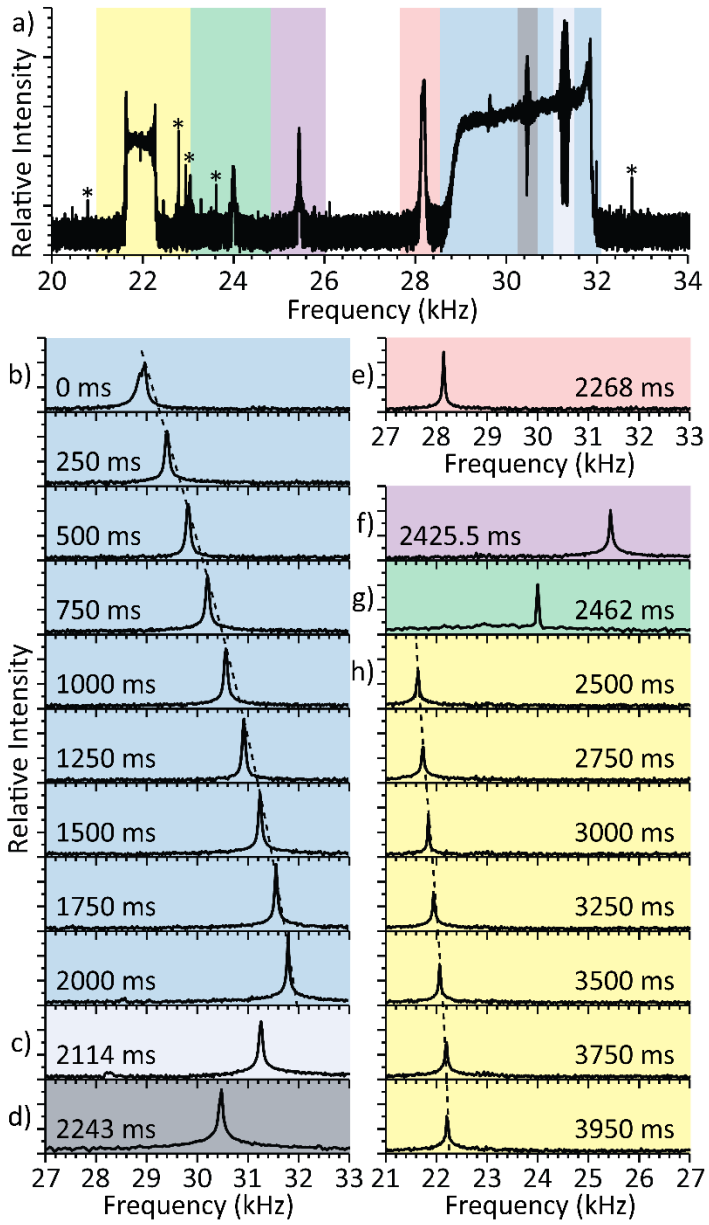

Figure 4.3: (a) Fourier transform of the full time-domain signal shown in Figure 4.2, and Fourier transforms of segments of data from that transient, (b) before any fragmentation events, (c) after the first fragmentation, (d) after the second, (e) third, (f) fourth, (g) fifth, and (h) after the sixth fragmentation. The segments in (b), (c), (e), and (h) are each 50 ms long, and the segments in (d), (f), and (g) are 23 ms, 35.5 ms, and 19 ms long, respectively, due to the short time between each of those fragmentation events. Regions in the short FT segments are highlighted in the same color in the FT of the full transient. Electronic noise in the transformed data is marked with asterisks.

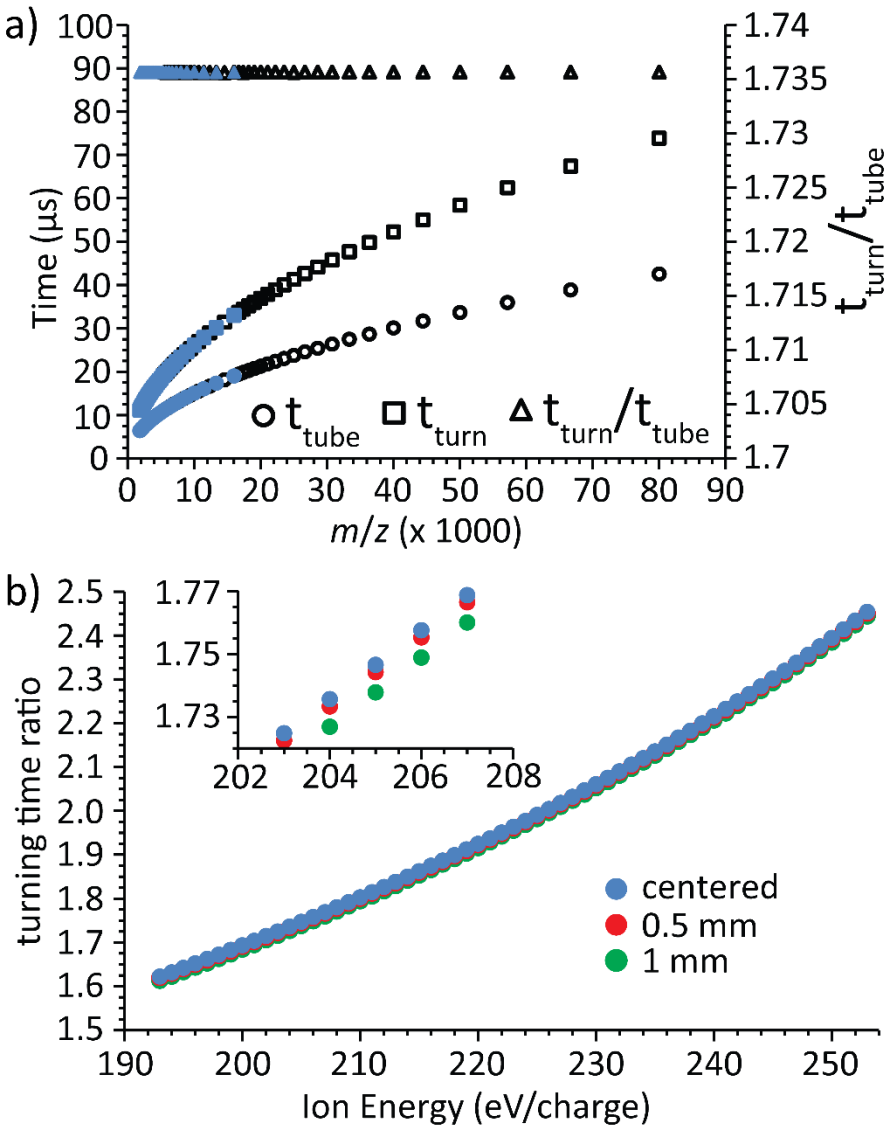

Figure 4.4: (a) Turnaround time, tube transit time, and turning time divided by tube transit time as a function of *m*/*z* for 80 kDa (filled blue points) and 8 MDa (empty black points) ions, and (b) the turning time ratio as a function of the ion kinetic energy per charge. The inset in (b) shows an expansion around 205 eV/charge demonstrating the small dependence of the turning time ratio on the initial position of the ion.

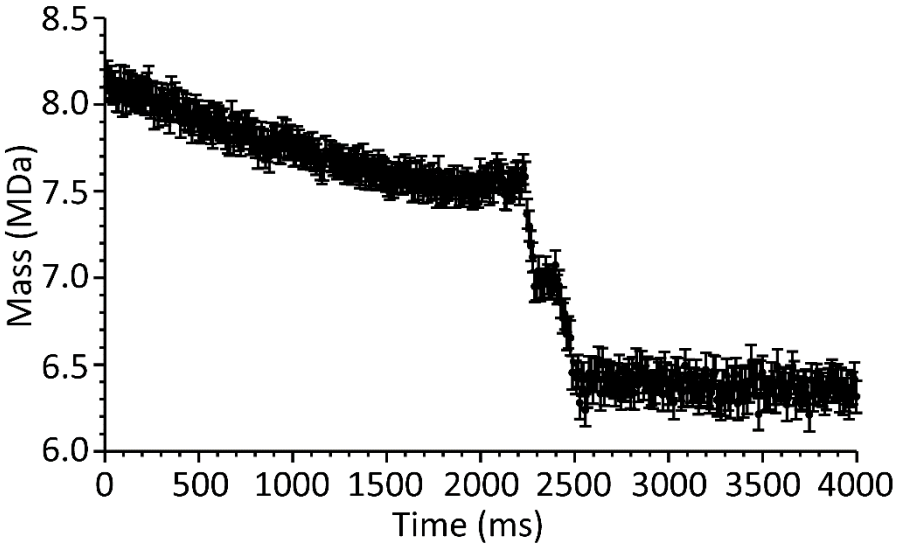

Figure 4.5: Mass of the PEG ion obtained from the Figure 4.2 time-domain data in each 10 ms interval throughout the 4.0 s recording time.

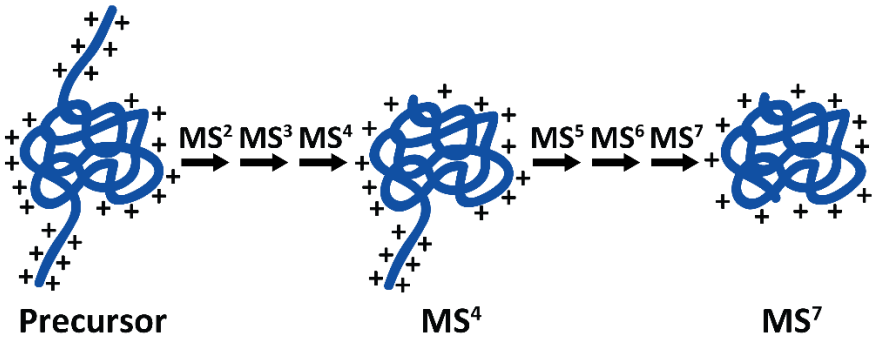

Figure 4.6: Illustration of the proposed conformation of the trapped PEG ion before fragmenting (left), the third fragment (middle), and the sixth fragment (right).

4.9 Supporting Information

4.9.1 Additional Experimental Details

4.9.1.1 Samples

Polyethylene glycol (PEG) with a nominal molecular weight of 8 MDa was obtained from Sigma Aldrich (St Louis, MO, USA) and was used without further purification. PEG solutions were prepared at a concentration of 60 nM in a 1:1 water-methanol solution.

4.9.1.2 Mass Spectrometry

Experiments were performed using the single particle analyzer of mass and mobility (SPAMM), a home-built charge detection mass spectrometer, a schematic of which is shown in Figure 4.1. Ions are formed by nanoelectrospray ionization using borosilicate capillaries that have tips pulled to an inner diameter of approximately 1 μm. A platinum wire is inserted into the capillary so as to contact the sample solution. A potential of +1-2 kV with respect to ground is applied to the capillary to initiate ion formation by electrospray. The resulting ions are transferred to vacuum using a Z-spray source (Waters, Milford, MA) modified to contain an extraction cone with a smaller 0.5 mm hole to improve differential pumping between the source and first vacuum stage. Typical voltages inside the source are +350 V for the exterior sample cone and +210 V for the interior extraction cone, with a pressure of 1 Torr between the cones. The source is heated to 80 °C for all samples.

After the extraction cone, ions are guided through the next vacuum stage at a pressure of 3×10^{-4} Torr by a pair of RF-only quadrupole ion guides (Ardara Technologies, Ardara, PA). The ion guides operate at a frequency of 1.89 MHz with a peak-to-peak potential of 1500 V and a DC offset potential of +204 V and +170 V for the first and second ion guides, respectively. The quadrupole ion guides are separated by a gate valve. The potential offset in the first ion guide defines the nominal energy of the ions. After the ion guides, ions pass through a lens with a potential of +180 V and into an electrostatic turning quadrupole (Ardara Technologies, Ardara, PA) in a third differentially pumped vacuum chamber at a pressure of 6×10^{-7} Torr. The turning quadrupole is used as an energy filter that works by bending ions within a selected energy range 90° into the detection chamber. The energy range selected for transmission into the trap depends on the potentials applied to the outside walls of the quadrupole and each pole, with each diagonally opposed pair of poles at the same potential. The walls, outer and inner poles were set to +140 V, +220 V and +120 V, respectively, which selects a distribution of ion energies centered at 209 eV/charge with a standard deviation of 3.2 eV/charge.

The energy selected ions are accelerated though a 1.0 mm conductance limit at a potential of -250 V into a final vacuum chamber with a pressure of 5×10^{-9} Torr where they are trapped and detected. The detection system consists of one stainless steel tube in between two conical trapping electrodes based on the design of Schmidt et al.[59] The tube has an inner diameter (ID) of 7.1 mm and is 28.2 mm long. This tube is held in place by insulators inside grounded shielding. The total distance separating the two trapping electrodes is 37.7 mm. The detector tube is connected to a CoolFET charge sensitive preamplifier (Amptek, Bedford, MA) containing an A250 preamplifier and JFET cooled to -50 °C by a Peltier cooler. The preamp is housed in a shielded box inside the vacuum chamber, and the signal is passed to a shaping amplifier consisting

of a differentiator, integrator and two voltage amplifiers (Amptek A275) and a signal filter outside the vacuum chamber. Data are recorded at a rate of 5 MHz on a computer with an analog to digital converter card (ATS9350, AlazarTech, Pointe-Claire, Canada) and stored for analysis offline. For trapping times longer than 2 s, the sampling rate is decreased to 2 MHz so that the entire trajectory can be recorded in one transient. The detector response measured using a test capacitor is 21 μV/charge.

Ions with approximately 200 eV/charge are trapped inside the detector when both cone electrodes are at 330 V. The electrode in the back of the trap is set to 330 V for the entire trapping event, and the front electrode is changed between an initial ground potential and 330 V with a MOSFET switch to allow ions into and out of the trap. After detecting a charge pulse greater than a set amplitude, the switch is triggered, and the front potential is raised and maintained for a predetermined maximum trapping time during which data is acquired. After the measurement, the front voltage is lowered for 5.0 ms to allow ions to leave and enter the trap. The fraction of events for which successful ion trapping occurs is approximately 40%.

An ion entering a detector tube induces an image charge of opposite sign on the tube. Inverting and shaping the square wave signal from that tube produces a pattern consisting of a leading positive peak and trailing negative peak for a positive ion. The amplitude of each peak is proportional to the charge of the ion, and the spacing between the peaks is proportional to the velocity of the ion.[19] The minimum charge on an ion for this signal pattern to be detected above the noise is approximately 225 charges. Data is analyzed with a program designed to find peaks of a consistent size and spacing that is described in detail elsewhere.[19]

4.9.2 Simulations

4.9.2.1 Determining Energy per Charge of Individual Ions

The ion energy was determined from the turning time ratio using data from simulations of ions traveling along the central axis of the trap. The relationship between the ion kinetic energy and turning time ratio was fit with a cubic polynomial and the ion energy for a given turning time ratio is determined from that polynomial fit.

The turning time ratio for a given energy depends on both the distance an ion enters the trap of the central axis and the angle at which the ion enters the trap. The uncertainty in the ion energy obtained from the turning time ratio was obtained by simulating ions that enter the trap off center and by simulating ions that enter the trap at various angles. At 1.0 mm off center, the uncertainty in the ion energy is ~0.5% and this is an upper limit because the radius of the trap entrance is only 0.75 mm. Similarly, ions can enter the trap at a maximum angle of 1.5° but these ions are not trapped. To determine the average turning time ratios for ions entering at an angle off the trap axis, 8 MDa and 1000 charge ions with 193-253 eV/charge and an initial trajectory 0.5° and 1° off axis were simulated with a maximum time of 10 ms during which time they made ~250 passes through the trap (Supporting Figure 4.1). The range of ion energies that can be trapped for ions entering the trap off center is narrower than for those that enter the trap on axis. For ions entering the trap 1° off center with energy in the middle of the trapping range, the turning time ratios are close to those for ions with 2 eV less energy traveling on the trap axis resulting in an energy uncertainty of ~1%. However, ions near the high and low end of the trapping range do not have stable trajectories for the full 10 ms. Ions with 193-194 and 246-253 eV/charge are not trapped, even though ions with this energy per charge are trapped when they start on the axis of

the trap. Thus, the distance off center from which the energy uncertainty is determined depends on the ion energy. The maximum turning time ratio for ions entering 1° off the trap axis is 2.21 for 245 eV/charge ions. However, ions with larger turning time ratios are observed in experiments. These ions must have entered the trap without such a large off-axis angle so the uncertainty in determining the ion energy is obtained for a lower off-center angle.

For ions entering the trap 0.5° off axis, average turning time ratios are similar to ions with up to 1 eV less energy traveling on the trap axis, resulting in an uncertainty of ~0.5%. The trapping range for these ions extends from 194-251 eV/charge. The maximum turning time ratio is 2.34 at 251 eV/charge, which is still less than the maximum turning time ratio of 2.45 at 253 eV/charge for ions entering on the trap axis. The energy uncertainty associated with ions entering off the trap axis correspondingly decreases for ions with high turning time ratios. To account for this effect of high energy ions not remaining trapped if they enter off the trap axis, the overall energy uncertainty for all energies was estimated at ~1%.

4.9.2.2 Ion Mobility of Precursor

To obtain the velocity of the precursor ion after losing mass in the absence of collisions, an ion with the initial mass and kinetic energy of the precursor that loses a constant mass in each time step was simulated. The simulated mass loss was 0.00274 Da in each 0.01 μs time step corresponding to the mass of the precursor at 1.9 s, which is when the precursor ion stopped losing mass in the experiment. The velocity was then calculated from the time between the ion crossing through the plane on each side of the tube in its last pass through the tube.

4.9.2.3 Calculation of Normalized Velocity Loss

The velocity of the precursor ion and sixth fragment ion decreases as a result of collisional dampening. The rate at which this occurs was normalized for the different ion lifetimes by dividing the percent velocity loss of both ions by their respective lifetimes. The ions have different oscillation frequencies and thus different distances traveled in a given time. To correct for this distance effect, the rates of velocity loss are normalized by dividing by their respective frequencies. The lifetime of the original precursor is 2.11 s and its average frequency is 30.56 kHz. The loss of velocity due to collisional dampening is 4.7%, and the normalized velocity decrease is 0.072% per thousand cycles. The lifetime of the final fragment is 1.52 s and its average frequency is 21.94 kHz. The velocity loss from collisional dampening is 1.7%, and the resulting normalized velocity decrease is 0.050% per thousand cycles.

4.9.3 Supporting Figure

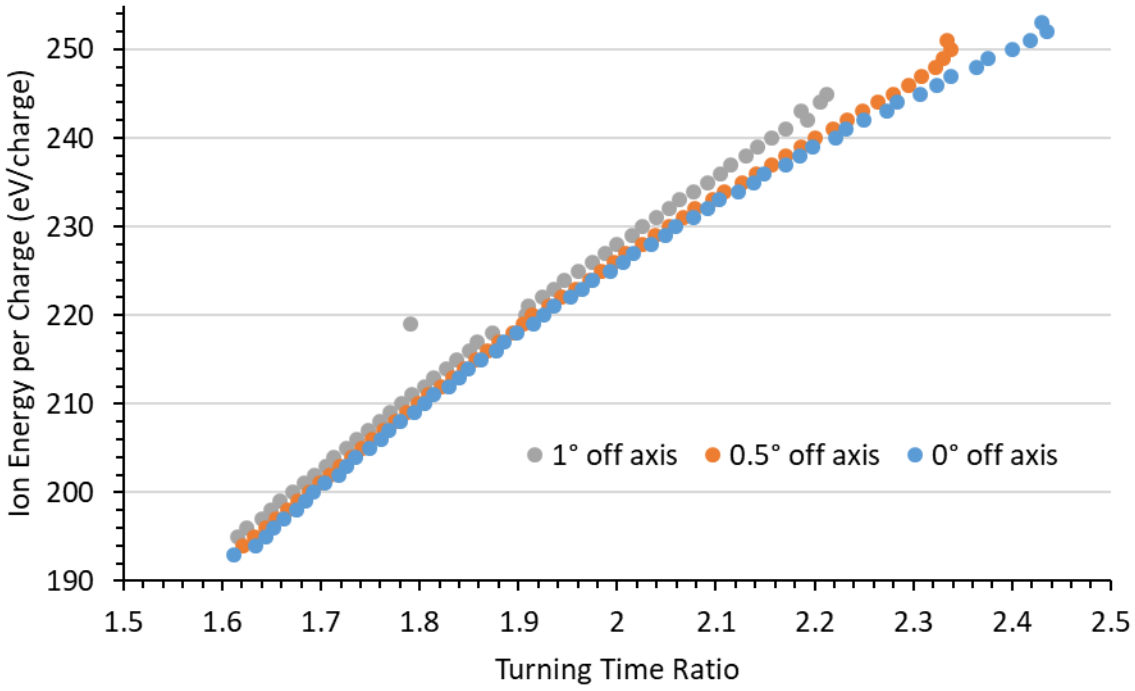

Supporting Figure 4.1: Ion energy per charge as a function of turning time ratio for ions starting on the center of the trap traveling parallel to the trap axis and at 0.5° and 1° off axis.

Chapter 5

Simultaneous Measurements of Mass and Collisional Cross Section of Single Ions with Charge Detection Mass Spectrometry

This chapter is reproduced with permission from:

Andrew G. Elliott, Conner C. Harper, Haw-Wei Lin, Anna C. Susa, Zijie Xia, Evan R. Williams

"Simultaneous Measurements of Mass and Collisional Cross Section of Single Ions with Charge Detection Mass Spectrometry" *Anal. Chem.* **2017**, *89* (14), 7701-7708

5.1 Abstract

The masses and mobilities of single multiply charged ions of cytochrome *c*, ubiquitin, myoglobin and bovine serum albumin formed by electrospray ionization are measured using charge detection mass spectrometry (CDMS). Single ions are trapped and repeatedly measured as they oscillate inside an electrostatic ion trap with cone electrodes for up to the maximum trapping time set at 500 ms. The histograms of the many single ion oscillation frequencies have resolved peaks that correspond to the different charge states of each protein. The *m*/*z* of each ion is determined from the initial oscillation frequency histogram, and the evolution of the ion energy with time is obtained from the changing frequency. A short-time Fourier transform of the time-domain data indicates that the increase in ion frequency occurs gradually with time with occasional sudden jumps in frequency. The frequency jumps are similar for each protein and may be caused by collision-induced changes in the ion trajectory. The rate of the gradual frequency shift increases with protein mass and charge state. This gradual frequency change is due to ion energy loss from collisions with the background gas. The total energy lost by an ion is determined from the latter frequency shifts normalized to a 500 ms lifetime and these values increase nearly linearly with measured collisional cross sections for these protein ions. These results show that the mass and collisional cross section of single multiply charged ions can be obtained from these CDMS measurements by using proteins with known collisional cross sections for calibration.

5.2 Introduction

Gaseous multiply charged molecules can be formed directly from solution using electrospray ionization (ESI) and can be readily analyzed with mass spectrometry. Molecular identification and detailed structural information can be obtained using a variety of powerful structural methods, including tandem mass spectrometry,[1-3] ion mobility,[4-7] and spectroscopy.[8-10] Multiply charged ions are more readily detected in instruments with charge sensitive detectors,

such as Fourier-transform ion cyclotron resonance (FT-ICR) and orbitrap mass analyzers, and these ions can be readily dissociated to obtain structural information, including protein sequence and sites of posttranslational modifications.[11, 12] Information about protein conformation,[4-7] stabilities,[13, 14] and conformational changes that occur in the transition from solution into the gas phase can be obtained from ion mobility measurements.[13-16] Large, macromolecular complexes can be analyzed with ESI MS where masses are obtained from resolved charge-state distributions. Resolving the individual charge states in a distribution can be challenging for very large complexes[3, 17] (greater than ~10 MDa) or for smaller complexes that are heterogeneous.[18, 19] This problem is especially difficult for synthetic polymers, where resolving the charge-state distributions of polymer ions formed by ESI, such as polyethylene glycol, has only been achieved for samples with average molecular weights of ~40 kDa.[19]

One solution to reduce the complexity of ESI spectra obtained from complex mixtures of large molecules and macromolecular complexes is to weigh ions individually so that other ions cannot interfere with the measurement. Information about the sample can be obtained by making many such measurements to provide a statistically representative sampling of the composition of the sample. Such single molecule mass measurements, in which both the *m*/*z* and *z* of each ion are measured, have been made using FT-ICR[20, 21] and quadrupole ion trap (QIT)[22-27] instruments. Although precise masses can be obtained, the measurements are relatively slow, making rapid measurements of the large numbers of ions necessary to obtain detailed information about complex samples impractical.

Both mass and charge measurements of individual ions can also be made using charge-detection mass spectrometry (CDMS), which has the advantage of high analysis speed. In CDMS, the charge of an individual ion is determined from the amplitude of the induced current as the ion passes through a conductive tube. The *m*/*z* is determined by the energy per charge of the ion and its velocity, where velocity is derived from the time required for the ion to pass through the conductive tube. Single pass CDMS has been used to measure the masses of highly charged micron sized cosmic dust particles,[28-31] viruses,[32] DNA,[33, 34] synthetic polymers,[35, 36] and nanoparticles.[37, 38] This technique is much faster than the QIT and FT-ICR single ion techniques, but the measurement of mass is considerably less precise.[32]

The accuracy of CDMS can be significantly improved by trapping ions and repeatedly measuring their induced signal. Benner first demonstrated an electrostatic dual ion mirror trap to recirculate an ion through the detector tube for 10 ms (450 cycles), thereby reducing charge uncertainty to ±2.3 elementary charges (*e*).[39] Jarrold and co-workers used an electrostatic cone trap to further reduce charge uncertainty to ±0.196 *e* by using cryogenic cooling and extended trapping times (3 s, 60,000 cycles).[40, 41] They also demonstrated a limit of detection of seven charges by trapping small protein ions and analyzing the CDMS data with a Fourier transform (FT).[40, 42] They showed that the individual charge states of proteins as small as ubiquitin (8.6 kDa) can be detected and resolved using this method.[42] A mass spectrum for bacteriophage P22 (52 MDa) was also obtained with this method and the narrow mass distribution indicated the transition of the intact virus into the gas phase.[43] Dugourd and coworkers have also implemented an ion trapping CDMS instrument in studies of the photodissociation of polyethylene glycol (PEG) and DNA ions.[44-47] A multiple detector tube CDMS ion trap design has also been used to measure the mass distributions of MDa PEG samples and polystyrene nanoparticles with diameters up to ~100 nm.[48]

The oscillation frequency of an ion inside a CDMS electrostatic ion trap increases as a result of collisions with background gas and loss of solvent molecules.[49, 50] Jarrold and coworkers

reported that some hepatitis B virus ions exhibit sudden changes in oscillation frequency that correspond to the loss of a singly charged fragment and suggested that this process was induced by electric fields in the trap.[49] Elliott et al. showed that sequential fragmentation of an ion can occur inside the trap.[50] In order to obtain the mass of each of the fragment ions, the energy of each of the ions was obtained from the ratio of the time required for an ion to turn around in the cone region to the time an ion travels through the detector. This ratio is independent of *m*/*z* but is a sensitive measure of ion energy. For a single 8.1 MDa PEG ion that was trapped for 4 s, loss of ~500 kDa of solvent molecules occurred during the first 2.1 s that the ion was trapped. This ion subsequently fragmented six times and the mass of each fragment ion was determined, demonstrating MS^7 of a single ion. Information about the ion mobility was obtained for the original precursor and the fragment ions from the collision induced frequency change in these measurements.[50]

Here, we demonstrate a method to relate the change in oscillation frequency observed for ions that do not fragment inside the ion trap to the total energy lost via collisions with background gas inside the trap. The charge-state distributions of four proteins ranging in mass from 8.6 kDa to 66.5 kDa are resolved in these CDMS measurements and the collisional cross sections of all these ions have been measured using ion mobility spectrometry. The total energy lost by a single ion directly correlates with the collisional cross sections measured for an ensemble of ions of the same protein in the same charge state. This relationship between the frequency change of a single ion inside a trap and the collisional cross section should make it possible to not only weigh individual ions using CDMS, but to obtain the collisional cross section of each ion by calibrating these data with ions that have known collisional cross sections.

5.3 Experimental

Polyethylene glycol (PEG) with a nominal molecular weight of 8 MDa, ubiquitin, cytochrome *c*, myoglobin and bovine serum albumin were obtained from Sigma Aldrich (St Louis, MO, USA) and were used without further purification. PEG solutions were prepared at a concentration of 60 nM in a 50:50 water-methanol solution. Protein solutions were prepared at a concentration of 10 µM in solutions of 75:25 water-methanol with 2% (v/v) acetic acid (ubiquitin, cytochrome *c* and myoglobin) and 50:50 water-methanol with 3% (v/v) acetic acid (BSA).

Collisional cross sections of some charge states of BSA have been reported previously by Covey and Douglas.[51] In order to have more complete data for all the charge states of BSA formed in these experiments, collisional cross sections were obtained from traveling wave ion mobility spectrometry (TWIMS) arrival time data that were acquired using a Waters Synapt G2Si (Waters, Milford, MA, USA). The traveling wave ion mobility cell was operated with a constant wave velocity of 550 m/s, wave height of 40 V, helium flow rate of 180 mL/min, and IMS (N_2) flow rate of 90 mL/min. Cytochrome *c*, ubiquitin and myoglobin ions, formed from solutions in which they are denatured, were used for calibration and cross sections were obtained from the arrival time distributions using the procedure described by Ruotolo et al.[5] These data are provided in the Supporting Information.

Single ion experiments were performed on the single particle analyzer of mass and mobility (SPAMM), a home-built charge detection mass spectrometer which is described in detail elsewhere.[48, 50] Ions are formed by nanoelectrospray ionization using borosilicate capillaries. The ions are transferred through a modified Z-spray source (Waters, Milford, MA) into a pair of RF-only quadruple ion guides and an energy selective electrostatic turning quadruple (both Ardara

Technologies, Ardara, PA) to the electrostatic cone trap containing the detector. The vacuum chamber housing the cone trap is at a pressure of 5 x 10^{-9} Torr. The detector consists of a single stainless steel tube located between the two cone electrodes of the cone trap.

An ion induces a charge pulse when it passes through the detector tube. These pulses are amplified and shaped by a CoolFET charge sensitive preamplifier and voltage amplifier (Amptek, Bedford, MA) to produce a leading positive and trailing negative peak on each pass. Because small protein ions are not sufficiently charged to be detected on a single pass through the detector, a random trapping approach is used in which the trap is closed and opened at regular intervals.[40] The voltage on the back of the trap is held at a trapping potential of +330 V throughout the entire trapping cycle. At the start of the trapping cycle, the potential of the front of the trap is lowered to 0 V for 8 ms to allow ions to enter the trap. The front electrode of the trap is then raised to the trapping potential and held there for a specified time (100 ms or 500 ms). The potential on the front of the trap is then lowered again to empty the trap and start the next trapping cycle. Data is analyzed with a LabVIEW program designed to perform a short-time Fourier transform of the time-domain data and the amplitude and frequency of the transformed signal are recorded in each time segment. The amplitude of a peak is proportional to the charge of the ion, and the square of the frequency is inversely proportional to the *m*/*z* of the ion. An ion is considered to be trapped and detected if the signal lasts for at least 85 ms. This occurs in approximately 5% of all random trapping events.

5.4 Results and Discussion

5.4.1 Changes in Frequency of Single Ions in CDMS

At a given kinetic energy and trap potential, the *m*/*z* of an ion is inversely proportional to the square of the frequency at which it oscillates inside the trap. However, the oscillation frequency of an ion changes with time due to collisions with the background gas that reduces the kinetic energy of the ion. Fragmentation also leads to a change in frequency. Fragmentation typically results in large, discrete frequency changes although more gradual changes in frequency can also occur owing to loss of solvent from large MDa ions initially injected into the trap.[49, 50] The gradual change in frequency for a single bovine serum albumin (BSA) ion that has 51 positive charges and that does not change in mass is illustrated in Figure 5.1. Also shown is the Fourier transform (FT) of two different lengths of the time domain data centered at 300 ms. Because the ion has fewer than 225 charges, the signal from each pass through the detector tube does not appear above the noise level in the time domain signal (Figure 5.1a). The FT data show the ion oscillated through the trap at an average frequency of ~67.8 kHz between 275 and 325 ms and between 250 and 350 ms (Figure 5.1b-c). Although the ion signal appears at the same frequency in both segments, the peak for the 100 ms segment is broader and is lower intensity. This peak broadening occurs because the frequency at which the ion oscillates changes during the time period of the transform. The ion oscillates at a wider range of frequencies over the longer time, resulting in a broader peak. The peak width for each time segment is related to the gradual frequency shift that occurs over time, and this shift increases with protein size. The peak intensity decreases because the ion spends a smaller fraction of the total transformed time segment oscillating at a particular frequency.

This gradual change in frequency is caused by collisions with the background gas that decrease the ion energy. Ions with less energy take longer to go through the detector tube in the

field free region, but travel a shorter distance into the cone electrode before turning around, resulting in a shorter time to return to the detector tube.[50] Because ions spend more time in the cone electrode and the time they spend in this region is more sensitive to energy, the overall oscillation frequency of an ion increases with decreasing ion energy.[50] The relationship between *m*/*z* and frequency, *f*, at a given trap potential is given by equation 5.1

$$f = C(E)\sqrt{\frac{z}{m}} \qquad \text{(eq. 5.1)}$$

where $C(E)$ is a proportionality constant that depends on the energy per charge of the ion. The value of $C(E)$ as a function of ion energy was determined via simulations in SIMION (see Supporting Information) and is given in equation 5.2

$$C(E) = -44.5E^2 + 1.45 \times 10^4 E + 1.32 \times 10^6 \qquad \text{(eq. 5.2)}$$

where E is in units of eV. The value of $C(E)$ does not depend on the *m*/*z* of the ion. The change in the oscillation frequency of the ion can thus be used to measure the loss in the ion energy that occurs as a result of collisions with the background gas. Because the number of collisions depends on the collisional cross section of an ion, information about the collisional cross section should be obtainable from these single ion measurements. Collisions can occur for ion velocities ranging from zero when the ion turns around in the cone electrode up to the maximum energy of the ion in the field free region. Thus, the cross sections obtained from these measurements will not necessarily be directly related to those measured under the precisely controlled conditions of ion mobility spectrometry done in drift tubes.

5.4.2 Oscillation Frequency to *m*/*z* Calibration

Measurements of small proteins were performed in order to investigate the relationship between collisional energy loss and collisional cross section. Small proteins have the advantage that the *m*/*z* and charge state of an ion can be unambiguously assigned in these CDMS measurements from the separated charge-state distributions[42, 52] and accurate cross sections as a function of charge state have been reported for a range of small proteins.[53]

A histogram of the oscillation frequencies of 8363 individual cytochrome *c* ions (Figure 5.2a) has resolved peaks, which correspond to ions that have different charge states. To reduce the effect of collision-induced energy loss on the measured frequency and ensure the distribution of ion energies is narrow and close to the energy selected with the turning quadrupole, only the first 25 ms of the 100 ms trapping time were used in the FT. The gap in the histogram between 86.7 kHz and 87.7 kHz corresponds to electronic noise which is removed by filtering. By comparing the separation between each frequency peak to the separation between *m/z* values for different charge states of cytochrome *c*, the charge state for each frequency peak can be unambiguously assigned. The *m/z* histogram resulting from this calibration is shown in Figure 5.2b. The *m/z* resolution of the mass spectrum is approximately 3% full width half maximum, which is lower than the ~2% resolution predicted based on the width of energies selected by the turning quadrupole. This is due to the changing frequency of the ion with time as a result of both energy loss and more discrete changes that occur likely because of changes in ion trajectory (*vide infra*). Ions that enter off the trap axis also oscillate at a higher frequency than ions with the same

m/*z* that enter on the trap axis, so differences in initial trajectory may also contribute to the decrease in resolution.[50] Jarrold and coworkers obtain ~1.5% *m*/*z* resolution with an energy selection resolution of ~0.6% for a similar FT-based single particle CDMS instrument. Although their *m/z* resolution is higher than the resolution reported here, the difference between the energy resolution and *m*/*z* resolution is similar. Thus, the difference in *m*/*z* resolution between the instruments is likely primarily due to the width of the energy distribution selected before the detector rather than the characteristics of the trap itself.

Histograms of single ion *m/z* values for three other proteins, ubiquitin, myoglobin and BSA obtained with 500 ms trapping times are shown in Figure 5.2c, 5.2d and 5.2e, respectively. The charge states are clearly separated in the mass spectra of ubiquitin and myoglobin as they are with cytochrome *c*. Different charge states can be partially resolved in the low charge, high *m/z* side of the BSA distribution, although the charge states are more difficult to distinguish at higher charge. The masses determined from these *m/z* measurements for ubiquitin, myoglobin and BSA are 8,610 ± 34, 16,949 ± 51, and 66,905 ± 113, respectively, and differ from the theoretical average masses by 0.30%, 0.01%, and 0.71%, respectively.

The trapping time depends on ion mass.[48, 52] About 75% of BSA ions are trapped for the entire 500 ms versus only 5% for ubiquitin. The average trapping times for BSA, myoglobin, cytochrome *c* and ubiquitin ions are 440 ms, 334 ms, 324 ms and 191 ms, respectively. One potential reason for this mass or size effect is that for a given *m*/*z*, lower mass ions have less momentum and may be more susceptible to collisional destabilization of their trajectories. Another contributing factor is that small ions, such as ubiquitin, with charge near the detection limit of the instrument, may not be recorded by the data analysis program if the signal falls below the noise threshold even though the ion remains trapped.

5.4.3 Origin of Frequency Changes of a Single Ion

The frequency shifts with time result in peak broadening in the FT of long segments of time-domain data. Fourier transforming short segments spaced across the trapping time reveals more details about how the frequency changes over time. The progression of the oscillation frequency of a single 15+ cytochrome *c* ion is shown in a time-frequency plot in Figure 5.3a obtained by FT of 25 ms time segments repeated at 5 ms intervals throughout the transient. Over the 500 ms trapping time, the ion oscillation frequency increased from 84.85 kHz to 85.42 kHz. This frequency increase results from two distinct types of frequency changes: small, continuous frequency shifts, such as the periods from 50-200 ms, 200-300 ms and 300-500 ms where the frequency changes only slightly, and large, discrete frequency shifts, such as the events at 50, 200 and 300 ms where the oscillation frequency increases suddenly. The oscillation frequencies of all cytochrome *c* ions increase over time with both types of frequency shifts contributing. Ubiquitin, myoglobin and BSA ions also exhibit this same behavior, with a gradual frequency increase over time punctuated by occasional sudden frequency jumps (single ion examples shown in Figures 5.3b, 5.3c and 5.3d). However, larger ions typically have fewer discrete shifts. The frequencies of ions from a sample of 8 MDa polyethylene glycol (single ion example shown in Figure 5.3e) increase gradually and only jump in frequency when fragmentation occurs.[50]

The rate at which each individual ion changes in frequency can be determined by finding the difference between the peak frequency measured in each 25 ms segment. For example, the ion in Figure 5.3a on average oscillated at 84.978 kHz in the 25 ms starting at 80 ms, and 84.990 kHz in the 25 ms starting at 85 ms, for a shift of 12 Hz in those 5 ms. The probability distribution of

the frequency shift in each 5 ms interval is shown for each protein in Figure 5.4. For the three smaller proteins, the most common change in frequency between two segments is zero Hz and the distribution of frequency shifts tails to larger frequency increases, with the tail increasing in intensity with protein mass. The most common frequency change for BSA is two Hz and tails to even higher frequency than the smaller proteins. The most likely cause for this wide range of gradual frequency shifts is reduction in the ion energy due to collisional energy loss. A change by one charge would result in a frequency change of ~650 Hz for a BSA ion with 55 charges and would cause an even larger change in frequency for the other smaller proteins. For a two Hz change in frequency to be caused by fragmentation, ubiquitin and cytochrome *c* ions would need to lose less than 1 Da, and myoglobin ions and BSA ions would lose ~1 or ~4 Da, respectively. Thus, these frequency changes almost certainly do not correspond to fragmentation. Each ion also has some probability of a small decrease in peak frequency over a single 5 ms interval, most likely caused by noise creating uncertainty in the location of the peak oscillation frequency.

An expansion of the frequency shift histogram at larger frequency increases is shown in Figure 5.4b. There are peaks in the frequency distribution at ~75 Hz and ~120 Hz for each protein. The frequency jumps occur more frequently for lower mass ions, with an average of ~5 events per 500 ms for cytochrome *c*, and ~0.2 per 500 ms for BSA. Ubiquitin ions have somewhat fewer jumps than cytochrome *c* and myoglobin because they are more often lost by the data analysis program immediately after a frequency jump because of their lower charge. The origin of these large frequency changes is not fully understood. If this occurred because of fragmentation and loss of a neutral molecule, each different charge state of each protein would need to lose a slightly different mass to correspond to the same 75 or 120 Hz frequency jump. For example, these frequency jumps correspond to loss of ~23 Da and ~36 Da from a 14+ cytochrome *c* ion but loss of ~150 Da and ~240 Da for a 49+ BSA ion. The discrete frequency jumps are unlikely to occur by a sudden loss of energy for a similar reason. Thus, the frequency jumps do not appear to be caused by changes to the mass, charge or energy of the ions. We hypothesize that the sudden frequency shifts may be the result of changes in the ion trajectory whilst in the trap. Trajectories off the central axis of the trap result in a faster turnaround time and a higher oscillation frequency at a given energy.[50] This mechanism is consistent with the trend towards fewer large shifts for higher mass ions, which have more momentum and are thus less likely to significantly change in trajectory after collisions occur.

5.4.4 Single Ion Collisional Cross Section Measurements

The energy loss by ions due to collisions in these experiments is related to the number of collisions that occur. Thus, determining the energy lost to collisions with the background gas provides a route to measuring collisional cross sections. However, the exact relationship between the energy lost and collisional cross section is complex due to the wide range of velocities at which collisions can occur inside the cone trap. The *m*/*z* of each protein ion can be obtained from the initial frequency, and the energy of the ion as a function of time can be determined from its frequency and *m*/*z* using eqs 5.1 and 5.2. The average initial ion energy is 202.4 eV/charge. However, the final energy of the ion cannot simply be determined from the total frequency change for each ion because this includes both gradual frequency changes and discrete frequency jumps, which are the result of two different processes. In order to isolate the time periods in which ions slowly changed in frequency and remove the effects of ion trajectory changes, all frequency shifts within 10 ms of the ion oscillation frequency jumping by greater than 50 Hz were filtered out.

The remaining frequency changes were averaged to find the frequency change over 5 ms and these data were normalized to find the final frequency after 500 ms in the absence of trajectory changes. With that final frequency, the final energy per charge of each charge state was obtained using eqs 1 and 2 and subtracted from the initial energy of 202.4 eV/charge. The total energy lost for each charge state was then determined by multiplying the energy per charge difference by the charge state.

A plot of the total energy lost by ubiquitin, cytochrome *c*, myoglobin and BSA ions versus nitrogen collisional cross section values from the literature for ions formed from denaturing solutions[53] is shown in Figure 5.5. The values for BSA were measured in nitrogen with TWIMS calibrated using the method of Ruotolo et al (see Supporting Information).[5] The total energy lost trends linearly with nitrogen collisional cross sections although there is more scatter in the data for the individual charge states of BSA. It is possible that some of the scatter for BSA is because of mis-assigned charge states because of insufficient *m*/*z* resolution (Figure 5.2e). Nonetheless, the different proteins can be readily distinguished by the differing amounts of energy lost to collisions and the energy loss trends with collisional cross section. Over the size range of the ions measured here, the trend between energy loss and cross section can be fit with a line with an R^2 of 0.98. A linear fit to the data for just the smaller three proteins results in a similar R^2 value with a slightly different slope. Over a wider range of masses and cross sections, this trend may not necessarily be as linear. However, the relationship between energy loss and collisional cross section should make it possible to determine collisional cross sections from these data for ions for which values have not been previously measured.

Jarrold and coworkers recently proposed that the energy per charge lost to collisions by an ion oscillating in a cone trap can be modeled with an exponential relationship.[49] However, the energy loss modeled using cross section values obtained from the literature for these protein ions does not match the energy loss trend we observe. The model predicts that cytochrome *c* 13+ loses energy per charge more slowly than 10+ ubiquitin under the same instrumental conditions. However, 13+ cytochrome *c* loses on average ~3.0 eV/charge to collisions over the course of 500 ms compared to ~1.8 eV/charge lost by 10+ ubiquitin. One possible explanation for the larger slope of the measured energy change with cross section is that the collisional cross sections of these ions likely depend on velocity. The Langevin cross sections for the proteins and charge states investigated here become larger than the hard sphere cross sections when the ion velocities are less than ~150-275 m/s (see Supporting Information). However, the Langevin cross sections should also increase with molecular size owing to the larger number of charges for larger proteins. In the absence of a more theoretical treatment of these data, collisional cross sections of ions can be determined by calibrating the energy loss with ions of similar mass and known cross sections.

5.5 Conclusions

The masses of single multiply charged ions can be readily measured using an electrostatic ion trap for proteins as small as ubiquitin. The ion oscillation frequency histograms for small proteins show well resolved peaks corresponding to different charge states making an assignment of *m*/*z* unambiguous. The masses obtained from these data are within 1% of the computed masses of different proteins between 8.6 kDa and 66.5 kDa. The ion oscillation frequency increases with time, both gradually as the ions lose energy to collisions with the background gas and more suddenly, likely a result of collision induced changes in trajectory. The rate at which the ion oscillation frequency gradually increases with time increases with ion mass, but the number of

frequency jumps decreases with ion mass. The gradual collisional dampening of the ion motion is related to the collisional cross section of these ions. The total energy lost per unit time is determined from the rate of the gradual frequency change, and these values increase linearly with collisional cross sections of these ions in nitrogen measured using other ion mobility methods.

The ion kinetic energies range from zero as the ion turns around inside the cone electrode to the full energy in the field free region of the detector tube. Because of the wide range of velocities, determining collisional cross sections directly from the change in energy is complex. The trend in energy loss observed here does not match that predicted from a model based on hard-spheres collisions which underestimates the energy lost by higher mass and charge ions. The Langevin cross sections is greater than the hard sphere cross section when the ion velocity is low, which occurs when the ion turns around in the cone trap. Thus, the collisional cross section measured in these experiments may only loosely correlate with high precision collisional cross sections measured in drift tubes. However, even without a theoretical relationship between collisional cross section and energy loss, the correlation between energy loss and previously measured collisional cross sections observed here can be used to establish a calibration against which the cross sections of other ions can be measured, similar to the calibration steps necessary to obtain collisional cross sections with TWIMS[5] or by dephasing of ion packets in FT-ICR MS.[54] Although the relationship observed here is linear over this range of protein masses, it is possible that calibration curves may not be linear over an even wider range of masses and collisional cross sections. A short-time FT method is demonstrated for the analysis of the frequency shift. However, the width of a FT peak obtained at longer times for larger ions that do not undergo sudden jumps in frequency should also be related to the collisional cross section values and the peak width could be used in determining these values for unknown ions. These results indicate that CDMS is a useful technique for simultaneously measuring both the mass and collisional cross section of single ions, expanding the structural information that can be obtained for complex mixtures of large ions that cannot be resolved using conventional MS instruments.

5.6 Acknowledgements

The authors thank Waters Corporation for their generous donation of equipment, including the Z-spray source used in this work, and the National Institutes of Health (R01GM096097 and 1S10OD020062-01) for funding.

5.7 References

(1) Wysocki, V. H.; Joyce, K. E.; Jones, C. M.; Beardsley, R. L. Surface-Induced Dissociation of Small Molecules, Peptides, and Non-Covalent Protein Complexes. *J. Am. Soc. Mass Spectrom.* **2008**, *19*, 190-208.

(2) Hernandez, H.; Robinson, C. V. Determining the stoichiometry and interactions of macromolecular assemblies from mass spectrometry. *Nat. Protoc.* **2007**, *2*, 715-726.

(3) Snijder, J.; Heck, A. J. R. Analytical Approaches for Size and Mass Analysis of Large Protein Assemblies. *Annu. Rev. Anal. Chem.* **2014**, *7*, 43-64.

(4) El-Baba, T. J.; Woodall, D. W.; Raab, S. A.; Fuller, D. R.; Laganowsky, A.; Russell, D. H.; Clemmer, D. E. Melting Proteins: Evidence for Multiple Stable Structures upon Thermal Denaturation of Native Ubiquitin from Ion Mobility Spectrometry-Mass Spectrometry Measurements. *J. Am. Chem. Soc.* **2017**, *139*, 6306-6309.

(5) Ruotolo, B. T.; Benesch, J. L. P.; Sandercock, A. M.; Hyung, S.; Robinson, C. V. Ion mobility–mass spectrometry analysis of large protein complexes. *Nat. Protoc.* **2008**, *3*, 1139-1152.

(6) Clemmer, D. E.; Jarrold, M. F. Ion Mobility Measurements and their Applications to Clusters and Biomolecules. *J. Mass. Spectrom.* **1997**, *32*, 577-592.

(7) Kintzer, A. F.; Sterling, H. J.; Tang, I. I.; Abdul-Gader, A.; Miles, A. J.; Wallace, B. A.; Williams, E. R.; Krantz, B. A. Role of the Protective Antigen Octamer in the Molecular Mechanism of Anthrax Lethal Toxin Stabilization in Plasma. *J. Mol. Biol.* **2010**, *399*, 741-758.

(8) Nagornova, N. S.; Rizzo, T. R.; Boyarkin, O. V. Highly Resolved Spectra of Gas-Phase Gramicidin S: A Benchmark for Peptide Structure Calculations. *J. Am. Chem. Soc.* **2010**, *132*, 4040-4041.

(9) Prell, J. S.; Flick, T. G.; Oomens, J.; Berden, G.; Williams, E. R. Coordination of Trivalent Metal Cations to Peptides: Results from IRMPD Spectroscopy and Theory. *J. Phys. Chem. A.* **2010**, *114*, 854-860.

(10) Seo, J.; Hoffmann, W.; Warnke, S.; Huang, X.; Gewinner, S.; Schöllkopf, W.; Bowers, M. T.; von Helden, G.; Pagel, K. An infrared spectroscopy approach to follow β-sheet formation in peptide amyloid assemblies. *Nat. Chem.* **2017**, *9*, 39-44.

(11) Catherman, A. D.; Skinner, O. S.; Kelleher, N. L. Top Down proteomics: Facts and perspectives. *Biochem. Biophys. Res. Commun.* **2014**, *445*, 683-693.

(12) Skinner, O. S.; Breuker, K.; McLafferty, F. W. Charge Site Mass Spectra: Conformation-Sensitive Components of the Electron Capture Dissociation Spectrum of a Protein. *J. Am. Soc. Mass Spectrom.* **2013**, *24*, 807-810.

(13) Han, L.; Hyung, S.; Mayers, J. J. S.; Ruotolo, B. T. Bound Anions Differentially Stabilize Multiprotein Complexes in the Absence of Bulk Solvent. *J. Am. Chem. Soc.* **2011**, *133*, 11358-11367.

(14) Samulak, B. M.; Niu, S.; Andrews, P. C.; Ruotolo, B. T. Ion Mobility-Mass Spectrometry Analysis of Cross-Linked Intact Multiprotein Complexes: Enhanced Gas-Phase Stabilities and Altered Dissociation Pathways. *Anal. Chem.* **2016**, *88*, 5290-5298.

(15) Servage, K. A.; Silveira, J. A.; Fort, K. L.; Clemmer, D. E.; Russell, D. H. Water-Mediated Dimerization of Ubiquitin Ions Captured by Cryogenic Ion Mobility-Mass Spectrometry. *J. Phys. Chem. Lett.* **2015**, *6*, 4947-4951.

(16) Clemmer, D. E.; Russell, D. H.; Williams, E. R. Characterizing the Conformationome: Toward a Structural Understanding of the Proteome. *Acc. Chem. Res.* **2017**, *50*, 556-560.

(17) Lössl, P.; Snijder, J.; Heck, A. J. R. Boundaries of Mass Resolution in Native Mass Spectrometry. *J. Am. Soc. Mass Spectrom.* **2014**, *25*, 906-917.

(18) O'Connor, P. B.; McLafferty, F. W. Oligomer Characterization of 4-23 kDa Polymers by Electrospray Fourier Transform Mass Spectrometry. *J. Am. Chem. Soc.* **1995**, *117*, 12826-12831.

(19) Robb, D. B.; Brown, J. M.; Morris, M.; Blades, M. W. Method of Atmospheric Pressure Charge Stripping for Electrospray Ionization Mass Spectrometry and Its Application for the Analysis of Large Poly(Ethylene Glycol)s. *Anal. Chem.* **2014**, *86*, 9644-9652.

(20) Smith, R. D.; Cheng, X.; Brace, J. E.; Hofstadler, S. A.; Anderson, G. A. Trapping, detection and reaction of very large single molecular ions by mass spectrometry. *Nature.* **1994**, *369*, 137-139.

(21) Bruce, J. E.; Cheng, X.; Bakhtiar, R.; Wu, Q.; Hofstadler, S. A.; Anderson, G. A.; Smith, R. D. Trapping, detection, and mass measurement of individual ions in a Fourier transform ion cyclotron resonance mass spectrometer. *J. Am. Chem. Soc.* **1994**, *116*, 7839-7847.

(22) Wuerker, R. F.; Shelton, H.; Langmuir, R. V. Electrodynamic containment of charged particles. *J. Appl. Phys.* **1959**, *30*, 342-349.

(23) Philip, M. A.; Gelbard, F.; Arnold, S. An absolute method for aerosol particle mass and charge measurement. *J. Colloid Interface Sci.* **1983**, *91*, 507-515.

(24) Hars, G.; Tass, Z. Application of quadrupole ion trap for the accurate mass determination of submicron size charged particles. *J. Appl. Phys.* **1995**, *77*, 4245-4250.

(25) Schlemmer, S.; Illemann, J.; Wellert, S.; Gerlich, D. Nondestructive high-resolution and absolute mass determination of single charged particles in a three-dimensional quadrupole trap. *J. Appl. Phys.* **2001**, *90*, 5410-5418.

(26) Nie, Z.; Tzeng, Y.; Chang, H.; Chiu, C.; Chang, C.; Chang, C.; Tao, M. Microscopy-based mass measurement of a single whole virus in a cylindrical ion trap. *Angew. Chem., Int. Ed.* **2006**, *45*, 8131-8134.

(27) Cai, Y.; Peng, W. P.; Kuo, S. J.; Lee, Y. T.; Chang, H. C. Single-particle mass spectrometry of polystyrene microspheres and diamond nanocrystals. *Anal. Chem.* **2002**, *74*, 232-238.

(28) Shelton, H.; Hendricks, C. D.; Wuerker, R. F. Electrostatic acceleration of microparticles to hypervelocities. *J. Appl. Phys.* **1960**, *31*, 1243-1246.

(29) Hendricks Jr., C. D. Charged droplet experiments. *J. Colloid Sci.* **1962**, *17*, 249-259.

(30) Keaton, P. W.; Idzorek, G. C.; Rowton Sr., L. J.; Seagrave, J. D.; Stradling, G. L.; Bergeson, S. D.; Collopy, M. T.; Curling Jr., H. L.; McColl, D. B.; Smith, J. D. A hypervelocity-microparticle-impacts laboratory with 100-km/s projectiles. *Int. J. Impact Eng.* **1990**, *10*, 295-308.

(31) Stradling, G. L.; Idzorek, G. C.; Shafer, B. P.; Curling Jr., H. L.; Collopy, M. T.; Blossom, A. A. H.; Fuerstenau, S. Ultra-high velocity impacts: cratering studies of microscopic impacts from 3 km/s to 30 km/s. *Int. J. Impact Eng.* **1993**, *14*, 719-727.

(32) Fuerstenau, S. D.; Benner, W. H.; Thomas, J. J.; Brugidou, C.; Bothner, B.; Siuzdak, G. Mass spectrometry of an intact virus. *Angew. Chem., Int. Ed.* **2001**, *40*, 542-544.

(33) Fuerstenau, S. D.; Benner, W. H. Molecular weight determination of megadalton DNA electrospray ions using charge detection time-of-flight mass spectrometry. *Rapid Commun. Mass Spectrom.* **1995**, *9*, 1528-1538.

(34) Schultz, J. C.; Hack, C. A.; Benner, W. H. Mass determination of megadalton-DNA electrospray ions using charge detection mass spectrometry. *J. Am. Soc. Mass Spectrom.* **1998**, *9*, 305-313.

(35) Viodé, A.; Dagany, X.; Kerleroux, M.; Dugourd, P.; Doussineau, T.; Charles, L.; Antoine, R. Coupling of size-exclusion chromatography with electrospray ionization charge-detection mass spectrometry for the characterization of synthetic polymers of ultra-high molar mass. *Rapid Commun. Mass Spectrom.* **2016**, *30*, 132-136.

(36) Ouadah, N.; Doussineau, T.; Hamada, T.; Dugourd, P.; Bordes, C.; Antoine, R. Correlation between the Charge of Polymer Particles in Solution and in the Gas Phase Investigated by Zeta-Potential Measurements and Electrospray Ionization Mass Spectrometry. *Langmuir.* **2013**, *29*, 14074-14081.

(37) Doussineau, T.; Désert, A.; Lambert, O.; Taveau, J.; Lansalot, M.; Dugourd, P.; Bourgeat-Lami, E.; Ravaine, S.; Duguet, E.; Antoine, R. Charge detection mass spectrometry for the characterization of mass and surface area of composite nanoparticles. *J. Phys. Chem. C.* **2015**, *119*, 10844-10849.

(38) Doussineau, T.; Bao, C. Y.; Antoine, R.; Dugourd, P.; Zhang, W.; D'Agosto, F.; Charleux, B. Direct molar mass determination of self-assembled amphiphilic block copolymer nanoobjects using electrospray-charge detection mass spectrometry. *ACS Macro Lett.* **2012**, *1*, 414-417.

(39) Benner, W. H. A Gated Electrostatic Ion Trap to Repetitiously Measure the Charge and m/z of Large Electrospray Ions. *Anal. Chem.* **1997**, *69*, 4162-4168.

(40) Contino, N. C.; Jarrold, M. F. Charge detection mass spectrometry for single ions with a limit of detection of 30 charges. *Int. J. Mass Spectrom.* **2013**, *345-347*, 153-159.

(41) Keifer, D. Z.; Shinholt, D. L.; Jarrold, M. F. Charge detection mass spectrometry with almost perfect charge accuracy. *Anal. Chem.* **2015**, *87*, 10330-10337.

(42) Pierson, E. E.; Contino, N. C.; Keifer, D. Z.; Jarrold, M. F. Charge detection mass spectrometry for single ions with an uncertainty in the charge measurement of 0.65 e. *J. Am. Soc. Mass Spectrom.* **2015**, *26*, 1213-1220.

(43) Keifer, D. Z.; Motwani, T.; Teschke, C. M.; Jarrold, M. F. Measurement of the accurate mass of a 50 MDa infectious virus. *Rapid Commun. Mass Spectrom.* **2016**, *30*, 1957-1962.

(44) Doussineau, T.; Paletto, P.; Dugourd, P.; Antoine, R. Multiphoton Dissociation of Electrosprayed MegaDalton-Sized DNA Ions in a Charge-Detection Mass Spectrometer. *J. Am. Soc. Mass Spectrom.* **2015**, *26*, 7-13.

(45) Antoine, R.; Doussineau, T.; Dugourd, P.; Calvo, F. Multiphoton dissociation of macromolecular ions at the single-molecule level. *Phys. Rev. A.* **2013**, *87*, 013435.

(46) Doussineau, T.; Antoine, R.; Santacreu, M.; Dugourd, P. Pushing the limit of infrared multiphoton dissociation to megadalton-size DNA ions. *J. Phys. Chem. Lett.* **2012**, *3*, 2141-2145.

(47) Doussineau, T.; Yu Bao, C.; Clavier, C.; Dagany, X.; Kerleroux, M.; Antoine, R.; Dugourd, P. Infrared multiphoton dissociation tandem charge detection-mass spectrometry of single megadalton electrosprayed ions. *Rev. Sci. Instrum.* **2011**, *82*, 084104.

(48) Elliott, A. G.; Merenbloom, S. I.; Chakrabarty, S.; Williams, E. R. Single particle analyzer of mass: a charge detection mass spectrometer with a multi-detector electrostatic ion trap. *Int. J. Mass Spectrom.* **2017**, *414*, 45-55.

(49) Keifer, D. Z.; Alexander, A. W.; Jarrold, M. F. Spontaneous Mass and Charge Losses from Single Multi-Megadalton Ions Studied by Charge Detection Mass Spectrometry. *J. Am. Soc. Mass Spectrom.* **2017**, *28*, 498-506.

(50) Elliott, A. G.; Harper, C. C.; Lin, H.; Williams, E. R. Mass, Mobility and MS^n Measurements of Single Ions Using Charge Detection Mass Spectrometry. *Analyst.* **2017**, *142* (15), 2760-2769.

(51) Covey, T.; Douglas, D. J. Collision cross sections for protein ions. *J. Am. Soc. Mass Spectrom.* **1993**, *4*, 616-623.

(52) Contino, N. C.; Pierson, E. E.; Keifer, D. Z.; Jarrold, M. F. Charge detection mass spectrometry with resolved charge states. *J. Am. Soc. Mass Spectrom.* **2013**, *24*, 101-108.

(53) Bush, M. F.; Hall, Z.; Giles, K.; Hoyes, J.; Robinson, C. V.; Ruotolo, B. T. Collision cross sections of proteins and their complexes: a calibration framework and database for gas-phase structural biology. *Anal. Chem.* **2010**, *82*, 9557-9565.

(54) Yang, F.; Voelkel, J. E.; Dearden, D. V. Collision Cross Sectional Areas from Analysis of Fourier Transform Ion Cyclotron Resonance Line Width: A New Method for Characterizing Molecular Structure. *Anal. Chem.* **2012**, *84*, 4851-4857.

5.8 Figures

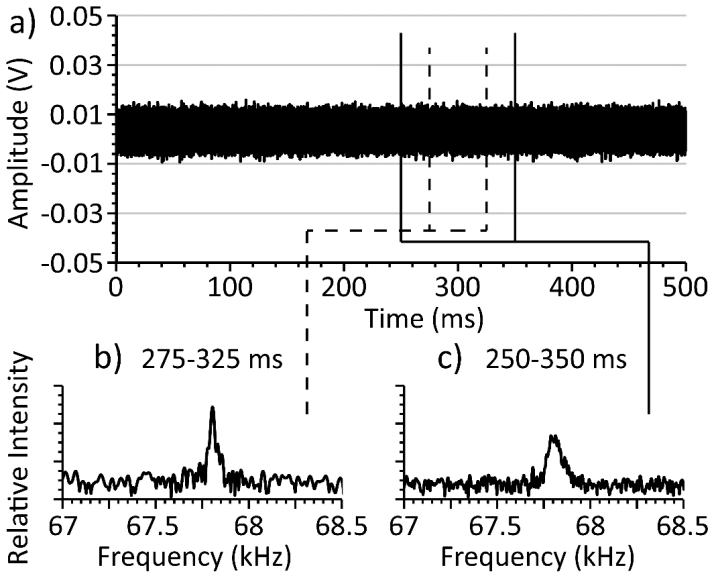

Figure 5.1: a) Time-domain signal of a 50+ BSA ion trapped for 500 ms, and Fourier transforms of segments of that transient centered at 300 ms that are b) 50 ms and c) 100 ms long.

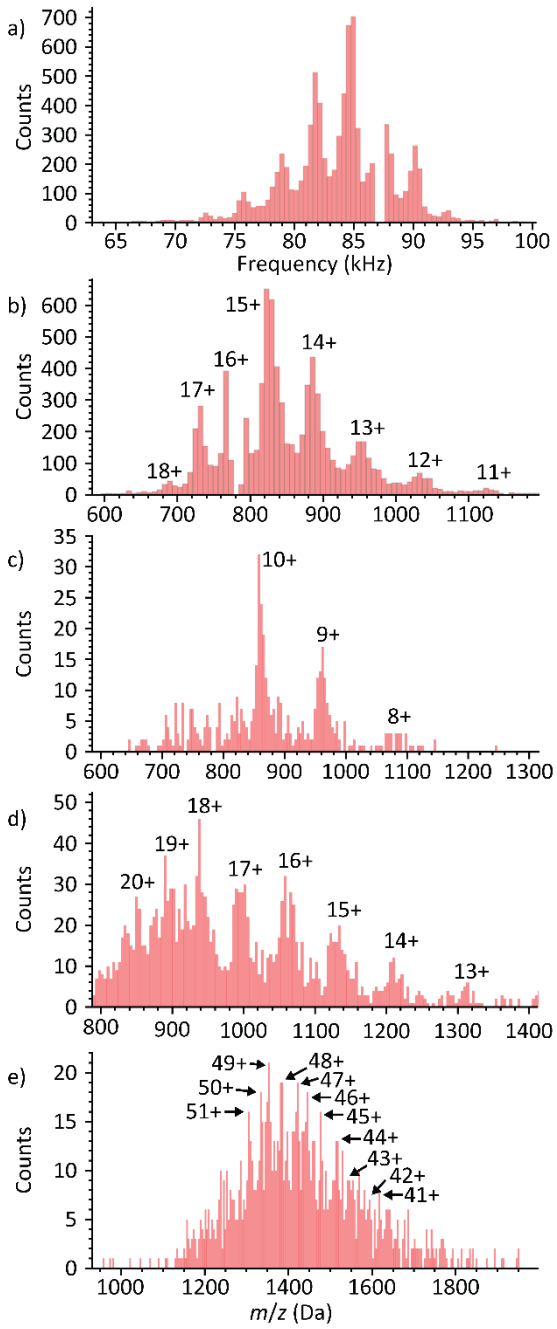

Figure 5.2: Histograms of a) the oscillation frequency of 8363 cytochrome *c* ions during the first 25 ms ions were trapped and b) the corresponding *m/z* of each ion determined from the data in a), the *m/z* histograms of c) ubiquitin, d) myoglobin, and e) BSA.

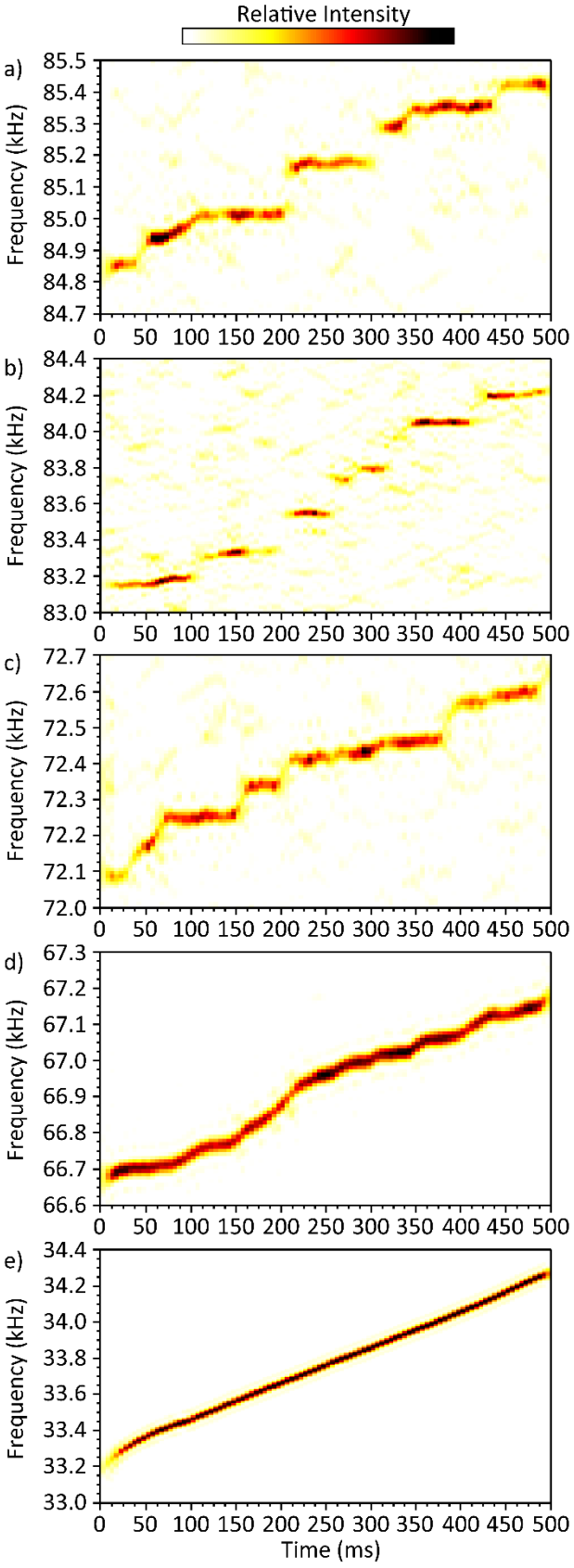

Figure 5.3: Short-time Fourier transforms of single trapped ions of a) 15+ cytochrome *c*, b) 10+ ubiquitin, c) 15+ myoglobin, d) 50+ BSA, and e) PEG.

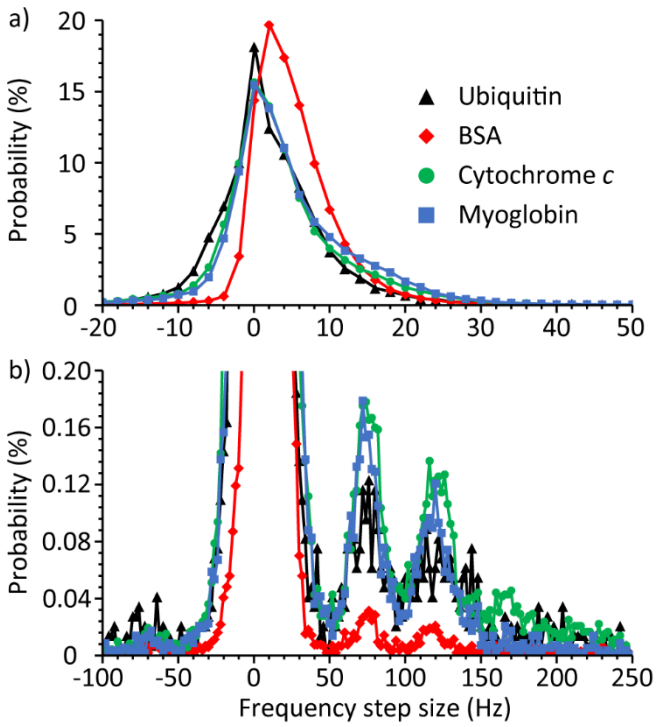

Figure 5.4: a) Probability distribution of the frequency step size in a 5 ms interval and b) an expansion of a) to show the frequency of the large discrete frequency shifts.

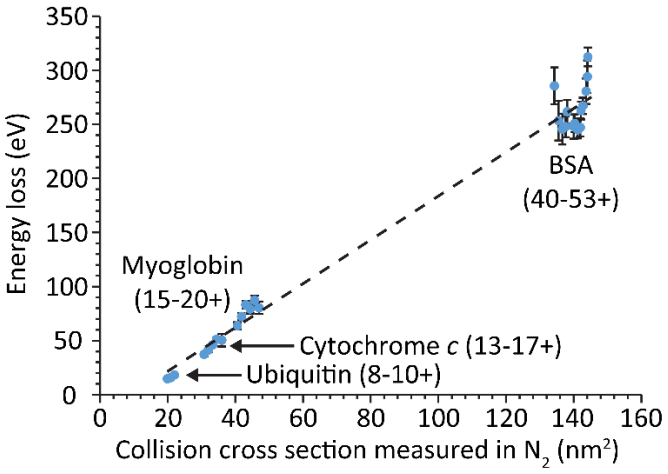

Figure 5.5: The energy lost over 500 ms for various charge states of ubiquitin, cytochrome *c*, myoglobin and BSA ions formed by ESI from solutions in which these proteins are denatured as a function of the measured collisional cross sections of the corresponding ions in N_2 reported in reference 53 and measured using TWIMS for BSA.

5.9 Supporting Information

5.9.1 Additional Experimental Information

5.9.1.1 Simulations to Determine Relationship between Frequency and Energy per Charge

Ion energy was determined from the oscillation frequency using data from SIMION ion trajectory simulations of ions traveling along the central axis of the trap using ions weighing 8 MDa and 12.4 kDa with 1000 and 15 charges, respectively. The simulated ion energies were between 193 and 253 eV/charge which is the range of energies that can be trapped in the electrostatic ion trap with the parameters used in the experiment. The time required for each cycle was obtained from the time between the ion entering the tube in one direction and reentering in the opposite direction after turning around in the cone electrode. The oscillation frequency is the inverse of the cycle time. The relationship between ion kinetic energy and oscillation frequency for each ion was fit with a quadratic polynomial. The equation for the best fit line for the 8 MDa ion is given in equation 5.3

$$f = -0.497E^2 + 1.62 \times 10^{\,2}E + 1.47 \times 10^4 \qquad \text{(eq. 5.3)}$$

and the equation for the best fit line for the 12.4 kDa ion is given in equation 5.4

$$f = -1.55E^2 + 5.06 \times 10^{\,2}E + 4.58 \times 10^4 \qquad \text{(eq. 5.4)}$$

The equation for the calibration constant, $C(E)$, between frequency and m/z at different energies, equation 5.2, was determined by multiplying the coefficients in equations 5.3 and 5.4 by the square root of the m/z of the ion used in that simulation. The coefficients for equation 5.2 calculated at the two different m/z values differ by less than 0.01% indicating that the coefficients do not depend on m/z.

5.9.1.2 Traveling Wave Ion Mobility Spectrometry (TWIMS) of Bovine Serum Albumin.

TWIMS was used to measure the cross sections of BSA ions with charges ranging from 36+ to 53+. These ions are formed by ESI from solutions in which the protein is denatured. To obtain cross sections from the TWIMS drift times, calibration with protein standards with known cross sections are typically used.[1] A calibration curve was generated by measuring the drift times of ubiquitin, cytochrome *c*, and myoglobin ions formed by ESI from solutions in which these proteins are denatured with charge states ranging from 7+ – 13+, 13+ – 19+ and 15+ – 24+, respectively. The drift times were corrected for the mass and charge dependence of flight time using the procedure described by Ruotolo et al.[1] and are shown as a function of known cross sections[2] in Supporting Figure 5.1. Drift times measured for BSA ions are similarly corrected and the collisional cross sections for each charge state are obtained using the calibration data. The values and estimated error[1] for BSA collisional cross sections are reported in Supporting Table 5.1. Although the measured collisional cross sections of BSA rely on extrapolation of the calibration beyond the range of calibrant collisional cross sections, the collisional cross section of 135.5 ± 6.3 nm^2 obtained for the 41+ charge state is in good agreement with the value of 140 nm^2 reported previously by Covey and Douglas.[3] Cross sections for the 36+ and 38+ charge state

measured with TWIMS are 128.8 ± 7.4 nm^2 and 131.1 ± 4.0 nm^2, respectively, which are also in good agreement with the values of 133 nm^2 and 137 nm^2 previously reported. Values for the other charge states have not been reported previously.

5.9.1.3 Calculation of Langevin Cross Sections

The Langevin cross section depends on the interaction potential between a charge particle and a polarizable molecule and is proportional to the charge of the ion and inversely proportional to the ion velocity. These cross sections are obtained in SI units from equation 5.5[4, 5]

$$\sigma = \frac{q\sqrt{\frac{\alpha}{\mu}}}{2v\varepsilon_0} \qquad \text{(eq. 5.5)}$$

where σ is the collisional cross section, q is the charge of the ion, α is the polarizability of the neutral collision partner, μ is the reduced mass of the ion and collision partner, v is the ion velocity and ε_0 is the permittivity of vacuum. The neutral collision partner in this calculation is N_2, which has a polarizability of 1.903 x 10^{-40} $C \cdot m^2 \cdot V^{-1}$.[6] Other neutral molecules, such as CO, are likely present in the vacuum chamber as well. The velocity at which the Langevin cross section is equal to the hard sphere cross section was calculated by solving for velocity in Equation S3 and using the hard sphere cross section of each charge state. The values are shown in Supporting Table 5.5. The Langevin cross section is larger when the velocity is below 233-264 m/s, 245-274 m/s, 214-247 m/s and 162-219 m/s for the 8+ – 10+ charge states of ubiquitin, 13+ – 17+ charge states cytochrome *c*, 15+ – 20+ charge states of myoglobin, and 36 – 53+ charge states of BSA, respectively.

5.9.2 Supporting Tables and Figure

Supporting Table 5.1. BSA Collisional Cross Section Measured with TWIMS and Total Energy Loss by Charge State

Charge State	Cross Section (nm^2)	Total Energy Loss (eV)
40+	134.3 ± 6.1	285 ± 17
41+	135.5 ± 6.3	253 ± 18
42+	136.6 ± 6.4	246 ± 14
43+	137.6 ± 6.5	248 ± 10
44+	138.1 ± 8.7	262 ± 11
45+	140.0 ± 8.9	248 ± 8
46+	140.2 ± 9.1	251 ± 8
47+	141.1 ± 9.2	245 ± 8
48+	141.9 ± 7.1	247 ± 8
49+	142.2 ± 7.2	263 ± 8
50+	142.2 ± 4.9	267 ± 8
51+	142.7 ± 7.5	281 ± 12
52+	144.0 ± 5.1	294 ± 15
53+	144.2 ± 5.5	312 ± 9

Supporting Table 5.2. Ubiquitin Collisional Cross Section and Total Energy Loss by Charge State

Charge State	**Cross Section (nm^2)^2**	**Total Energy Loss (eV)**
8+	19.9	15 ± 2
9+	20.9	16 ± 1
10+	22.0	18 ± 1

Supporting Table 5.3. Cytochrome *c* Collisional Cross Section and Total Energy Loss by Charge State

Charge State	**Cross Section (nm^2)^2**	**Total Energy Loss (eV)**
13+	30.8	37 ± 2
14+	32.0	41 ± 2
15+	33.3	46 ± 2
16+	34.5	51 ± 1
17+	36.0	50 ± 6

Supporting Table 5.4. Myoglobin Collisional Cross Section and Total Energy Loss by Charge State

Charge State	Cross Section $(nm^2)^2$	Total Energy Loss (eV)
15+	40.6	64 ± 3
16+	41.8	72 ± 3
17+	43.1	83 ± 3
18+	44.4	79 ± 4
19+	45.7	87 ± 5
20+	47.0	80 ± 6

Supporting Table 5.5. Velocity at which the Langevin cross section is equal to the hard spheres cross section.

Protein	Charge State	Velocity (m/s)
Ubiquitin	8+	233
	9+	250
	10+	264
Cytochrome *c*	13+	245
	14+	253
	15+	261
	16+	269
	17+	274
Myoglobin	15+	214
	16+	222
	17+	228
	18+	235
	19+	241
	20+	247
BSA	36+	162
	37+	164
	38+	168
	39+	170
	40+	172
	41+	175
	42+	178
	43+	181
	44+	184
	45+	186
	46+	190
	47+	193
	48+	196
	49+	200
	50+	203
	51+	205
	52+	209
	53+	213

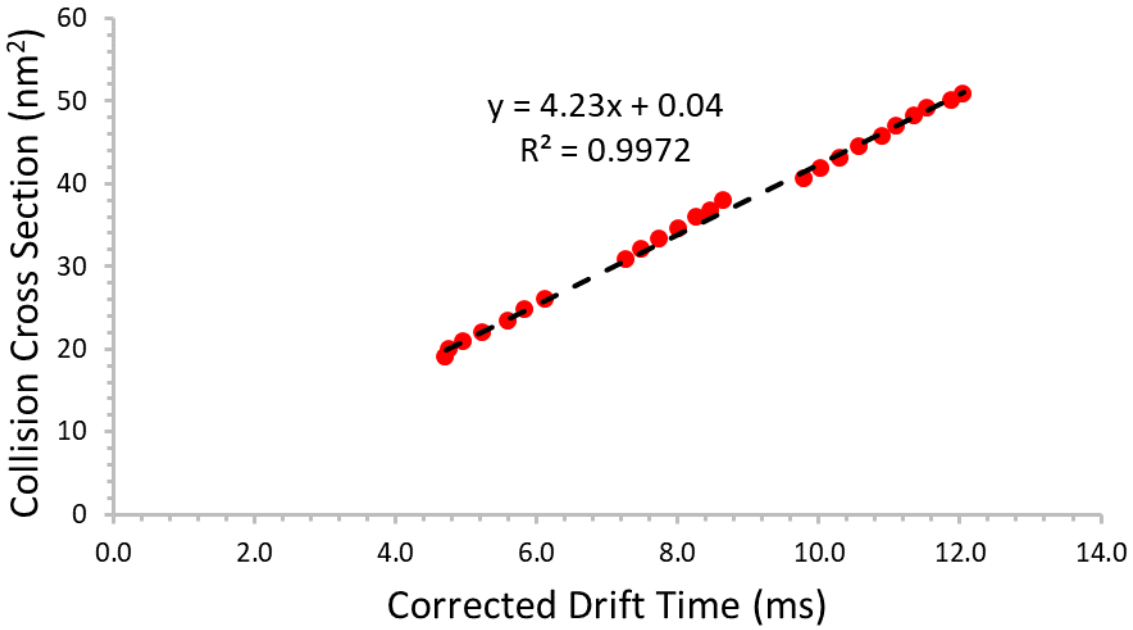

Supporting Figure 5.1. Calibration plot of corrected drift time with respect to ubiquitin, cytochrome *c*, and myoglobin cross section.

5.9.3 Supporting Information References

(1) Ruotolo, B. T.; Benesch, J. L. P.; Sandercock, A. M.; Hyung, S.; Robinson, C. V. Ion mobility–mass spectrometry analysis of large protein complexes. *Nat. Protoc.* **2008**, *3*, 1139-1152.

(2) Bush, M. F.; Hall, Z.; Giles, K.; Hoyes, J.; Robinson, C. V.; Ruotolo, B. T. Collision cross sections of proteins and their complexes: a calibration framework and database for gas-phase structural biology. *Anal. Chem.* **2010**, *82*, 9557-9565.

(3) Covey, T.; Douglas, D. J. Collision cross sections for protein ions. *J. Am. Soc. Mass Spectrom.* **1993**, *4*, 616-623.

(4) Guan, S.; Li, G.; Marshall, A. G. Effect of ion-neutral collision mechanism on the trapped-ion equation of motion: a new mass spectral line shape for high-mass trapped ions. *Int. J. Mass Spectrom. Ion Processes.* **1997**, *167*, 185-193.

(5) Su, T.; Bowers, M. T. Ion-polar molecule collisions: the effect of ion size on ion-polar molecule rate constants; the parameterization of the average-dipole-orientation theory. *Int. J. Mass Spectrom. Ion Phys.* **1973**, *12*, 347-356.

(6) Olney, T. N.; Cann, N. M.; Cooper, G.; Brion, C. E. Absolute scale determination for photoabsorption spectra and the calculation of molecular properties using dipole sum-rules. *Chem. Phys.* **1997**, *223*, 59-98.

Chapter 6

Effects of Individual Ion Energies on Charge Measurements in Fourier Transform Charge Detection Mass Spectrometry (FT-CDMS)

This chapter is reproduced with permission from:

Andrew G. Elliott, Conner C. Harper, Haw-Wei Lin, Evan R. Williams

"Effects of Individual Ion Energies on Charge Measurements in Fourier Transform Charge Detection Mass Spectrometry (FT-CDMS)" *J. Am. Soc. Mass Spectrom.* **2018**, DOI: 10.1007/s13361-018-2094-8

6.1 Abstract

A method to correct for the effect of ion energy on charge measurements of individual ions trapped and weighed with charge detection mass spectrometry (CDMS) is demonstrated. Ions with different energies induce different signal patterns inside an electrostatic ion trap. The sum of the amplitudes of the fundamental and second harmonic frequencies in the Fourier transform of the induced signal, which has been used to obtain the ion charge, depends on both ion energy and charge. The amplitudes of the fundamental frequencies of ions increase over time as ions lose energy by collisions with background gas and solvent loss from larger ions. Model ion signals are simulated with the same time domain amplitude at different energies and frequencies and the resulting fundamental frequency amplitudes are used to normalize real ion signals for energy and frequency effects. The fundamental frequency amplitude decreases dramatically below 20 kHz and increases by ~17% from the highest energy to lowest energy that is stable with a given trap potential at all frequencies. Normalizing the fundamental frequency amplitude with the modeled amplitudes removes the systematic changes in the charge measurement of polyethylene glycol (PEG) and other ions and makes it possible to signal average the amplitude over long times, which reduces the charge uncertainty to 0.04% for a PEG ion for a 500 ms measurement. This method improves charge measurement accuracy and uncertainty, which are important for high accuracy mass measurement with CDMS.

6.2 Introduction

Electrospray ionization (ESI) can transfer large molecules and molecular complexes into the gas phase as multiply charged ions for their identification or structural analysis with mass spectrometry (MS). Masses of ions can be determined from the spacings between peaks in a charge state distribution produced by molecules or complexes with the same mass or from the isotopic

spacing of a single charge state, with all information obtained from ensemble measurements of many different ions. Heterogeneity in the masses of ions, both intrinsic to the analyte and due to salt and solvent adduction, can lead to broad, unresolved peaks which obscure the charge state separation necessary for mass measurement when isotopic or adduct resolution is not possible.[1] Charges and masses have been measured for highly purified virus capsids up to ~18 MDa, but the upper mass limit is significantly lower for more heterogeneous samples, such as native viruses and synthetic polymers.[2-4] The issue of heterogeneity can be eliminated if the mass of each ion is determined individually, such as has been demonstrated in Fourier transform ion cyclotron resonance (FT-ICR)[5-7] and quadrupole ion trap (QIT) mass spectrometry.[8-15] Although accurate mass measurements can be made with these techniques, the long measurement time for each ion makes them impractical to use for analyzing complex samples.

Charge detection mass spectrometry (CDMS) is an alternative method for single ion MS that is faster than the FT-ICR and QIT techniques. In CDMS, single ions induce a charge pulse as they pass through a conductive detection tube. The charge of the ion is proportional to the amplitude of the charge pulse, and the *m*/*z* of the ion is proportional to its velocity, which is obtained from the duration of the charge pulse. The simplest implementation of CDMS, in which an ion passes once through a single detector, has been used to study a variety of different samples.[16-25] A single tube CDMS measurement is fast, but has the disadvantage of high uncertainty (>75 e) in the charge measurement for each individual ion. Because the ion detection is nondestructive, the signal from an ion can be averaged from multiple measurements in order to reduce uncertainty in the charge measurement. Techniques involving electrostatic ion traps,[26-29] arrays of aligned detector tubes,[30-32] and a combined ion trap and array detector[33] have all been implemented to repetitively weigh an individual ion. However, most recent developments have been based on the single detector ion trap design first demonstrated by Benner, in which ions were trapped for up to 450 passes through the detector tube resulting in a charge uncertainty of 2.3 *e*.[26] Dugourd and coworkers have used this design to investigate the photodissociation of polyethylene glycol (PEG) and DNA ions.[27, 34-36] Jarrold and coworkers also used the single tube ion trap to develop a Fourier transform CDMS (FT-CDMS) technique in which the ion *m*/*z* is obtained from the oscillation frequency and the charge is obtained from the amplitude of the oscillation frequency and second harmonic frequency.[28, 37] An important feature of FT-CDMS is a low detection limit (~6 *e*), enabling the measurement of small, less highly charged proteins, such as ubiquitin and cytochrome *c* and large protein complexes including pyruvate kinase and numerous different virus particles.[38-40] They have also demonstrated an uncertainty in the charge measurement of 0.196 *e* rmsd, which was obtained with cryogenically cooled detector electronics and extended ion trapping times up to 3 s.[37, 41]

Extending the trapping period reduces the uncertainty in the charge measurement caused by random noise, but other sources of uncertainty also affect the mass measurement. The oscillation frequency of an ion trapped for CDMS can change significantly while it oscillates inside the trap.[42-44] These frequency shifts can be caused not only by changes in the ion *m*/*z* through discrete fragmentation events and gradual mass loss due to solvent evaporation, but also by changes in the ion energy after collisions with the background gas. The relationship between energy and frequency leads to uncertainty in the *m*/*z* measurement for ions with different energies. Ions entering the trap with a wide range of energies or changing energy inside the device can obfuscate mass measurements. Energy filtering before the ion trap decreases the overall spread of ion energies that reaches the trap. This improves the uncertainty in the *m*/*z* obtained only from an initial frequency measurement, but not at later times when the energy and frequency of an ion

changes inside the trap. High resolution energy filtering can also reduce the rate at which ions enter the trap for dilute solutions for which few ions are formed, diminishing the throughput of the mass measurement.

Instead of using an energy filter, the ion energy can be measured dynamically while the ion is trapped by measuring the turning time ratio (TTR), the ratio of the time the ion takes to turn around in the trapping electrode to the time the ion takes to travel through the detector electrode.[43] The TTR is related to the duty cycle or fraction of each cycle through the trap an ion spends in the detector tube. With less energy, ions turn around faster in the field region but take longer to transit the detector tube in the field free region, leading to a higher duty cycle and higher oscillation frequency. Ion energies can also be measured using the ratio between the amplitudes of the first and second harmonics in the FT spectrum.[45] This ratio is highly dependent on the ion energy because the entire pattern of harmonic amplitudes changes when the duty cycle and thus the pattern of the periodic waveform induced by an ion changes. Thus, two ions with the same charge state and m/z with different energies will have different TTRs and different amplitudes at their fundamental frequencies, resulting in uncertainty in the charge measurement. With these in situ energy measurement techniques, CDMS can be used for tandem MS[43] and ion mobility measurements of single ions.[43-45]

Here, we demonstrate a method to normalize FT-CDMS charge measurements for ion energy effects using the energy of each ion in situ during the mass measurement. The amplitude of the fundamental frequency in the FT of a real ion signal is scaled by the fundamental frequency amplitude of a model ion signal simulated at a range of frequencies and TTR values with a constant time domain amplitude. Without the normalization, energy loss during the trapping period results in a systematic measurement error where the amplitude of the fundamental frequency increases steadily while each ion is trapped. The normalization essentially eliminates the slope in the measured amplitude over time for all ions. For highly charged ions that lose a large amount of energy, removing this systematic error in the charge measurement makes it possible to signal average the charge measurement over long times, reducing the uncertainty by up to two orders of magnitude.

6.3 Experimental

PEG with a nominal molecular weight of 4 MDa and bovine serum albumin (BSA) were obtained from Sigma-Aldrich (St. Louis, MO, USA) and were used without further purification. PEG was prepared at a concentration of 120 nM in 50:50 water-methanol and BSA was prepared at 10 μM in 50:50 water-methanol with 3% (v/v) acetic acid.

Experiments were performed using a home-built charge detection mass spectrometer (Figure 6.1) that is described in detail elsewhere.[43] Briefly, ions are formed by nanoelectrospray ionization using borosilicate capillaries pulled to tips with an inner diameter of ~1.5 μm. Ions enter the instrument through a modified Z-Spray source (Waters, Milford, MA, USA) and are transferred to the trap region by a pair of RF-only quadrupole ion guides and an energy selective electrostatic turning quadrupole (Ardara Technologies, Ardara, PA, USA). The electrostatic cone trap is in a differentially pumped chamber at a pressure of approximately 4×10^{-9} Torr. A detector, which consists of a single 28.2 mm long, 7.1 mm inner diameter stainless steel tube, is located between the electrodes of the trap.

When an ion passes through the detector tube, it induces a charge pulse on the tube. The charge pulse is amplified by a CoolFET charge sensitive preamplifier, linear voltage amplifier,

and shaping amplifier (Amptek, Bedford, MA, USA). Data is recorded on two detection channels, one using the output from the linear amplifier and the other using the output of the shaping amplifier. The shaping amplifier produces a pair of peaks at the leading and trailing ends of the charge pulse. Ions with >300 charges can be detected above the noise in the time domain signal on a single pass through the detector tube using the shaped signal. Thus, for high charge ions, such as those formed from 4 MDa PEG, the shaped detection channel is used to control the operation of the ion trap. The peak produced by an ion entering the detector rises above a specified level, triggering the raising of the potential of the front electrode to match the constant potential of the back electrode for a specified time (500 ms in these experiments). For low charge ions such as smaller proteins that are not sufficiently charged to be detected on a single pass, a random trapping scheme where the trap is opened and closed at regular intervals is used. In this scheme, the front electrode potential is held at 0 V for 1 ms then raised to match the constant potential of the back electrode for the specified trapping time (500 ms here), then lowered again to 0 V to allow the trapped ion to leave and restart the measurement cycle.

The time domain signals generated by a trapped, oscillating ion are analyzed offline with LabVIEW programs described in detail previously.[33, 44] Trapped high charge ions are identified using a program that finds peaks of consistent size and spacing in the shaped detection channel that persist for at least 5 ms. Trapped low charge ions are identified by finding signals that last for at least 85 ms using a program that performs a short-time Fourier transform (STFT) routine and records the fundamental frequency and amplitude of the fundamental and a specified set of harmonics for each segment. The shaped signal has a better signal-to-noise (S/N) than the unshaped channel for ion detection and is therefore used to determine whether an ion is trapped. However, the shaping amplifier distorts the pattern of harmonic frequency amplitudes, so the unshaped signal is used for all analysis of the amplitudes of the fundamental and harmonic frequencies of ions. The segment length used in the STFT is adjusted depending on the sample. The segment length is chosen to optimize the balance between the signal-to-noise ratio improvement provided by a longer segment with the amplitude dampening caused by the ion frequency shifting during that time. For the 4 MDa PEG sample, the segment length is set to 5 ms, and for BSA the segment length is set to 25 ms.

6.4 Results and Discussion

6.4.1 Charge Measurement of Single Ions

In CDMS, trapped ions produce periodic signals from which independent measures of m/z, charge, and hence mass can be obtained. Uncertainty in the m/z and charge measurements can be reduced with longer trapping times. The frequency of the ion oscillation is obtained from a Fourier transform (FT) of the time-domain signal induced by an ion. The oscillation frequency is related to the ion m/z and ion energy, and the amplitudes of the fundamental and harmonic frequencies are related to the ion charge and ion energy. The ion energy decreases during the time that it is trapped due to collisions with the background gas and, for some ions, mass loss owing either to solvent evaporation or fragmentation.[42-44] Energy loss due to collisions and solvent evaporation leads to an increase in the oscillation frequency. When the ion has less energy, it spends more time transiting through the detection tube owing to the lower velocity in this field free region but turns around faster inside the trapping electrodes.[43] Thus, the ratio between the turnaround time and tube transit time or turning time ratio (TTR) decreases as the ion energy decreases, which causes the

oscillation frequency to increase. Because the pattern of amplitudes at the fundamental frequency and higher harmonic frequencies depends on the ion energy, a FT spectrum of the induced signal changes over time as well.[45]

The effect of changes in ion energy on the signal pattern produced by a polyethylene glycol (PEG) ion with 2496 ± 1 charges trapped for 500 ms is illustrated in Figure 6.2a and 6.2b. The oscillation frequency of the ion increases from 19.3 kHz between 5 and 10 ms (blue trace, Figure 6.2a and 6.2b) to 21.7 kHz between 495 and 500 ms (orange trace, Figure 6.2a and 6.2b). At these two times, the TTR measured from the shaped channel time domain signal (Figure 6.2a) decreases from 2.31 to 1.85 (see Supporting Information). The unshaped signal (Figure 6.2b) resembles a rectangular wave pulse train with a negative pulse while the ion is in the tube and positive pulse while the ion is turning around. The duty cycle, the fraction of the waveform with a negative pulse, increases from 30.2% to 35.1%, corresponding to the change in TTR. In the FT spectrum of the unshaped signal, the amplitude of the fundamental frequency increases by ~11% between these two time periods (Figure 6.2c). The relative amplitudes of the harmonic frequencies change as well, with the fourth and seventh harmonics increasing, and the second, third, fifth, sixth, and eighth harmonics decreasing between the two time periods. Higher harmonic frequencies beyond the eighth harmonic also change in amplitude, each with their own pattern. Although the fundamental and harmonic amplitudes change with time, the amplitude of the signal pulse in the time domain does not change. This clearly demonstrates that the change in the amplitude of the fundamental and harmonic frequencies is due to changing ion energy and not ion charge, which remains constant throughout the measurement. This illustrates the challenge of determining the ion charge from the amplitudes of the fundamental frequency and just one or a few harmonic frequencies in the FT spectrum as they change over time.

The amplitude of the periodic time-domain signal induced by an ion is proportional to the ion charge. For an ideal periodic signal, the time domain amplitude can be obtained from the sum of the amplitudes of the fundamental frequency and each of the harmonic frequencies in the FT spectrum. Signal-to-noise ratios and sampling rate limitations make including many higher order harmonic frequencies in this sum challenging for real CDMS ion signals, especially for low charge ions. As a result, the charge of the ion is instead typically taken to be proportional to the amplitude of the fundamental or the sum of the fundamental and second harmonic frequency, the two most intense frequencies.[37] However, this proportionality is only exact when comparing signal patterns that have the same duty cycle and therefore produce the same pattern of harmonics. Because the pattern of harmonic frequencies changes as the ion energy decreases with time, the proportionality between charge and the amplitudes of a single or set of harmonic frequencies also changes. Determining the charge from FT amplitudes without considering the ion energy during the time segment in each transform can thus lead to errors in charge measurements.

To illustrate the errors in determining ion charge that can occur if the ion energy is not taken into account, the apparent charge obtained from the amplitude of the fundamental frequency of the ion from Figure 6.2 is shown as a function of time in Figure 6.3 (blue triangles). The amplitude monotonically increases over the entire 500 ms trapping time. Calibrating the charge measurement at the initial ion energy, the slope of these data suggests that the ion gains one charge every ~1.8 ms (~280 charges over 500 ms) during this trap time. However, the time-domain signal shows that no change in charge occurs for this ion. This discrepancy is a clear indication of a systematic measurement error that occurs because the ion energy decreases over time. This error increases significantly over time, so the apparent charge obtained from the average amplitude of segments in the first 100 ms (2525 *e*) is smaller than apparent charge using the average amplitude

of all segments in the entire trapping time (2647 *e*). Signal averaging for longer times only increases the uncertainty and changes the charge obtained in these measurements because the uncertainty is predominantly caused by a systematic error rather than random noise.

The systematic error is mitigated somewhat by summing the fundamental and second harmonic frequencies (Figure 6.3, black points). The summed amplitude increases in the first ~200 ms before reaching a maximum and decreases with a smaller slope over the final ~200 ms. Using local regression to fit the nonlinear change in amplitude over time, the summed amplitude varies by ~1.2% from its maximum to its minimum, corresponding to a ~1.2% or ~31 *e* change in charge based on the charge calibration at the initial ion energy. The change in amplitude for the summed amplitudes is smaller than for the fundamental frequency alone because the second harmonic decreases in amplitude over the range of TTRs the ion has while trapped which partially compensates for the increase in amplitude of the fundamental frequency that occurs with time. However, there is still a systematic measurement error because the amplitude of the second harmonic frequency changes at a different rate than the amplitude of the fundamental frequency. For high charge ions, such as this PEG ion, the amplitudes of additional higher order harmonics are above the noise. Each harmonic frequency changes in amplitude with a different trend as the TTR changes over time (see Supporting Information). Some combination of different harmonics may further reduce the systematic measurement error, which is the primary factor in the overall uncertainty in the charge measurement made using the amplitude of the fundamental frequency or the sum of the amplitudes of the fundamental and second harmonic frequencies for this ion. However, the S/N is lower for these higher frequency harmonics, so adding their amplitudes to the fundamental amplitude increases the uncertainty caused by random noise. Between the reduced systematic error and increased random error, adding additional harmonics can either increase or decrease the overall uncertainty, depending on the charge of the ion and the rate at which the ion energy changes with time.

Changes in the ion energy and thereby TTR and fundamental frequency amplitude also occur over time for much smaller protein ions. Measuring the resulting systematic change in amplitude for these protein ions can be challenging because their slower energy loss reduces the relative change in the fundamental frequency amplitude over the trapping time. That relative change in charge also corresponds to a smaller absolute change in charge because the protein ions have fewer charges. Thus, for a single ion, the systematic amplitude change can be obscured by random noise. However, the systematic amplitude change can still be observed by combining data from many single ion measurements. Figure 6.4a shows the most common fundamental frequency amplitude measured for a 48+ bovine serum albumin (BSA) ion at different times in the 500 ms trapping period obtained from a Gaussian fit of the amplitude distribution at each time for a sample of 246 ions. The best fit line corresponds to a ~1% or ~0.5 *e* change in charge over 500 ms. Although the increase in amplitude with longer trap times is small, the p-value for the slope is 1×10^{-4}, indicating that it is statistically significant. The increase in amplitude cannot be caused by a change in the charge state of the ions. This would result in a sudden change in oscillation frequency of at least ~600 Hz due to the change in the ion m/z, and this was not observed for any of these ions. Instead, the increase in amplitude occurs because the ions slowly lose energy, ~4.2 eV per charge, over the 500 ms trapping time. This change in energy results in a longer duty cycle (increasing from 35.7% to 36.3%) and a lower TTR (decreasing from 1.80 to 1.76). The pattern of the harmonic frequency amplitudes changes accordingly, with a larger proportion of the time domain amplitude partitioned into the fundamental frequency. Because the BSA ions lose less energy than the much larger PEG ion shown previously, the systematic change in amplitude due

to energy change is much smaller. The distribution of amplitudes caused by random noise variance is only slightly shifted by the systematic amplitude change. As a result, the overall distribution of BSA amplitudes is still nearly Gaussian, and the uncertainty in the mean amplitude still decreases over the entire 500 ms trapping time. At longer trapping times, however, the systematic effect of the changing harmonic amplitudes limits the improvement in the uncertainty if the ion energy and TTR are not taken into account.

6.4.2 Normalizing Fundamental Frequency Amplitudes for Energy

The amplitude of a fundamental frequency in the FT of a trapped ion signal depends on the frequency, TTR, and charge of the ion, but is linearly proportional to charge at any given combination of frequency and TTR. The effects of frequency and TTR on the charge measurement can be essentially eliminated by rescaling each amplitude measurement to normalize for these factors. The general scheme for this fundamental amplitude to charge normalization (FACN) is as follows. First, simulated ion signals are created with the same amplitude in the time domain for a wide range of different TTRs and frequencies. Each simulated signal is transformed to obtain the resulting amplitude of the fundamental frequency in the FT. All differences in the fundamental frequency amplitudes are then the result of varying amplitudes of the harmonic frequencies and not the amplitude of the time domain signal. The amplitude of the fundamental frequency of an ion is then divided by the amplitude of the fundamental frequency of the simulated signal that has the same frequency and TTR as the ion, to normalize for any differences in the amplitude caused by the different pattern of harmonic frequency amplitudes. This FACN approach to accounting for the effects of ion energy on the amplitude of the fundamental frequency has two advantages. First, the fundamental frequency is the best frequency to normalize because it has the highest S/N and correspondingly the least relative uncertainty caused by random noise of any harmonic frequency. Random noise introduced to the measurement by adding higher harmonics that have lower S/N than the fundamental frequency can lower the overall S/N even though the systematic error is reduced. Second, scaling based on measured TTR also normalizes the amplitude of the fundamental frequency for any effects of differences in the ion trajectory. Although TTR depends primarily on the ion energy, it is also affected by the ion trajectory. Ions with trajectories off the central axis of the trap turn around faster in the trapping electrode and have a slightly lower TTR than ions with the same energy on the trap axis.[43] This leads to slightly different TTRs and duty cycles for ions with the same energy because ions do not necessarily all follow the same trajectory. However, the pattern of harmonic amplitudes reflects the actual TTR and duty cycle measured for the ion, rather than the ion energy directly. After applying the resulting normalization factor, ion signals can be compared with the same proportionality between charge and peak amplitudes.

In order to determine these normalization factors, the ion signal was simulated at a series of frequencies and TTRs using a method that has been described previously.[45] Briefly, signals ranging from 5 to 95 kHz and 1.6 to 2.4 in TTR were generated with the same maximum amplitude at the midpoint of the charge pulse. SIMION simulations indicate that this is the most extreme range of TTRs for trapped ions in this cell geometry. The rise time and shape of the charge pulse were determined from Green's reciprocity theorem and simulations of the trap geometry in SIMION.[46] RC decay was then iteratively applied across each simulated signal using a time constant of 20 μs to match the waveforms produced by real ions.[47] A comparison between the simulated and real signals for ions at ~20 kHz with 2.15 TTR and ~61 kHz and 1.80 TTR are shown in Figure 6.5a and 6.5b, respectively. The signal for the real ion is averaged over 5 ms with

a comb filter that uses the locations of peaks in the shaped detection channel as reference points to add the signal to itself, and then scaled to the same amplitude as the simulated signal. The signals closely match during the charge pulse (corresponding to the ion travelling through the detector), but there is a small deviation in the decay shortly after the end of the charge pulse, especially at lower frequencies. RC decay significantly affects the shape of the lower frequency signal so the amplitude corresponding to the ion travelling halfway through the tube is decreased and the waveform deviates more significantly from a rectangular pulse train. The RC decay also changes the proportionality between the charge and the amplitude at the start of the pulse because some of the charge decays during the long rise time of the pulse. RC decay while the ion is not in the detector tube also makes measuring that amplitude in the time domain more challenging.

Results from the simulated signals (gray points, Figure 6.6a) show the effect of both TTR and RC decay on the amplitude of the fundamental frequency of the ion signal. The amplitude of the fundamental frequency is lower for higher values of TTR, corresponding to lower duty cycles, at all frequencies. At a single frequency, the amplitude at a TTR of 1.6 is ~17% larger than the value at a TTR of 2.4. At a single TTR, the fundamental amplitude changes only slightly between 40 and 95 kHz but drops off quickly below 20 kHz due to the effect of RC decay on the shape of the induced signal. As the charge pulse shifts from resembling a rectangular pulse train to something closer to a sawtooth wave at low frequency, more intensity in the FT spectrum shifts from the fundamental frequency to higher harmonic frequencies. To determine the scaling factor for actual ion signals with frequencies and TTRs between the simulated signals, the FT fundamental amplitudes from the simulated signals were modeled with a function that is exponential in frequency and linear in TTR with a single cross term given by equation 6.1:

$$\text{Normalization Factor} = a_1 e^{a_2 f} + a_3 TTR + a_4 TTR e^{a_2 f} + a_5 \qquad \text{(eq. 6.1)}$$

which produces the colored surface shown in Figure 6.6a. To improve the fit to the simulated amplitudes, the data were divided in three groups, from 5 to 20 kHz, 20 to 50 kHz and 50 to 95 kHz and each group was fit separately. The resulting sets of coefficients are provided in the Supporting Information. The exponential relationship between the scaling factor and frequency makes correctly scaling the amplitude at low frequency challenging. Because the scaling factors change rapidly in this regime, small errors in the modeled waveform can lead to larger uncertainty in the fundamental frequency amplitude and the resulting scaling factor. This could best be remedied by using higher ion energies in the trap resulting in higher fundamental frequencies or by increasing the RC time constant of detection system.

Measuring the TTR of each trapped ion accurately is important to effectively correct the amplitude measurement and hence the measure of the ion charge. A method to determine the TTR from the harmonic amplitude ratio (HAR) between the first and second harmonics has recently been demonstrated using ions that have a fundamental frequency of approximately 40 kHz.[45] Using the same simulations as above, the relationship between HAR and TTR can be determined at all frequencies (Figure 6.6b). Similarly to the fundamental amplitude, the HAR-TTR relationship changes only slightly above 40 kHz and changes significantly at lower frequencies. With this surface, the TTR can be determined for any ion that has detectable fundamental and second harmonic frequencies. This method is more generally applicable than the two methods that have previously been used to measure the TTR of an ion while it is trapped.[43, 44] For ions with more than ~300 charges, TTR can be measured from the time-domain signal after the square wave signal is passed through a shaping amplifier, which produces peaks that correspond to the ion entering

and exiting the detector tube.[43] For ions with fewer charges, the TTR has been determined from the oscillation frequency for ions with known *m*/*z* values.[44] This method requires that the ion is measured under instrument conditions where the relationship between the initial oscillation frequency and *m*/*z* is calibrated using the resolved charge state distribution of an ion with known mass. The HAR method is applicable to ions of any charge and unknown *m*/*z*. Thus, the TTR and the amplitude normalization factor can be determined for ions with a wider range of frequencies and charges than previously demonstrated.

6.4.3 Fundamental Amplitude to Charge Normalization for Individual Ions

Using the relationship between fundamental frequency amplitude, oscillation frequency and TTR, effects of changes in ion energy or trajectory on the charge measurement can be significantly reduced. The effect of the FACN method for the high charge PEG ion is demonstrated in Figure 6.3 (red squares). For each 5 ms segment, the original fundamental amplitude was divided by a different normalization factor obtained from equation 6.1. The frequency and TTR of the ion during each segment were measured in the FT spectrum using the unshaped signal and time-domain signal using the shaped signal, respectively. The slope of the best fit line is ~60 times smaller than that for the non-normalized fundamental amplitude (Figure 6.3, blue triangles). The R^2 for the linear fit is 0.012 and the p-value for the slope is 0.27. Using local regression to find a nonlinear change in the FACN amplitude, the maximum variation from the initial measurement is reduced by a factor of ~5 compared to the sum of the first and second harmonic frequency amplitudes. Because of the reduced dependence on TTR and frequency, the FACN amplitude can be accurately converted directly to a charge measurement. The standard deviation for the measured charge in each segment is 11 *e*, resulting in a charge uncertainty of 2.2 *e* after 125 ms and 1.1 *e* after the 500 ms trapping time. The charge uncertainty decreased by a factor of two after increasing the trapping time by a factor of four, following the expected dependence on the square root of the trapping time. Without the FACN, there is a lower limit to the charge uncertainty that can be obtained with increasing trapping time that is determined by the rate at which an ion loses energy. With no normalization, the charge uncertainty improves with longer trapping times until energy loss creates a large enough systematic change in amplitude that the overall distribution of amplitudes broadens significantly.

The FACN method is similarly effective for ions with any charge. Figure 6.4b shows the amplitudes that result from applying the appropriate normalization factors to the same sample of 48+ BSA ions shown in Figure 6.4a. Because these ions have too little charge to be directly observed in the time domain signal, the TTR for each ion was determined from the measured frequency and the *m*/*z* assigned to the ion based on its charge state. After applying the FACN, the signal amplitude induced by the BSA ions does not change significantly over the course of the trapping time. The slope of a best fit line is -7.4×10^{-7}, which is opposite in sign and ~14 times smaller in magnitude than the slope of the un-normalized data. The p-value for the slope is 0.77 which indicates that the time of the segment is not a significant factor in the measured amplitude. Because the amplitudes shown are from the entire sample of 48+ BSA ions, the variance in these data corresponds to an uncertainty in the average amplitude induced by a 48+ ion of 0.04 *e*, which is an uncertainty in the calibration. For individual ions in this charge state, the charge uncertainty of an ion measured for 500 ms is 0.58 *e* which is comparable to the charge uncertainty of 0.49 *e* reported by Jarrold and coworkers for ions trapped for ~400 ms [38]. The slightly lower charge uncertainty reported by Jarrold and coworkers is likely due to the lower temperature of their

preamplifier (~125 K) compared to ~225 K in the instrument described here [41]. After correcting for differences in trapping time and temperature, the measurement uncertainty in both instruments is similar. The FACN does not result in a significant charge uncertainty improvement because the ions lose only a small amount of energy to collisions so failing to correct for TTR change introduces less error in the charge measurement for these smaller ions. The normalization becomes more important at longer trapping times, and for larger ions that lose energy more quickly.

The absolute charge uncertainty for individual BSA ions measured here is also less than it is for the PEG ion. Jarrold and coworkers have previously noted that the uncertainty in the charge measurement depends on the charge of the ion.[37] They attributed this to a combination of $1/f$ noise that increases the electrical noise for high m/z ions and a duty cycle effect that scales with charge. Here, applying the FACN significantly reduces the duty cycle effects of energy and trajectory, but the charge uncertainty for the PEG ion is still 1.9 times larger than that for the BSA ions. Approximately half of the difference in uncertainty can be attributed to $1/f$ noise. The baseline noise is ~30% higher at 20 kHz than at 65 kHz, and the FACN further increases the noise because the PEG ion is at higher TTR and lower frequency where the fundamental frequency amplitude is reduced. This frequency effect will tend to increase the noise for large ions which are often at high m/z and oscillate at lower frequency, but results in the same noise level for all ions at a given frequency and TTR. The remainder of the increased charge uncertainty is likely caused by duty cycle effects that the FACN does not completely account for. However, even with this small charge dependence for the absolute charge uncertainty, the relative charge uncertainty significantly improves so that it decreases with increasing charge. Without the FACN, the systematic change in amplitude caused by energy loss is the dominant source of charge uncertainty for high charge ions. All ions with the same TTR change have the same relative change in amplitude, which creates a lower limit on the relative uncertainty in the charge measurement. For the PEG ion, the un-normalized fundamental frequency amplitude varies by ~11% from the beginning to the end of the transient. With the FACN, the relative charge uncertainty is just 0.04%. With such a small relative charge uncertainty, m/z uncertainty is the primary factor in the overall mass uncertainty even with an absolute charge uncertainty of 1.1 e.

6.5 Conclusions

Charge measurements in FT-CDMS can be improved by taking into account the effects of ion energy and oscillation frequency on the signal induced by an ion. The signal pattern or duty cycle depends on these factors, which in turn affects how the amplitude of the charge pulse in the time domain is distributed into the fundamental frequency and each of the harmonic frequencies in the frequency domain. Thus, determining the ion charge using only the fundamental frequency amplitude or the amplitudes of the fundamental and second harmonic frequencies leads to errors in the charge measurement. These errors can be significantly reduced with a correction method that uses the measured TTR and frequency to normalize the fundamental frequency amplitude for the effects of ion energy and detector electronics on the amplitude of signals in the frequency domain. The FACN method is especially important for large ions with high charge for which the change in amplitude is significantly larger than the random noise in the charge measurement. The fundamental frequency amplitude of a PEG ion with 2496 charges which gradually loses ~36 eV/charge over the 500 ms trapping time increases by 11% without the normalization and is essentially constant with the normalization. Because the normalized amplitude is constant, the

charge measurement can be signal averaged over the entire trapping time, reducing the relative uncertainty in the charge to 0.04%.

Jarrold and coworkers have recently shown the dependence of the ion oscillation frequency on energy is significantly decreased in a trap that uses a harmonic potential.[48] The effect of energy on the fundamental frequency was reduced by an order of magnitude, leading to a factor of four improvement in the *m*/*z* resolution. The ion trap was also designed to obtain a duty cycle of 50% at the specified ion energy to eliminate the second harmonic and maximize the amplitude of the fundamental frequency to reduce the uncertainty in the charge measurement. However, with a detection tube of finite length, the duty cycle and the resulting charge measurement depend on the ion energy, even in a trap with harmonic potentials. For two ions with the same *m*/*z* and different energies in a harmonic trap, the lower energy ion will take longer to travel through the detector, and less time to turn around outside the detector. As a result, the ions have a different duty cycle and a different pattern of harmonic amplitudes, just as in the trap demonstrated here. Measuring the ion energy and using the FACN can remove these duty cycle effects. This approach has the added advantage that tracking how the ion energy changes over time also provides information about the ion cross section and makes MS/MS measurements possible.[43-45] Energy filtering to select a small slice of the ion population into the trap is also unnecessary with this approach. Accurate charge measurements can be made over a wide range of initial ion energies after measuring the ion energy in situ and normalizing the amplitude to remove duty cycle effects, establishing a universal charge calibration. Less energy filtering is advantageous for analyzing dilute samples from which few ions are formed, so all ions that can be trapped are actually measured. Measuring the ion energy and normalizing the fundamental frequency amplitude for that measured energy is thus an important way to reduce the influence of ion energy on the charge and mass measurement.

6.6 Acknowledgements

This material is based upon work supported by the National Science Foundation under CHE-1609866. The authors thank Professors Gert von Helden, Martin F. Jarrold and David E. Clemmer for many helpful discussions and for their pioneering contributions to instrumentation and ion mobility spectrometry.

6.7 References

(1) Lössl, P.; Snijder, J.; Heck, A. J. R. Boundaries of Mass Resolution in Native Mass Spectrometry. *J. Am. Soc. Mass Spectrom.* **2014**, *25*, 906-917.

(2) Snijder, J.; Rose, R. J.; Veesler, D.; Johnson, J. E.; Heck, A. J. Studying 18 MDa virus assemblies with native mass spectrometry. *Angew. Chem., Int. Ed.* **2013**, *52*, 4020-4023.

(3) Weiss, V. U.; Bereszczak, J. Z.; Havlik, M.; Kallinger, P.; Gösler, I.; Kumar, M.; Blaas, D.; Marchetti-Deschmann, M.; Heck, A. J. R.; Szymanski, W. W.; Allmaier, G. Analysis of a Common Cold Virus and Its Subviral Particles by Gas-Phase Electrophoretic Mobility Molecular Analysis and Native Mass Spectrometry. *Anal. Chem.* **2015**, *87*, 8709 8717.

(4) Robb, D. B.; Brown, J. M.; Morris, M.; Blades, M. W. Method of Atmospheric Pressure Charge Stripping for Electrospray Ionization Mass Spectrometry and Its Application for the Analysis of Large Poly(Ethylene Glycol)s. *Anal. Chem.* **2014**, *86*, 9644-9652.

(5) Smith, R. D.; Cheng, X.; Brace, J. E.; Hofstadler, S. A.; Anderson, G. A. Trapping, detection and reaction of very large single molecular ions by mass spectrometry. *Nature.* **1994**, *369*, 137-139.

(6) Bruce, J. E.; Cheng, X.; Bakhtiar, R.; Wu, Q.; Hofstadler, S. A.; Anderson, G. A.; Smith, R. D. Trapping, detection, and mass measurement of individual ions in a Fourier transform ion cyclotron resonance mass spectrometer. *J. Am. Chem. Soc.* **1994**, *116*, 7839-7847.

(7) Chen, R.; Wu, Q.; Mitchell, D. W.; Hofstadler, S. A.; Rockwood, A. L.; Smith, R. D. Direct charge number and molecular weight determination of large individual ions by electrospray ionization Fourier transform ion cyclotron resonance mass spectrometry. *Anal. Chem.* **1994**, *66*, 3964-3969.

(8) Wuerker, R. F.; Shelton, H.; Langmuir, R. V. Electrodynamic containment of charged particles. *J. Appl. Phys.* **1959**, *30*, 342-349.

(9) Philip, M. A.; Gelbard, F.; Arnold, S. An absolute method for aerosol particle mass and charge measurement. *J. Colloid Interface Sci.* **1983**, *91*, 507-515.

(10) Hars, G.; Tass, Z. Application of quadrupole ion trap for the accurate mass determination of submicron size charged particles. *J. Appl. Phys.* **1995**, *77*, 4245-4250.

(11) Schlemmer, S.; Illemann, J.; Wellert, S.; Gerlich, D. Nondestructive high-resolution and absolute mass determination of single charged particles in a three-dimensional quadrupole trap. *J. Appl. Phys.* **2001**, *90*, 5410-5418.

(12) Cai, Y.; Peng, W. P.; Kuo, S. J.; Lee, Y. T.; Chang, H. C. Single-particle mass spectrometry of polystyrene microspheres and diamond nanocrystals. *Anal.Chem.* **2002**, *74*, 232-238.

(13) Nie, Z.; Tzeng, Y.; Chang, H.; Chiu, C.; Chang, C.; Chang, C.; Tao, M. Microscopy-based Mass Measurement of a Single Whole Virus in a Cylindrical Ion Trap. *Angew. Chem., Int. Ed.* **2006**, *45*, 8131-8134.

(14) Bell, D. M.; Howder, C. R.; Johnson, R. C.; Anderson, S. L. Single CdSe/ZnS nanocrystals in an ion trap: Charge and mass determination and photophysics evolution with changing mass, charge, and temperature. *ACS Nano.* **2014**, *8*, 2387-2398.

(15) Peng, W.; Lin, H.; Lin, H.; Chu, M.; Yu, A. L.; Chang, H.; Chen, C. Charge-Monitoring Laser-Induced Acoustic Desorption Mass Spectrometry for Cell and Microparticle Mass Distribution Measurement. *Angew. Chem., Int. Ed.* **2007**, *46*, 3865-3869.

(16) Shelton, H.; Hendricks, C. D.; Wuerker, R. F. Electrostatic Acceleration of Microparticles to Hypervelocities. *J. Appl. Phys.* **1960**, *31*, 1243-1246.

(17) Hendricks Jr., C. D. Charged droplet experiments. *J. Colloid Sci.* **1962**, *17*, 249-259.

(18) Keaton, P. W.; Idzorek, G. C.; Rowton Sr., L. J.; Seagrave, J. D.; Stradling, G. L.; Bergeson, S. D.; Collopy, M. T.; Curling Jr., H. L.; McColl, D. B.; Smith, J. D. A hypervelocity - microparticle - impacts laboratory with 100-km/s projectiles. *Int. J. Impact Eng.* **1990**, *10*, 295-308.

(19) Stradling, G. L.; Idzorek, G. C.; Shafer, B. P.; Curling Jr., H. L.; Collopy, M. T.; Blossom, A. A. H.; Fuerstenau, S. Ultra-high velocity impacts: cratering studies of microscopic impacts from 3 km/s to 30 km/s. *Int. J. Impact Eng.* **1993**, *14*, 719-727.

(20) Fuerstenau, S. D.; Benner, W. H. Molecular Weight Determination of Megadalton DNA Electrospray Ions Using Charge Detection Time-of-Flight Mass Spectrometry. *Rapid Commun. Mass Spectrom.* **1995**, *9*, 1528-1538.

(21) Schultz, J. C.; Hack, C. A.; Benner, W. H. Mass Determination of Megadalton-DNA Electrospray Ions Using Charge Detection Mass Spectrometry. *J. Am. Soc. Mass Spectrom.* **1998**, *9*, 305-313.

(22) Fuerstenau, S. D.; Benner, W. H.; Thomas, J. J.; Brugidou, C.; Bothner, B.; Siuzdak, G. Mass spectrometry of an intact virus. *Angew. Chem., Int. Ed.* **2001**, *40*, 542-544.

(23) Doussineau, T.; Kerleroux, M.; Dagany, X.; Clavier, C.; Barbaire, M.; Maurelli, J.; Antoine, R.; Dugourd, P. Charging megadalton poly(ethylene oxide)s by electrospray ionization. A charge detection mass spectrometry study. *Rapid Commun. Mass Spectrom.* **2011**, *25*, 617-623.

(24) Doussineau, T.; Désert, A.; Lambert, O.; Taveau, J.; Lansalot, M.; Dugourd, P.; Bourgeat-Lami, E.; Ravaine, S.; Duguet, E.; Antoine, R. Charge Detection Mass Spectrometry for the Characterization of Mass and Surface Area of Composite Nanoparticles. *J. Phys. Chem. C.* **2015**, *119*, 10844-10849.

(25) Doussineau, T.; Mathevon, C.; Altamura, L.; Vendrely, C.; Dugourd, P.; Forge, V.; Antoine, R. Mass determination of entire amyloid fibrils by using mass spectrometry. *Angew. Chem., Int. Ed.* **2016**, *55*, 2340-2344.

(26) Benner, W. H. A Gated Electrostatic Ion Trap To Repetitiously Measure the Charge and m/z of Large Electrospray Ions. *Anal. Chem.* **1997**, *69*, 4162-4168.

(27) Doussineau, T.; Yu Bao, C.; Clavier, C.; Dagany, X.; Kerleroux, M.; Antoine, R.; Dugourd, P. Infrared multiphoton dissociation tandem charge detection-mass spectrometry of single megadalton electrosprayed ions. *Rev. Sci. Instrum.* **2011**, *82*, 084104.

(28) Contino, N. C.; Jarrold, M. F. Charge detection mass spectrometry for single ions with a limit of detection of 30 charges. *Int. J. Mass Spectrom.* **2013**, *345-347*, 153-159.

(29) Adamson, B. D.; Miller, M. E. C.; Continetti, R. E. The aerosol impact spectrometer: a versatile platform for studying the velocity dependence of nanoparticle-surface impact phenomena. *EPJ Tech. Instrum.* **2017**, *4*, 2.

(30) Gamero-Castaño, M. Induction charge detector with multiple sensing stages. *Rev. Sci. Instrum.* **2007**, *78*, 043301.

(31) Smith, J. W.; Siegel, E. E.; Maze, J. T.; Jarrold, M. F. Image Charge Detection Mass Spectrometry: Pushing the Envelope with Sensitivity and Accuracy. *Anal. Chem.* **2011**, *83*, 950-956.

(32) Barney, B. L.; Daly, R. T.; Austin, D. E. A multi-stage image charge detector made from printed circuit boards. *Rev. Sci. Instrum.* **2013**, *84*, 114101.

(33) Elliott, A. G.; Merenbloom, S. I.; Chakrabarty, S.; Williams, E. R. Single Particle Analyzer of Mass: A Charge Detection Mass Spectrometer with a Multi-Detector Electrostatic Ion Trap. *Int. J. Mass Spectrom.* **2017**, *414*, 45-55.

(34) Doussineau, T.; Antoine, R.; Santacreu, M.; Dugourd, P. Pushing the Limit of Infrared Multiphoton Dissociation to Megadalton-Size DNA Ions. *J. Phys. Chem. Lett.* **2012**, *3*, 2141-2145.

(35) Antoine, R.; Doussineau, T.; Dugourd, P.; Calvo, F. Multiphoton dissociation of macromolecular ions at the single-molecule level. *Phys. Rev. A.* **2013**, *87*, 013435.

(36) Halim, M. A.; Clavier, C.; Dagany, X.; Kerleroux, M.; Dugourd, P.; Dunbar, R. C.; Antoine, R. Infrared laser dissociation of single megadalton polymer ions in a gated electrostatic ion trap: the added value of statistical analysis of individual events. *Phys. Chem. Chem. Phys.* **2018**, *20*, 11959-11966.

(37) Keifer, D. Z.; Shinholt, D. L.; Jarrold, M. F. Charge Detection Mass Spectrometry with Almost Perfect Charge Accuracy. *Anal. Chem.* **2015**, *87*, 10330-10337.

(38) Pierson, E. E.; Contino, N. C.; Keifer, D. Z.; Jarrold, M. F. Charge Detection Mass Spectrometry for Single Ions with an Uncertainty in the Charge Measurement of 0.65 e. *J. Am. Soc. Mass Spectrom.* **2015**, *26*, 1213-1220.

(39) Keifer, D. Z.; Pierson, E. E.; Jarrold, M. F. Charge detection mass spectrometry: weighing heavier things. *Analyst.* **2017**, *142*, 1654-1671.

(40) Lutomski, C. A.; Lyktey, N. A.; Pierson, E. E.; Zhao, Z.; Zlotnick, A.; Jarrold, M. F. Multiple Pathways in Capsid Assembly. *J. Am. Chem. Soc.* **2018**, *140*, 5784–5790.

(41) Contino, N. C.; Pierson, E. E.; Keifer, D. Z.; Jarrold, M. F. Charge Detection Mass Spectrometry with Resolved Charge States. *J. Am. Soc. Mass Spectrom.* **2013**, *24*, 101-108.

(42) Keifer, D. Z.; Alexander, A. W.; Jarrold, M. F. Spontaneous Mass and Charge Losses from Single Multi-Megadalton Ions Studied by Charge Detection Mass Spectrometry. *J. Am. Soc. Mass Spectrom.* **2017**, *28*, 498-506.

(43) Elliott, A. G.; Harper, C. C.; Lin, H.; Williams, E. R. Mass, Mobility and MS^n Measurements of Single Ions Using Charge Detection Mass Spectrometry. *Analyst.* **2017**, *142*, 2760-2769.

(44) Elliott, A. G.; Harper, C. C.; Lin, H.; Susa, A. C.; Xia, Z.; Williams, E. R. Simultaneous Measurements of Mass and Collisional Cross-Section of Single Ions with Charge Detection Mass Spectrometry. *Anal. Chem.* **2017**, *89*, 7701-7708.

(45) Harper, C. C.; Elliott, A. G.; Lin, H.; Williams, E. R. Determining Energies and Cross Sections of Individual Ions Using Higher-Order Harmonics in Fourier Transform Charge Detection Mass Spectrometry (FT-CDMS). *J. Am. Soc. Mass Spectrom.* **2018**, *29*, 1861-1869.

(46) Alexander, J. D.; Graham, L.; Calvert, C. R.; Kelly, O.; King, R. B.; Williams, I. D.; Greenwood, J. B. Determination of absolute ion yields from a MALDI source through calibration of an image-charge detector. *Meas. Sci. Technol.* **2010**, *21*, 045802.

(47) Weinheimer, A. J. The charge induced on a conducting cylinder by a point charge and its application to the measurement of charge on precipitation. *J. Atmos. Ocean. Technol.* **1988**, *5*, 298-304.

(48) Hogan, J. A.; Jarrold, M. F. Optimized Electrostatic Linear Ion Trap for Charge Detection Mass Spectrometry. *J. Am. Soc. Mass Spectrom.* **2018**, *29*, 2086-2095.

6.8 Figures

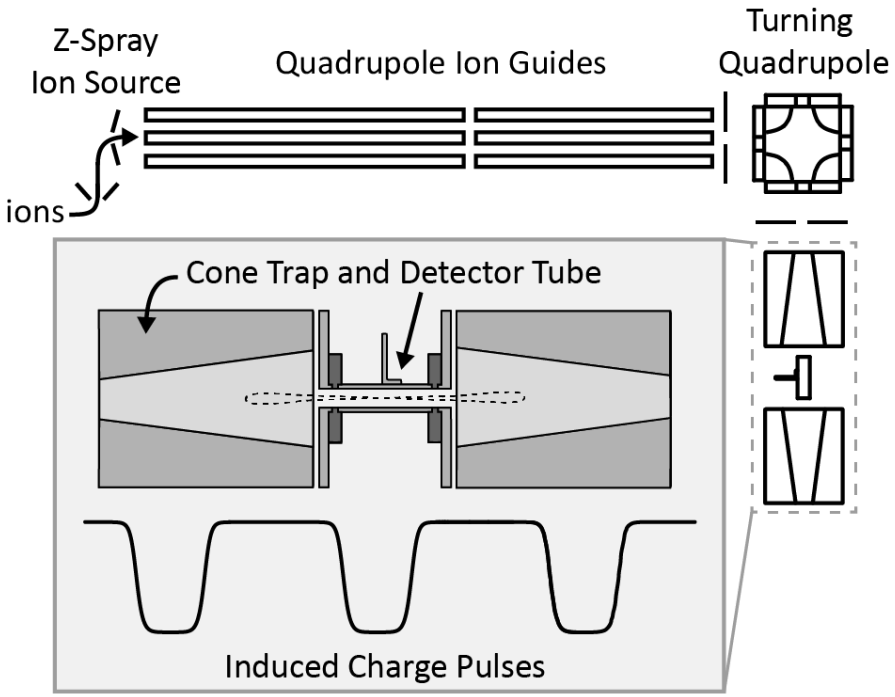

Figure 6.1: Overview of the instrument used in these experiments. The highlighted section of the diagram shows the detector tube and ion trap in detail, as well as an example trajectory for a trapped ion and the corresponding induced charge pulses. The shorter, negative, part of the waveform corresponds to the pulse induced by an ion.

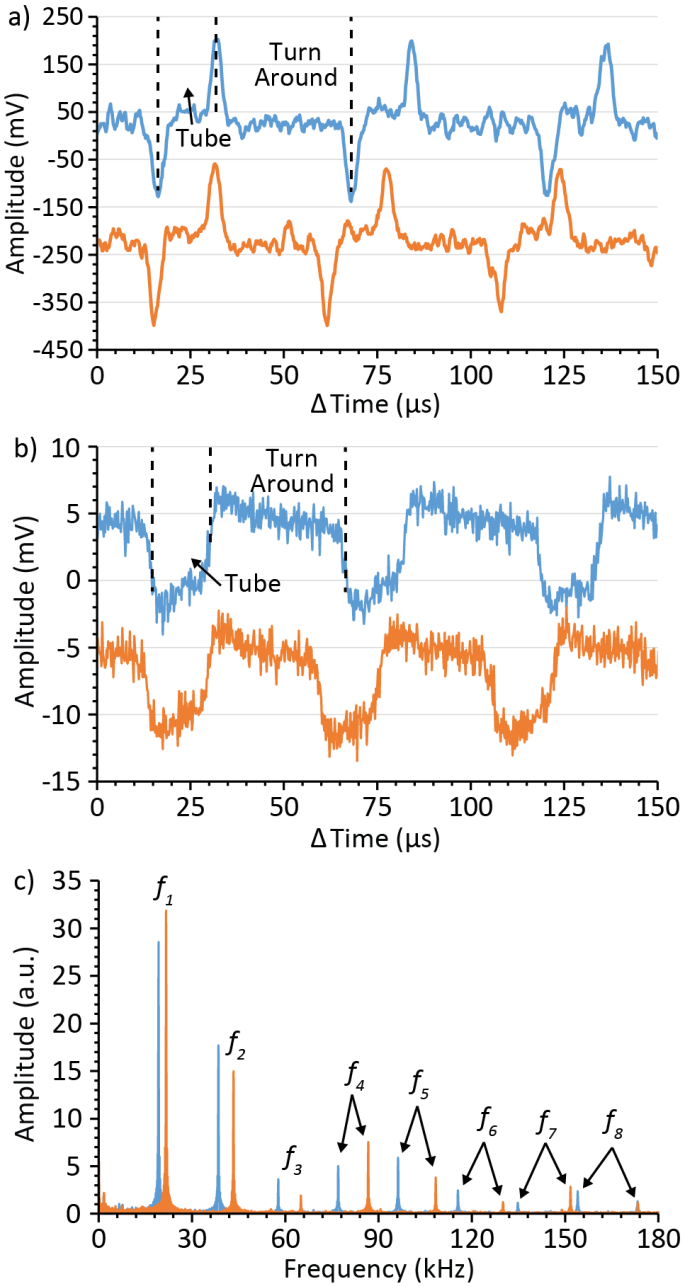

Figure 6.2: a) Shaped channel time domain signal and b) unshaped channel time domain signal for PEG transient starting at different times (blue: 5.12 ms into transient, orange: 495.08 ms into transient). c) FTs of 5 ms segments of data starting at 5 ms (blue) and 495 ms (orange)

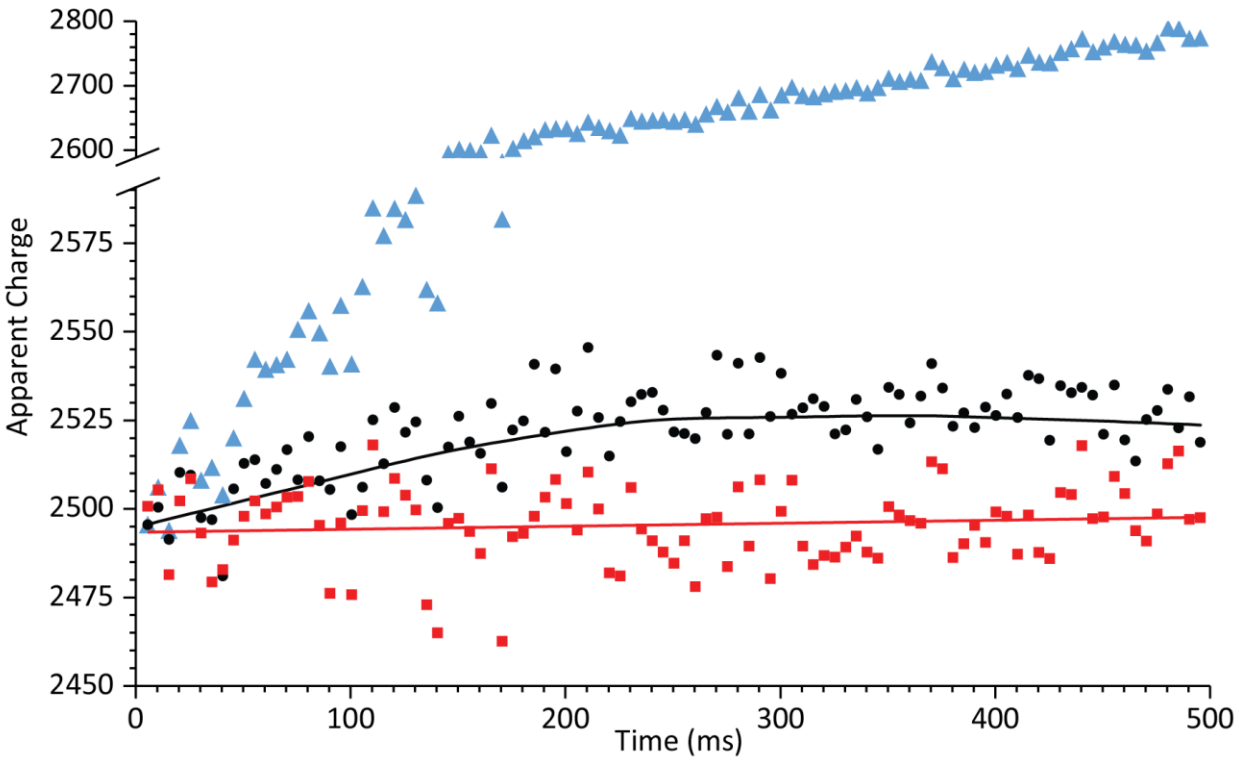

Figure 6.3: Comparison of the time evolution of the apparent charge of the PEG ion shown in Figure 6.2 determined from the fundamental frequency amplitude (blue triangles), sum of the fundamental and second harmonic frequency amplitudes (black circles and black line showing local regression) and using the fundamental amplitude charge normalization (red squares and red line showing linear regression). For the normalized data, the charge response of the detector was calibrated with protein ions in resolved charge states. For the non-normalized data, the apparent charge was determined by assigning the initial amplitude measurement to the ion charge (2496 *e*) and scaling the remaining points accordingly.

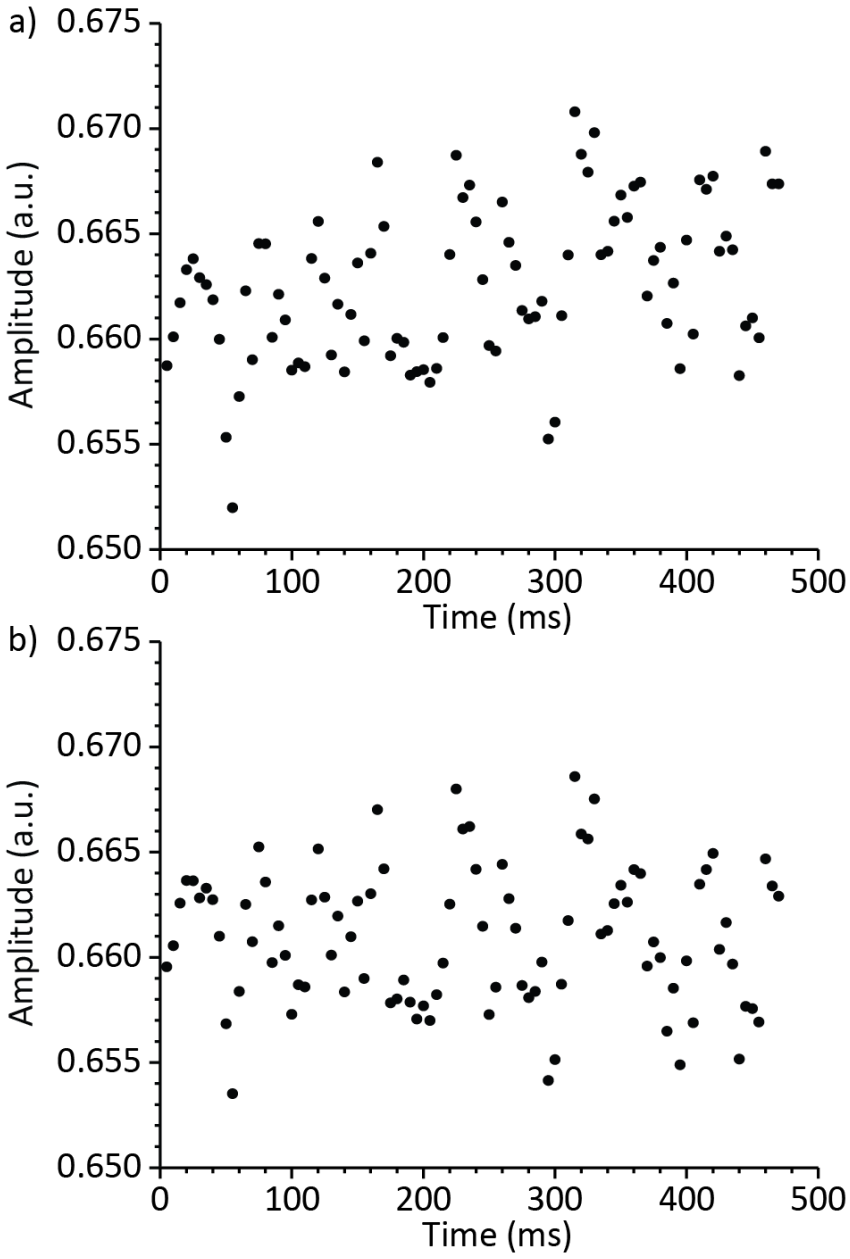

Figure 6.4: a) Most probable fundamental frequency amplitude and b) most probable normalized fundamental frequency amplitude for a sample of 246 48+ BSA ions at different times throughout the transient.

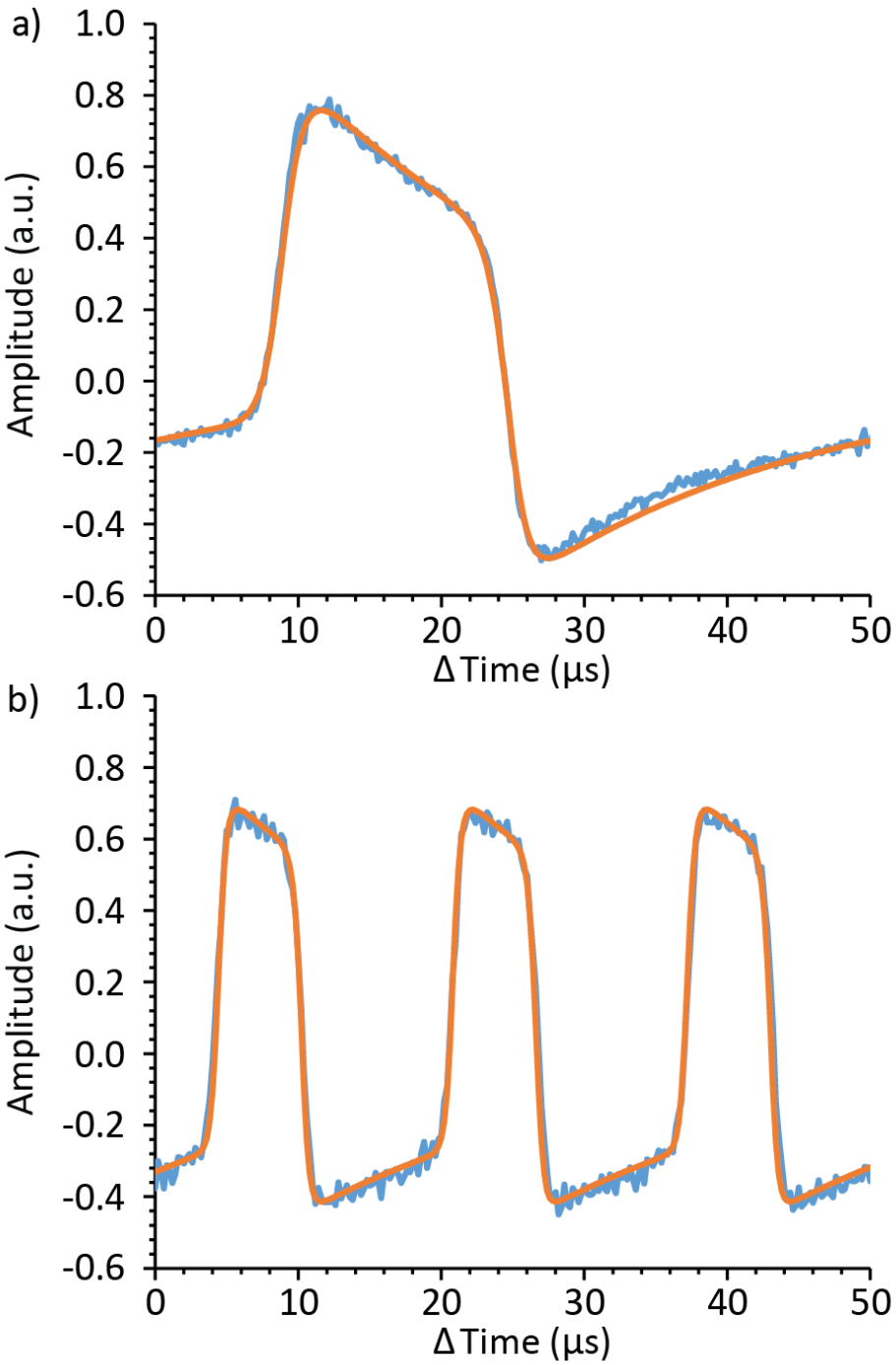

Figure 6.5: Comparison between real and simulated signals at a) ~20 kHz and b) ~60 kHz. Real signals are shown in blue and simulated signals are shown in orange.

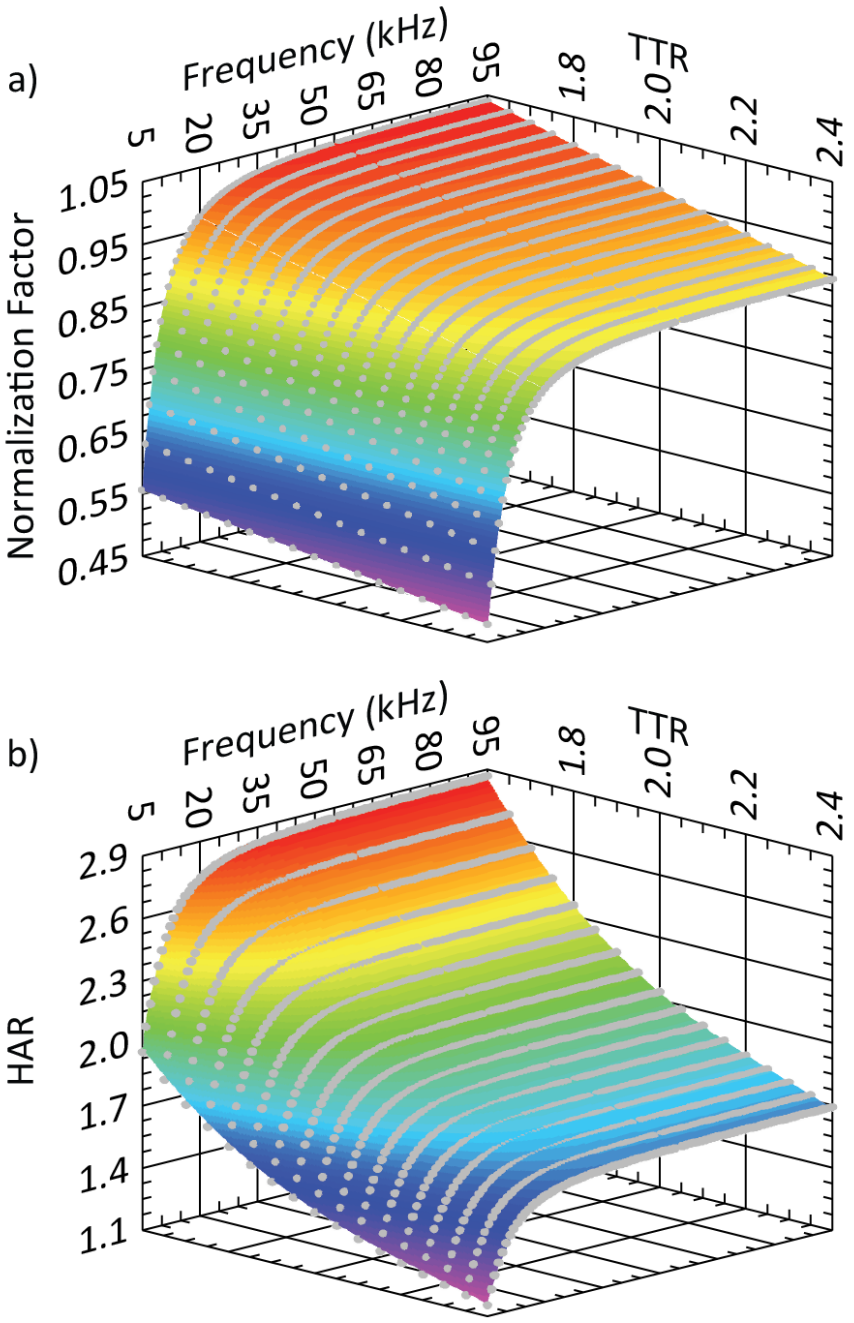

Figure 6.6: a) Fundamental amplitude to charge normalization surface and, b) harmonic ratio surface determined from simulated model ion signals. The simulated points are shown in gray, and the surface fit to those points is shown in color.

6.9 Supporting Information

6.9.1 Supporting Table and Figures

Supporting Table 6.1: Coefficients for Obtaining Normalization Factor with Equation 6.1

Coefficient	5-20 kHz	20-50 kHz	50-95 kHz
a_1	-1.377	-0.5131	-0.1304
a_2	-1.763	-0.9208	-0.4551
a_3	-0.1787	-0.1849	-0.1862
a_4	0.1916	0.07144	0.01776
a_5	1.286	1.331	1.340

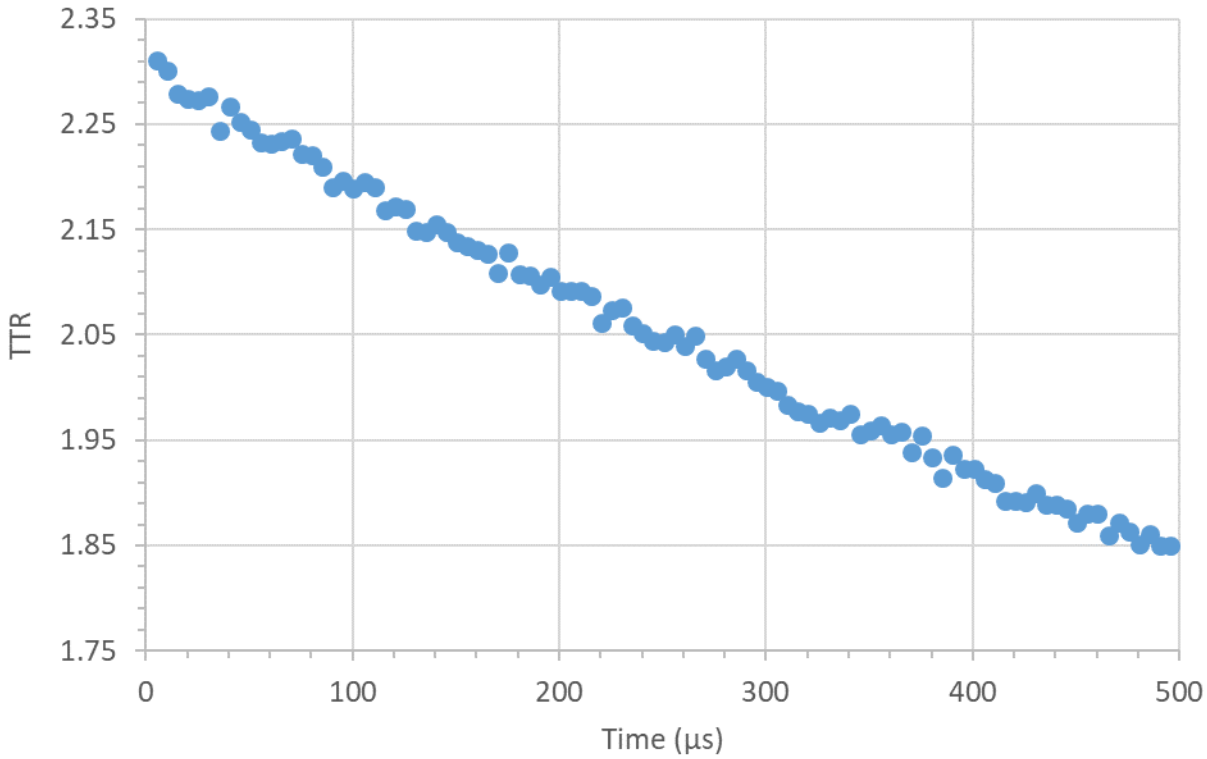

Supporting Figure 6.1: Average TTR of the PEG ion in Figure 6.1 in each 5 ms long segment throughout the trapping time

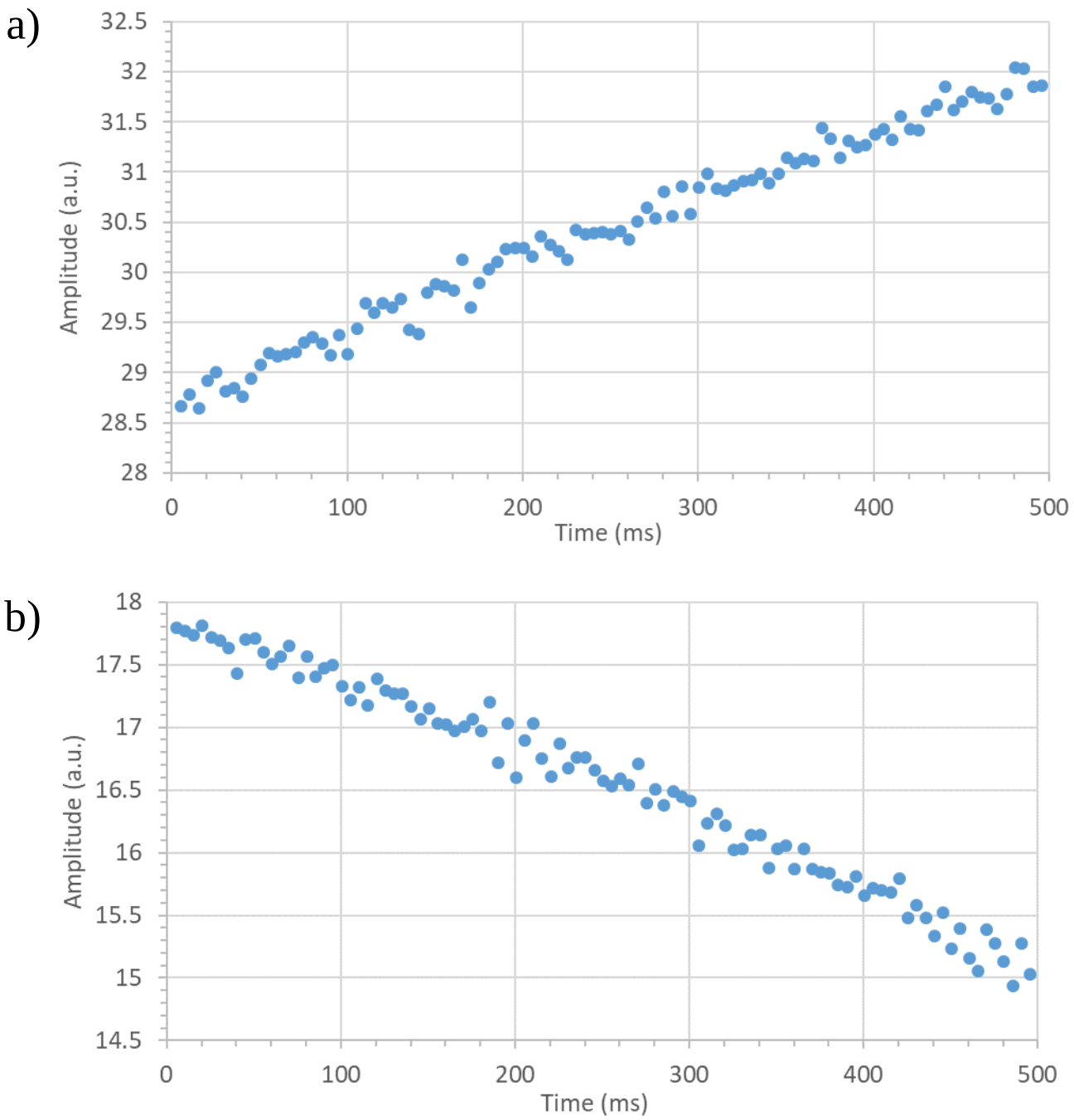

Supporting Figure 6.2: a) Fundamental frequency amplitude and b) second harmonic frequency amplitude for FTs of 5 ms long segments of the PEG ion in Figure 6.1 over time. The arbitrary units are the same for each graph. The amplitude of the fundamental increases by more than the amplitude of the second harmonic decreases, leading to a systematic change in the sum of the amplitudes of the two harmonics.

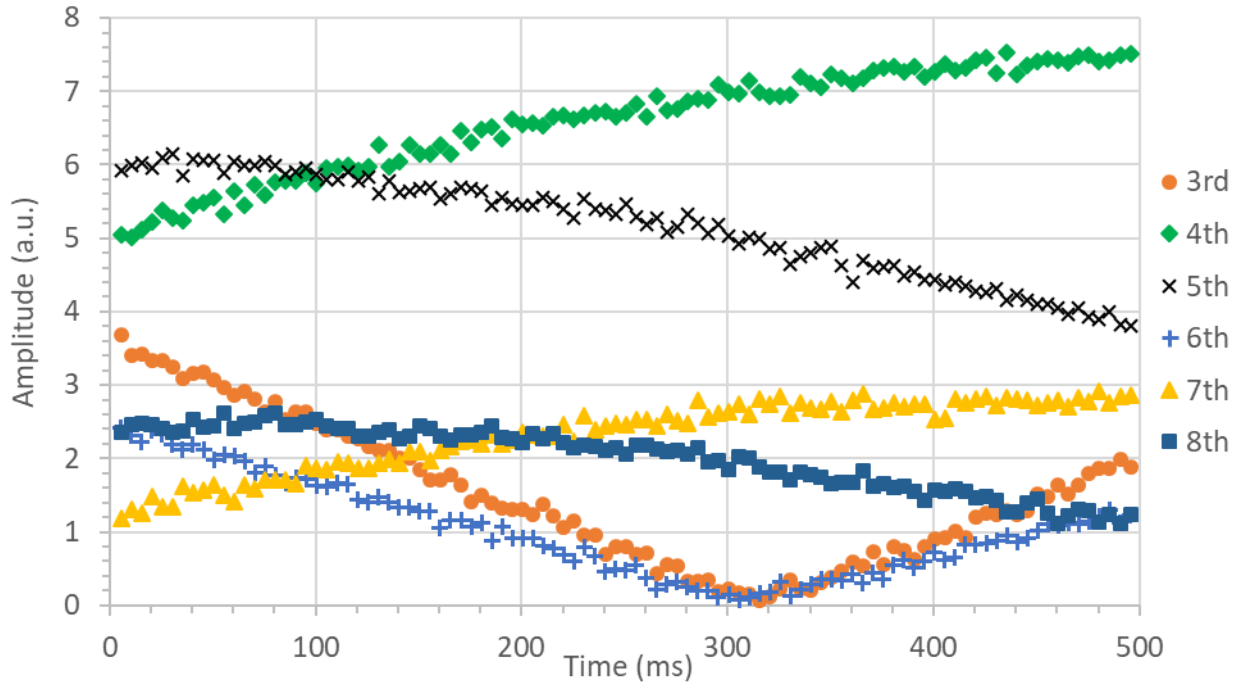

Supporting Figure 6.3: Amplitudes of the third to eighth harmonics for FTs of 5 ms long segments of the PEG ion in Figure 6.1 over time. The units in this graph are on the same scale as the units used in Supporting Figure 6.2.

Chapter 7

Summary and Future Directions

The work in this dissertation provides an array of new techniques to improve mass spectrometry methods for analyzing samples that consist of complex mixtures of high mass molecules. These techniques are based on measuring individual ions with charge detection mass spectrometry (CDMS) to overcome the problems heterogeneity in the ion population creates for conventional mass spectrometers that measure ensembles of ions. Measuring one ion at a time removes the chemical noise of other ions with similar mass to charge ratios (m/z) that interfere with the mass measurement. CDMS has advantages over other single ion detection methods in the speed of the measurement as well as the simplicity of the device. A new type of CDMS detector combining the array and ion trap methods for remeasuring ions was shown to analyze ions with a similar precision to other trapping CDMS instruments (Chapter 3). Methods to determine the ion energy during the measurement time were developed, making it possible to use CDMS for tandem MS (Chapter 4) and ion mobility (Chapters 4 and 5) measurements that increase the amount of structural information CDMS can provide beyond the ion mass. Energy measurements also enable a charge correction method that improves the precision of charge measurements in CDMS for high mass ions (Chapter 6), so that the ion m/z is the primary source of uncertainty in the mass of the ion.

The primary focus of the work in these experiments has been developing new CDMS instrumentation and data analysis techniques to weigh and obtain other structural information about samples that cannot be measured with conventional mass spectrometry techniques. An important next step is to then use the instrument to analyze samples beyond test analytes like PEG or small proteins. One system of interest is the carboxysome, a bacterial organelle that concentrates carbon dioxide inside a protein shell to improve the efficiency of carbon fixation by RuBisCO enzymes inside the shell. MS can help determine how the carboxysome forms and how RuBisCO and other proteins are packed inside the shell with the help of an intrinsically disordered protein. Carboxysomes are typically ~100 nm or larger, so measuring the mass of particles with different number of RuBisCOs loaded inside would be challenging with conventional MS but should be possible with CDMS, which has no upper mass limit. Another potential analyte for CDMS is HDL and LDL cholesterol particles, which conventional blood tests only measure the approximate concentration of. Combining mass and size measurements made with CDMS can give a fuller picture of how much of each type of particle there is, which may be useful in more accurately treating heart disease. Measuring new samples can also help improve the techniques discussed here by providing additional data to help calibrate the relationship between the energy an ion loses in the CDMS ion trap and its cross section.

Further improvements to CDMS techniques could also help make CDMS more useful for general commercial use. A key factor in single ion MS is the ability to rapidly measure a large number of ions so the mass spectrum has a high dynamic range. Increasing the measurement rate beyond the best case ~1 ion per second observed here is desirable for future CDMS methods. One

potential method to improve the measurement rate is multiplexing the instrument with multiple detectors and ion traps so that many ions can be measured at the same time. Currently, much of the ion current generated by the source is wasted by directing the ions towards the detector when the trap is closed. Using additional ion traps and deflecting ions into each different trap in turn with each trap opening could use that current more efficiently. A second method to increase the measurement rate is to multiplex inside each ion trap by measuring multiple ions in the trap at the same time. Preliminary results indicate that at least ~10 ions can be detected simultaneously without affecting the frequency, charge, or frequency shifting rate measured for each ion. The key factor in maintaining single ion measurements with multiple ions in the detector is the ability to measure the ion energy while it is trapped. Thus, more ions with different initial energies and similar m/z values can be allowed into the trap at the same time without overlapping frequencies.

Additional instrumental modifications could help improve the precision of the mass measurement as well as the rate of data collection. Aerodynamic acceleration provides high mass ions with extra energy per charge over the energy set by the DC offset potential of the RF-only ion guides. Trapping ions in the source region with those ion guides should allow additional collisions between the ions and the background gas to thermalize the ions closer to the energy set in the ion guides. Ensuring all ions have a similar energy should reduce any bias in the masses measured that comes from selecting certain energies with the turning quadrupole. Narrowing the range of ion energies produced by the source also allows more ions to be deflected at a single setting on the turning quadrupole so that more ions can enter the detector and be trapped. Modifying the detector with a shorter detector tube with a smaller inner diameter could also lead to more ions trapped for longer times, further increasing the data collection rate. Reducing the mass of the detector may also reduce its capacitance and help reduce noise in the detection channel. A shorter detector would also lead to a higher oscillation frequency, decreasing the effect of $1/f$ noise on the charge measurement. One drawback of a shorter detector is ions with a wider range of trajectories can travel between each cone electrode without hitting the walls of the detector, increasing uncertainty in obtaining the ion energy from the turning time ratio (TTR). This effect can be countered by shrinking the through holes in the entrance to the trap and in the shielding plates between the cone electrodes and the detector tube. Restricting the trap so only ions on the axis are trapped improves the precision of using the TTR to measure energy, m/z and mass.